ABSTRACT

McCOY, BRAD CHRISTOPHER. Enhanced Sustainability Concrete Mixtures: Effects of Elevated Temperature Exposure on Changes in Microstructure and Elastic Properties and the Development of Modified Layered-Sectional Analysis for Forensic Investigation. (Under the direction of Dr. Michael L. Leming and Dr. Rudolf Seracino.)

Part I of this report discusses the findings of an investigation of the relationships between changes in microstructure and elastic properties of lightweight and conventional, enhanced sustainability concrete (ESC) mixtures resulting from elevated temperature exposure. The shear modulus (G) and dynamic elastic (Young's) modulus (E_d) was determined from resonant frequency of nominal 25 mm (1 in.) thick by 100 mm (4 in.) diameter disk specimens, tested wet and dry, before and after exposure to 150 C (300 F) and 300 C (570 F). The crack densities ($\in$) before and after exposure were estimated from wet and dry G values of the disk. A critical finding was that the relationship between initial crack density and changes in crack density were similar regardless of the fly ash content implying that ESC mixtures can be used similarly to conventional mixtures in elements exposed to elevated temperatures. This study confirmed the well established effects of strength on damaged concrete members due to elevated temperature exposures, and found statistically significant differences between changes in crack density of mixtures containing fly ash and those containing slag cement.

Part II of this report describes the development of a modified layered-sectional analysis (MLSA) providing the engineer with a tool to assess structural behavior of concrete beams with localized damage, a problem not well suited to classical, closed form solutions. The MLSA framework was then used to examine how concrete materials with enhanced sustainability would perform in service after damage associated with a

short intense fire. The elastic (Young's) modulus of the ESC mixtures was determined in a companion study for undamaged and damaged conditions before and after exposure to 300 C. The elastic properties were incorporated into the MLSA, which predicted satisfactory structural performance of the evaluated ESC beams with localized damage due to fire.

Enhanced Sustainability Concrete Mixtures: Effects of Elevated Temperature Exposure on Changes in Microstructure and Elastic Properties and the Development of Modified Layered-Sectional Analysis for Forensic Investigation

by
Brad Christopher McCoy

A thesis submitted to the Graduate Faculty of
North Carolina State University
in partial fulfillment of the
requirements for the Degree of
Master of Science

Civil Engineering

Raleigh, North Carolina

2011

APPROVED BY:

_____	_____
Michael L. Leming, PhD	Rudolf Seracino, PhD
Committee Co-Chair	Committee Co-Chair

_____
David W. Johnston, PE, PhD

DEDICATION

To my wife, Stephanie, and children, Gabriel and Michael, for their unending love and support throughout this project and in life.

BIOGRAPHY

Brad McCoy is a Major in the United States Army. He enlisted in the army as an artillery cannon crew member in 1995 and later earned his B.S. in Civil Engineering from the United States Military Academy (USMA) at West Point, NY in 2001 after which he was commissioned a Second Lieutenant in Corps of Engineers. Brad has served as a Mechanized Engineer Platoon Leader, the Aide-de-Camp to the Commanding General (CG) of Fort Irwin, and the Aide-de-Camp to the CG of the Civilian Police Assistance Training Team headquartered in Baghdad, Iraq. Brad became in Infantry Officer in March of 2004, and as an Infantry Officer has served as the Assistant Operations Officer (Chief of Plans) and later Operations Officer for the 2nd Battalion, 508th Parachute Infantry Regiment (2-508 PIR), and the Company Commander for Headquarters and Headquarters Company (HHC) of 2-508 PIR. Brad has combat deployments in support of Operation Iraqi Freedom and Operation Enduring Freedom.

Brad entered the Master of Science program at North Carolina State University in 2009. Following the completion of the M.S. program, Brad will be assigned as an instructor in the Department of Civil and Mechanical Engineering at USMA.

Brad is married to the former Stephanie Wright of Manteca, California. They have two children, Gabriel and Michael.

ACKNOWLEDGMENTS

This project was possible thanks to the guidance and collaboration of Dr. Michael Leming and Dr. Rudolf Seracino, to whom I am incredibly grateful; thank you for your wisdom, support and patience. I also extend my gratitude to Dr. David Johnston for his service on my committee and professional insight. Material and concrete specimens were provided by Mr. Godwin Amekeudi and Mr. Ken Vickers of Argos USA, Raleigh Division and compressive strength tests were conducted by Mr. David Emery of Argos USA. Mr. Allen Avery and Mr. Gabriel Ballestas of Argos USA assisted in concrete specimen preparation and testing. Additionally, Mr. James Crenshaw of F&R Laboratory in Richmond, VA conducted the static elastic modulus testing for the project. Dr. Reid Castrodale of Carolina Stalite Company also provided assistance throughout the project.

I offer special thanks to Dr. Juan José Recalde who developed the analytical methodology and worked with me to share his lessons learned, and to Dr. Ufuk Dilek who provided field test data for the damaged double-tee case study members. Mr. Jerry Atkinson and Mr. Johnathan McEntire at the Constructed Facilities Laboratory (CFL) provided invaluable support with specimen preparation a testing; thank you for your expertise and friendship. Additionally, thank you to Mr. James Cox, who also provided assistance during the experimental testing phase of the project.

I am eternally grateful to my family and friends who provided continuous love and support throughout this endeavor.

TABLE OF CONTENTS

LIST OF TABLES

LIST OF FIGURES

NOTATION

A = cross-sectional area of concrete specimen

d = diameter of disk specimen

dmg = subscript indicating damage, for example G_{dmg} = damaged shear modulus

E_c = static elastic Young's modulus

E_{cs} = secant elastic Young's modulus

E_d = dynamic elastic Young's modulus

E_{pe} = effective elastic Young's modulus

E_t = tangent elastic Young's modulus

EI_{eff} = effective flexural rigidity

F = axial force

f = fundamental cyclic natural frequency

f_c = compressive concrete stress

f'_c = ultimate compressive concrete stress

f_{ct} = tensile concrete stress

f_p = stress in prestressing steel

f_s = stress in mild steel reinforcement

f_y = yield stress

G = shear modulus

M = moment

M_b = balanced moment

M_{cr} = cracking moment

p = pressure

s = seconds

t = thickness of concrete specimen

u = subscript indicating undamaged, for example G_u = undamaged shear modulus

V_s = volume of API vacuum chamber

v_s = shear wave velocity

$\in$ = crack density parameter

ε_c = concrete strain

ε_{cr} = concrete cracking strain

ε_p = strain in prestressing steel after loading

ε_{pe} = effective strain in prestressing steel

ε_0 = strain at peak stress

ϕ = angle of curvature

ν = Poisson's ratio

ρ = mass density of concrete

Ω_0 = dimensionless frequency parameter

EXECUTIVE SUMMARY

Part I:

Part I is an investigation into the effects of elevated temperature exposure to 150 C and 300 C, and to 300 C only on six different concrete mixtures. The concrete mixtures evaluated were selected to provide comparison of conventional and lightweight aggregate mixtures with 20% fly ash (conventional SCM quantity), 60% slag cement (routine sustainability), and 60% fly ash (enhanced sustainability) mixture proportions. The effects of exposure examined were changes in crack density and shear modulus.

The experimental methodology used a resonant frequency technique to non-destructively determine the shear modulus for the test specimens in each condition. The dynamic elastic (Young's) modulus was estimated using the shear modulus measurement and a reasonable estimate for Poisson's ratio. Crack density was calculated using the measured shear modulus in wet and dry conditions. The non-destructive nature of the testing allowed for replicate specimens to be evaluated before and after exposure to 150 C and 300 C or 300 C only.

Statistical analysis revealed that there was no significant difference between exposure to 150 C and 300 C and exposure to 300 C only. This allowed for the two exposure types to be grouped together and therefore the specimens were evaluated as either undamaged or damaged.

The results of the investigation concluded that stiffer, stronger mixtures exhibited larger increases in crack density due to exposure for both slag cement and fly ash

mixtures, and while enhanced sustainability mixtures (conventional and lightweight) had a higher undamaged crack density, the increase in crack density due to exposure was significantly less than the conventional or routine sustainability compositions. The initial stiffness, G_u, and SCM type had statistically significant effects on changes in crack density. Additionally, the lightweight aggregate mixtures were found to have reduced effects on crack density due to exposure for all compositions, which is consistent with transition zone effects in lightweight aggregate concrete mixture.

Part II:

Part II is the development of a modification to the layered-sectional analysis technique to provide analysis of flexural members with varying degrees of stiffness vertically and transversely through the cross-section. The investigation uses data from a case study in which a prestressed double-tee flexural member was damaged in a fire, and was subsequently load tested.

The modified layered-sectional analysis (MLSA) technique uses a discretized, cellular cross-section that allows the material properties of each cell to be uniquely specified. The dynamic elastic (Young's) modulus (E_d) can be easily obtained with routine testing, and controls deformation, was adjusted for specific cells based on damage gradients established from ACI 216.1-07. The MLSA technique allows the user to define stress-strain relationships for tension and compression in each cell.

The MLSA technique was used to produce a moment-curvature response at the cross-section evaluated. This technique can be used singularly for strength analysis at a

point along the member, or conducted at multiple points along a member to create a family of moment-curvature responses which can be used to determine the load deflection behavior of the member.

This study used a family of 21 moment-curvature responses to model the damaged double-tee member based upon the field investigation data provided in the case study. The results of the 21 moment-curvature responses were incorporated into a beam analysis software program to calculate the load deflection behavior, which was compared to the actual deflections at each increment of the load test. The predicted deflections from the MLSA framework and beam analysis software differed from the actual load test results by 1%.

The results of this study concluded that the MLSA framework provides a computationally efficient technique for the investigating engineer to determine the load deflection response of damaged concrete members with varying material properties. The data needed for the investigating engineer to accurately model the damaged member is easily gathered using standard practices conducted during the field investigation phase of a forensic study.

PART I

CRACK DENSITY AND ELASTIC PROPERTIES OF SUSTAINABLE CONCRETES

Brad C. McCoy, Michael L. Leming, and Rudolf Seracino

1.0 Introduction

Sustainability and asset management are important and related aspects of managing the built environment. Owners or agencies that provide operations and maintenance oversight of facilities, interested in using sustainable construction materials for new construction, or the repair or retrofit of existing structures, must ensure that those materials have acceptable durability.

The use of portland cement concrete is recognized by the U.S. Green Building Council as a sustainable material and its use can help attain points toward a LEED™ certification (U.S. Green Building Council 2008). Concrete is generally accepted as a sustainable material because it can provide acceptable durability under many circumstances, is regionally available, recyclable, and environmentally benign in service.

The specifications needed to achieve the desired levels of durability in concrete structures exposed to various environmental effects were largely developed after identification from failures in practice. Frost attack, sulfate attack, alkali-silica reactivity and heat of hydration effects were first indentified in structures already in service. The

construction industry has developed specifications and test methods from over one hundred years of "trial and error" case studies predominantly based on moderate strength, portland cement concrete mixtures. Application of standard test methods may not be appropriate for a mixture with a significantly different microstructure, such as mixtures with enhanced sustainability characteristics, because the existing state of knowledge relies so heavily on comparison to field studies.

By definition, a sustainable material must be durable, but different concrete mixtures do not necessarily respond the same way to given exposures. The potential difficulty in extrapolating results from one general type of concrete to another has been well documented in the case of higher strength concrete mixtures, for example. Current standards and specifications for frost attack in moderate strength concrete cannot be directly extended to high strength concrete (ACI 201.2-08; Zia *et al.* 1993), and the behavior of high strength concrete exposed to high temperatures is significantly different from that of moderate strength concrete (Phan and Carino 2002; Recalde and Leming 2009).

Although studies in North America have shown high-performance concrete production is possible with concrete mixtures containing as much as 60% fly ash by mass of the total cementitious materials (Malhotra 2002), more research is needed to develop an understanding of mechanisms and effects of deterioration of these mixtures. Further studies are also needed to expand the knowledge base of the behavior of enhanced sustainability concrete (ESC) exposed to extreme events such as fire.

Engineers require material data for design of reinforced concrete members, but simple comparison of changes in mechanical properties to either an established specification or to a control mixture may not be sufficient to address all aspects of serviceability. Changes in microstructure affecting mechanical properties may not have the same relationship for all cementitious material systems. An understanding of behavior at the fundamental, microstructural level will therefore improve the understanding of deterioration mechanisms and rates of these mixtures in severe exposures.

This paper describes a method for estimating crack density ($\in$) based on differences in shear modulus (G) between wet and dry specimens, originally developed by Recalde (2009). This paper then describes the differences in crack density between several types of concrete mixtures resulting from relatively short exposures to 300 C (570 F) and examines the relationship between initial $\in$ and change in $\in$ related to composition of the cementitious material and type of aggregate used. The response of ESC to short term fire exposure is not well established, and the results of this study also provide data for use in structural analysis of concrete beams produced with ESC and exposed to elevated temperatures.

The study described in this paper examined the effects of relatively short, 300 C (570 F) exposures on the elastic properties and changes in crack density of different types of concrete mixtures. Mixtures were produced using conventional concrete materials with either commercially common proportions or proportions that would enhance sustainability of the mixture. Both conventional and lightweight aggregates were used in

combination with cementitious systems composed of either (1) 20% fly ash (control), (2) 60% fly ash, enhanced sustainability, or (3) 60% slag cement, routine sustainability. Tests were conducted on disks approximately 25 mm (1 in.) thick and 100 mm (4 in.) in diameter.

This study also examined the relationship between changes in $\in$ based on composition. Results determined that changes in the microstructure of concrete, as assessed by changes in crack density compared with initial crack density, due to exposure to elevated temperatures, appears to be more sensitive to differences in cementitious materials than to differences in aggregate type or cementitious material proportions. Similarity in results between conventional and enhanced sustainability concrete suggests that the ESC examined in this study behave very similarly to conventional concretes produced with the same cementitious materials.

1.1 Research Significance

The information provided in this paper should be of interest to the practicing engineer concerned with assessing or evaluating concrete mixtures, particularly those with enhanced sustainability, that could be exposed to a short, intense fire in service. Experimental values of the shear and elastic modulus of several types of mixture are provided. This paper should also be of interest to the researcher investigating the microstructure of concrete mixtures with different cementitious systems. The ability to easily and effectively evaluate changes in the microstructure of concrete specimens by estimating changes in crack density after either standard test method exposures or

exposures in a research setting would be a significant benefit in helping evaluate test results between different mixtures, particularly mixtures with enhanced sustainability. This ability would improve fundamental understanding of the behavior of all concrete mixtures, and would likely reduce the time between development of concrete mixtures with enhanced sustainability and their utilization in practice.

2.0 Background

Portland cement production process also produces CO_2 emissions that are of environmental concern. Portland cement production in 2000 reportedly contributed over 3 percent of the global CO_2 emissions from fossil fuel combustion and cement production (Hanle *et al.* 2004). Mehta (2002) reported that the 2006 levels of CO_2 emissions from portland cement production was greater than 7% of the total global emission. Additionally, the total energy required to produce one ton of portland cement is 3.7 million Btu (3.9 Gj) (Mehta and Monteiro 2006). Reductions in portland cement and increased use of supplementary cementitious materials (SCM) in the form of fly ash, slag cement, or silica fume can help enhance the sustainability of concrete by reducing energy consumption, CO_2 emissions, NO_x levels, and other particulates and pollutants from the portland cement production process (Lepech *et al*. 2008). By using recycled fly ash or blast furnace slag cement to partially replace portland cement, the environmental impact of coal power plants, steel production and portland cement manufacturing are all reduced (Mehta 2002; Malhotra 2002).

The American Concrete Institute, as do many others, describes sustainable construction or development as a process that meets the needs of the present without compromising the future generation's ability to meet their needs. Sustainability in construction can reduce energy consumption and pollutant emissions. Concrete that reduces the amount of portland cement required, such as with increased volumes of SCMs, can be said to have enhanced sustainability (Mehta 2002).

The successful use of any construction material, including conventional, lightweight, or ESC mixtures, requires that the material support the anticipated applied loads and respond to the anticipated environmental exposures over the life of the structure without excessive loss of serviceability. Acceptance and approval of mixtures by the engineer of record (EOR) requires sufficient documentation to verify the material's structural properties and durability to design exposures. The current level of understanding of durability, effects of aggressive environments, and the mechanisms associated with those effects relies heavily on experimental observations, largely based on moderate strength, portland cement mixtures. Many of the new enhanced sustainability mixtures with relatively low portland cement content have limited or no service records (Recalde 2009).

Lightweight aggregate concrete has better thermal insulation compared to concrete with conventional granitic aggregate. ACI Committee 216 (2007) reports that 3 in. (75 mm) of lightweight concrete has the same thermal conductivity as 4 in. (100 mm) of conventional weight concrete, and therefore, lightweight concrete materials are often used to help attain life-safety requirements for exposure to fire. Lightweight aggregate

can also reduce environmental impact by creating a usable product out of otherwise unusable shale and slate materials (Holm 1995).

Considerable potential exists for the use of ESC in infrastructure applications. According to the U.S. Census Bureau (2008), over $20.5 trillion (in constant 1996 dollars) worth of total construction was completed between 1964 and 2002, and $5.5 trillion completed between 2003 and 2007 (U.S. Census Bureau 2009). Although the current economy has slowed, the total worth of construction costs in October 2010 was $809.5 billion (U.S. Census Bureau 2010). In an ASCE (2009) report, a general rating of "D" described much of the infrastructure in the U.S., noting that a significant amount of work is needed to repair, rehabilitate, upgrade, replace or expand many of the structures. Continued construction and increased interest in sustainability indicate a likely increase in demand for ESC in the future.

The use of ESC mixtures in new work or rehabilitation could significantly reduce pollutant emissions, however, their use in practice is scarce, in part due to limited studies examining the fundamental response of these concrete mixtures to extreme exposures (Recalde 2009). A further complication is that current test methods may not be entirely appropriate for evaluating concrete with enhanced sustainability. Because acceptance criteria for durability often rely on comparison to field studies, assessment of changes in the microstructure of concrete mixtures, including ESC mixtures, exposed to damaging environments would provide a better understanding of behavior of these concretes. A

more fundamental method of comparing changes in microstructure, as well as changes in mechanical properties, would improve evaluation of unconventional materials.

3.0 Analytical Testing Methodology

Recalde (2009) developed a test methodology to determine the crack density of concrete specimens. The method was based on analysis of shear modulus (G) of thin concrete disks, approximately 25 mm (1 in.) thick and 100 mm (4 in.) in diameter, in wet and dry conditions, before and after damage, using analytical techniques derived from O'Connell and Budiansky (1974). Recalde (2009) demonstrated that the experimental and analytical techniques could be used to compare deterioration of various concrete mixtures due to elevated temperature exposures.

3.1 Experimental Determination of Dynamic Elastic (Young's) Modulus and Shear Modulus

The shear modulus of thin disks cut from cores or cylinders can be estimated efficiently and economically with low cost equipment using the methodology developed by Leming, Nau and Fukuda (1998) based on analytical methods described by Hutchinson (1979). An accelerometer with signal conditioning and acquisition equipment, as shown in Figure 3.1, can be used to determine the resonant frequency of a thin concrete disk in free-free vibration. The resonant frequency can be used with the mass and geometry of the disks to determine the shear modulus, G. The dynamic elastic (Young's) modulus, E_d, can then be estimated, as shown in Equation 3.1, using a reasonable estimate of Poisson's ratio (ν).

$$E_d = 2(1+\nu)\rho\left(\frac{\pi f d}{\Omega_0}\right)^2 \tag{3.1}$$

where

E_d = dynamic elastic (Young's) modulus, psi (Pa)

ν = Poisson's ratio

ρ = mass density of the disk, lb/in.^{3} (kg/m^3)

f = frequency, Hz

d = diameter of the disk, in. (mm)

Ω_0 = dimensionless frequency parameter associated with the first mode of vibration defined in terms of f as

$$\Omega_0 = \frac{\pi f d}{v_s} \tag{3.2}$$

with

$$v_s = \sqrt{\frac{G}{\rho}} \tag{3.3}$$

where

v_s = shear wave velocity, ft/s (m/s)

G = shear modulus, Mpsi (GPa)

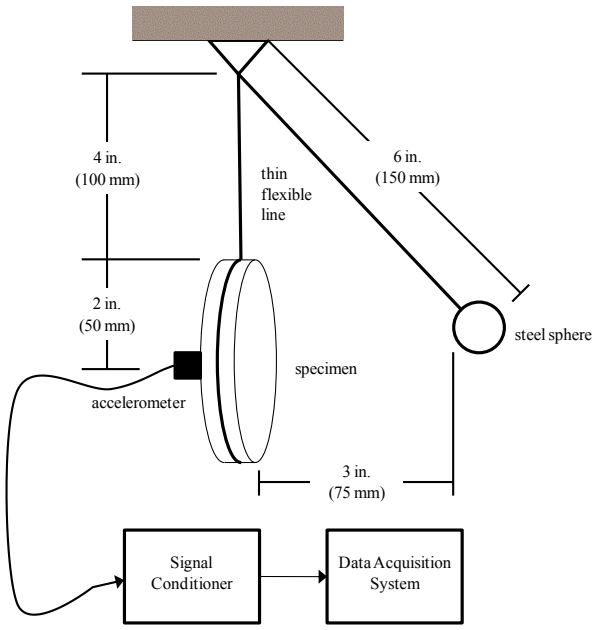

Fig. 3.1: Resonant Frequency Test Apparatus

3.2 Crack Density Changes in Damaged Concrete

Recalde's (2009) analysis was derived from work by O'Connell and Budiansky (1974) showing the relationship between shear modulus and crack density parameter for cracked, isotropic materials at various degrees of saturation assuming flat, ellipsoidal cracks. O'Connell and Budiansky (1974) developed relationships between the ratios of effective, or cracked, moduli to uncracked moduli for isotropic materials with a given ν, and moisture contents ranging from dry to saturated up to a theoretical maximum of 9/16 for $\in$. The crack density parameter is the calculated crack density assuming isolated, flat ellipsoidal cracks of a particular aspect ratio. The equations developed by O'Connell and Budiansky showed that the effects of varying ν on elastic (E), shear (G) and bulk (K) moduli ratios were small, and that differences in assumptions of crack geometry

produced negligible differences in numerical values of the moduli. The analysis demonstrated that large cracks reduce the moduli more than a great number of small cracks with the same total crack area. O'Connell and Budiansky applied the results to rock mechanics, but the extension to concrete is direct.

Recalde demonstrated that $\in$ of thin concrete disks could be determined from the shear moduli of disks dry and wet, having soaked in water for at least 24 hours, (G_{dry} and G_{wet}) without exact knowledge of either ν or G_0, the uncracked shear modulus. Recalde (2009) showed that $\in$ can be derived from an iterative solution of Equations 3.4 through 3.7:

$$\frac{G_{dry}}{G_0} = 1 - \frac{32}{45}(1-\nu_{dry})\left[1 + \frac{3}{(2-\nu_{dry})}\right] \in \tag{3.4}$$

and

$$\frac{G_{wet}}{G_0} = 1 - \frac{32}{45}(1-\nu_{wet})\left[\frac{3}{(2-\nu_{wet})}\right] \in \tag{3.5}$$

where

G_{dry} = shear modulus of air dried concrete, Mpsi (GPa)

G_{wet} = shear modulus for soaked concrete, Mpsi (GPa)

G_0 = shear modulus for uncracked concrete, Mpsi (GPa)

ν_{dry} = Poisson's ratio for air dried concrete

ν_{wet} = Poisson's ratio for soaked concrete

$\in$ = crack density parameter (dimensionless), with

$$\in_{dry} = \frac{45}{16}\frac{(\nu_0 - \nu_{dry})}{(1-\nu_{dry}^2)}\left[\frac{(2-\nu_{dry})}{(1+3\nu_0)(2-\nu_{dry})-2(1-2\nu_0)}\right] \quad (3.6)$$

and

$$\in_{wet} = \frac{45}{16}\frac{(\nu_0 - \nu_{wet})}{(1-\nu_{wet}^2)}\frac{(2-\nu_{wet})}{(2\nu_0 - 1)} \quad (3.7)$$

where

ν_0 = Poisson's ratio for uncracked concrete (0.30 for this study)

An iterative solution is used to find values for ν_{dry}, ν_{wet}, and G_0 such that $\in_{wet} = \in_{dry}$ and $0 < \nu_{dry} < \nu_{wet} < 0.5$. Recalde (2009) found that the sensitivity of $\in$ is ± 0.01 for $0.15 \le \nu_0 \le 0.30$, therefore, changes in $\in$ are insensitive to any reasonable value of ν_0.

4.0 Experimental Testing Methodology

Three conventional weight mixtures with granitic aggregate (C) and three lightweight mixtures (L) with expanded shale aggregate were tested in this study. Three cementitious material systems were examined in combination with conventional and lightweight aggregate. The cementitious material in the control mixture contained 20% fly ash (F2). One mixture, designated routine sustainability, contained 60% slag cement (S6). The amount of slag cement used is at the high end but still easily within the quantities found in common use. The other mixture, designated enhanced sustainability, contained 60% fly ash by weight of the cementitious materials (F6). The compositions and properties are shown in Table 4.1.

Table 4.1: Mixture Composition, Fresh and Hardened Concrete Properties

		CF2	CF6	CS6	LF2	LF6	LS6
Mixture Composition							
Portland Cement (Type II) pcy (kg/m^3)		500 (297)	250 (148)	250 (148)	500 (297)	250 (148)	250 (148)
Fly Ash (Class F) pcy (kg/m^3)		125 (74)	375 (222)	---	125 (74)	375 (222)	---
Slag Cement (Grade 100) pcf (kg/m^3)		---	---	375 (222)	---	---	375 (222)
Sand (Natural, C33) pcy (kg/m^3)		1085 (644)	985 (584)	1100 (653)	1330 (789)	1235 (733)	1370 (813)
Stone (# 67 C33) pcy (kg/m^3)		1800 (1068)	1800 (1068)	1800 (1068)	---	---	---
Lightweight (#67 C330) pcy (kg/m^3)		---	---	---	875 (519)	875 (519)	875 (519)
Water pcy (kg/m^3)		283 (168)	283 (168)	283 (168)	283 (168)	283 (168)	283 (168)
Fresh Concrete Properties							
Slump in. (mm)		3 ¼ (80)	4 ¼ (110)	2 (50)	2 ¾ (70)	4 (100)	2 ¼ (60)
Air Content		6.2%	6.1%	4.9%	4.2%	4.4%	5.2%
Unit Weight pcf (kg/m^3)		140.4 (2246)	136.8 (2188)	141.2 (2287)	117.4 (1881)	113.5 (1818)	118.6 (1876)
Temperature at Casting F (C)		64 (17.8)	64 (17.8)	63 (17.2)	64 (17.8)	64 (17.8)	63 (17.2)
Peak Temperature Rise F (C)		91 (32.8)	79 (76.1)	80 (26.7)	92 (33.3)	81 (27.2)	80 (26.7)
Hardened Concrete Properties							
Compressive Strength psi (MPa)	7 d	3680 (25.4)	1030 (7.1)	2980 (20.5)	3910 (27.0)	1130 (7.8)	2540 (17.5)
	28 d	5110 (35.2)	1870 (12.9)	7130 (49.1)	5990 (41.3)	2530 (17.4)	7960 (54.9)
	56 d	5880 (40.5)	2390 (16.5)	7950 (54.8)	6940 (47.8)	3740 (25.8)	8700 (60.0)
Static Elastic Modulus Mpsi (GPa)		3.33 (23.0)	2.48 (17.1)	3.87 (26.7)	3.35 (23.1)	2.62 (18.1)	3.94 (27.2)
Dry Unit Weight pcf (kg/m^3)		139.5 (2235)	133.7 (2142)	142.1 (2276)	113.2 (1813)	105.4 (2409)	117.1 (1877)

Note: All mixtures contained water reducing and air entraining admixtures, and were proportioned to have as near similar constituents as possible; fresh and hardened properties were expected to vary. Dry Unit Weight was measured after 90 days of air drying at 68 F (20 C).

4.1 Sample Curing and Specimen Preparation

Fourteen 4 in. x 8 in. (100 mm x 200 mm) cylinders were fabricated for each of the six mixtures. One cylinder had a thermocouple inserted and was stored in an insulated container to record adiabatic temperature rise over time for the first 24 hours. All samples were sealed for initial curing in accordance with ASTM C31-08 for 48 hours. After removing the samples from the molds, they were cured in accordance with ASTM C31-08 until testing. Three cylinders from each mixture were removed from curing after 36 days. Two disks, approximately 25 mm (1 in.) were sawn from the middle of the cylinder as shown in Figure 4.1 to provide six disks per mixture. The disks and the ends of the cylinders were then allowed to cure for an additional 20 days before testing.

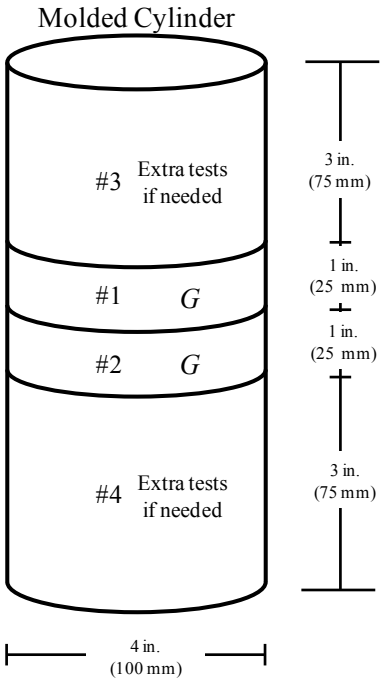

Fig. 4.1: Molded Cylinder and Thin Disk Specimen Schematic

4.2 Testing Schedule

After mixing, the following tests were conducted in accordance with the appropriate ASTM standards of the fresh concrete: slump (ASTM C143-08), air content – pressure method (ASTM C231-09), air content – volumetric method (lightweight concrete) (ASTM C173-09), density (ASTM C138-09), and temperature (ASTM C1064-08).

Compressive strength (ASTM C39 -10) was determined at 7, 28, and 56 days, the age at which the disks were removed from curing for testing. The age of 56 days was selected to attain reasonable strength for the 60% fly ash mixture. The shear and elastic moduli of the disks were determined before and after elevated temperature exposure. Static elastic (Young's) modulus (E_c) was determined after 56 days of moist curing in general accordance with ASTM C469-02. Results for f_c, unit weight and temperature rise are reported in Table 4.1.

Disks were stored in water until tested. Upon removal from the water, the surface water was removed from the specimen to improve the connection between the accelerometer and test specimen. After measuring the initial undamaged resonant frequency to determine G_{wet}, and estimate $E_{d,\text{wet}}$, the specimens were allowed to air dry at 20 ± 2 C (68 $\pm$ 5 F) for 3 weeks. Air drying over an extended period was used in an attempt to minimize cracking due to rapid drying. The disks were then tested in the dry condition to determine G_{dry} , and estimate $E_{d,\text{dry}}$.

Selected disks were then exposed to elevated temperatures. Two disks were exposed to 300 C (570 F) only and two disks to both 150 C and 300 C (300 F and 570 F). Disks

exposed to both 150 C and 300 C (300 F and 570 F) were allowed to air dry for 7 days before the subsequent exposure at 300 C (570 F) to minimize potential spalling due to trapped water in the specimen resulting from testing wet. Following each exposure, the specimens were tested in the dry condition and then submersed in a water bath for 7 days before being tested in the wet condition to obtain *G* and *E* values wet and dry in the damaged state. Two disks from each batch were kept undamaged, but stored as the other disks to help account for any differences due to additional curing.

Resonant frequency was determined at least three times for each condition. Mass was measured to the nearest 0.01 g before each test. The thickness and diameter were measured to the nearest 0.01 mm at four locations and averaged to determine the average thickness and diameter of each disk prior to the first test.

Hardened unit weights were determined based on mass and nominal volume of the cylinder as a check on fresh unit weight and were calculated to the nearest 0.1 pcf (1.6 kg/m^3). Although mixture LS6 does not meet the typical specification for lightweight concrete (115 pcf, 1840 kg/m^3) found in building construction, it was considered to be a lightweight mixture for the purposes of this study because the aggregate used in mixture LS6 is expanded shale, a typical lightweight aggregate, and the mixture is only 2% heavier than 115 pcf (1840 kg/m^3).

5.0 Results and Discussion

Statistical analysis was conducted using the JMP® (SAS© 2010) software program. Time series analysis found no serial correlation or pattern in the data, indicating that the

sequence of data collection did not affect the results. Various models were examined in which the initial crack density, shear modulus, and changes in both $\in$ and G were adjusted for the quantity of paste of each mixture. No analytical benefit was found with these adjustments. Full details of the statistical analysis are provided in Appendix B.

5.1 Differences in Exposure

The decrease in shear modulus with exposure to either 150 C and 300 C (300 F and 570 F) or the 300 C (570 F) alone is shown in Table 5.1. Analysis of the effects of differences in exposures on G was conducted using single factor analysis of variance (ANOVA), with a 95% confidence interval. Single factor ANOVA, or one-way analysis, is a comparison of the variation within a group to the variation across groups (NIST 2010). That analysis found no statistically significant difference between the two exposure groups (P = 0.63). Because E is derived from G, and $\in$ was derived from measurements of G wet and dry, these factors would also be expected to show no statistically significant difference. ANOVA analysis confirmed that expectation. This finding is consistent with those reported by Recalde and Leming (2009), whose study did not include lightweight concrete. For all remaining analysis, no distinction was made between disks exposed to 150 C and 300 C (300 F and 570 F) or to 300 C (570 F) only.

Table 5.1: Reduction in Shear Modulus (*G*) with Exposures 150 C + 300 C and 300 C Only

	CF2	CF6	CS6	LF2	LF6	LS6
ΔG: 150 C +300 C Mpsi (GPa)	0.606 (4.18)	0.400 (2.76)	0.868 (5.99)	0.461 (3.18)	0.374 (2.58)	0.722 (4.98)
ΔG: 300 C Only Mpsi (GPa)	0.633 (4.36)	0.411 (2.83)	0.828 (5.71)	0.429 (2.96)	0.328 (2.26)	0.636 (4.49)

5.2 Effects of Aggregate and SCM on Shear Modulus and Crack Density

One purpose of this study was to examine the effects of aggregate, type of SCM and quantity of SCM (%SCM) on mechanical properties and, more importantly, on changes in crack density with damage. Analysis of the effects of aggregate (L or C), type of SCM (F or S), and %SCM (20% or 60%) on shear modulus, undamaged crack density, and on the changes in these characteristics after exposure, was conducted using simple hypothesis testing based on Student-t distribution to account for the limited degrees of freedom. Analysis did not consider cross-correlation effect because those were examined as discussed later in this report.

Table 5.2 gives the dynamic shear modulus, both undamaged and damaged by exposure, undamaged crack density, and change in crack density with exposure, of the mixtures tested. Table 5.3 shows the results of the hypothesis testing.

The results indicate that the mechanical properties of the undamaged specimens are, as expected, clearly dependent on the type of aggregate and type of SCM used. The use of lightweight aggregate is known to have a large effect on the stiffness of concrete (ACI

216.1-07). The smaller undamaged crack density ($\in_u$) values for lightweight aggregate mixtures are consistent with transition zone effects reported in previous studies of lightweight aggregate mixtures (Vaysburd 1992; Holm 1995; Holm, Ooi and Bremner 2003), but may also be the result of reduced cracking due to less restraint by lower modulus aggregate on initial drying.

Table 5.2: Average Microstructural and Elastic Properties by Mixture Composition

	CF2	CF6	CS6	LF2	LF6	LS6
G_u Mpsi (GPa)	1.52 (10.5)	1.06 (7.27)	1.61 (11.1)	1.12 (7.75)	0.888 (6.12)	1.21 (8.33)
G_{dmg} Mpsi (GPa)	0.901 (6.21)	0.650 (4.48)	0.764 (5.26)	0.679 (4.68)	0.537 (3.70)	0.529 (3.65)
$E_{d,u}$ Mpsi (GPa)	3.80 (26.2)	2.64 (18.2)	4.03 (27.8)	2.81 (19.4)	2.22 (15.3)	3.02 (20.8)
$E_{d,dmg}$ Mpsi (GPa)	2.25 (15.5)	1.62 (11.2)	1.91 (13.2)	1.70 (11.7)	1.34 (9.25)	1.32 (9.12)
$\in_u$	0.233	0.287	0.264	0.224	0.261	0.226
$\Delta\in$	0.266	0.256	0.296	0.254	0.259	0.299

Note: subscript "u" indicates undamaged state; subscript "dmg" indicates damaged specimens. Shear modulus and elastic modulus values are dry condition.

Table 5.3: Statistically Significant Effect of Material on Shear Modulus and Crack Density

Factors	Measured Parameters			
	G_u	ΔG	$\in_u$	$\Delta\in$
%SCM	No (0.125)	No (0.661)	***Yes*** (0.0002)	No (0.942)
SCM Type	***Yes*** (0.003)	***Yes*** (< 0.0001)	No (0.463)	***Yes*** (< 0.0001)
Aggregate	***Yes*** (< 0.0001)	No (0.078)	***Yes*** (0.005)	No (0.246)

Note: the probability that the means of the groups are statistically the same at a 95% confidence interval is shown in parentheses for each class of composition material. ***Yes*** *= Factor has statistically significant effect on the measured parameter; No = Factor is not statistically significant for the measured parameter. Values in parenthesis are P-values based on student-t distribution*

The use of fly ash or slag cement is similarly known to affect the stiffness and strength of concrete. The lack of SCM quantity effect is likely related to the very limited number of percentages examined and by the very large effects of aggregate and SCM type affecting the shear modulus. The effect of SCM type, but not aggregate type on the reduction in shear modulus with exposure was not expected. The difference in transition zone characteristics was expected to affect the change in shear modulus, *a priori*. However, the damage due to these levels of temperature exposure occurs primarily in the paste, and the aggregate effect would be statistically significant at a 90% confidence interval. Additional study with larger number of types of mixtures could help resolve this issue.

The differences in pattern of statistical significance for crack density and shear modulus (Table 5.3), and the orthogonal response between significance of effects on crack density and effects on changes in crack density, support several important conclusions and observations. The effects of composition on relationships between shear modulus, damage, and crack densities are not simple. Additional analysis is required to examine factors and provide insight into the relationships between changes in mechanical properties and changes in microstructure as measured by changes in crack density. This analysis is provided and discussed later in this report. Another observation is that even though the value of crack density was derived from measured values of the shear modulus, the effects of composition appear to be different for $\in_u$ and G_{dry}. This

observation would suggest that important aspects of the microstructure are being captured by the crack density parameter in ways not found by simple analysis of the mechanical properties alone. This observation also suggests that analysis should be conducted separately on relationships of various factors on changes in shear modulus and changes in crack density. Additional research on the nature of the crack system, including microscopic examination, would be useful to support these observations.

5.3 Relationship Between Initial Shear Modulus and Changes in Shear Modulus

Changes in G were found to be directly related to G_u. Figure 5.1 shows that increased changes in G, that is, more damage, are found in stronger mixtures, those with higher G_u. This is consistent with previous studies (Phan and Carino 2002; Recalde and Leming 2009) on the effects of elevated temperature exposure of high strength concrete; a stiffer, stronger material is more "brittle."

Figure 5.1 also indicates that G_u is strongly affected by mixture composition, with a difference between concretes containing slag cement and those containing fly ash. The slag cement mixtures behaved similarly to the fly ash mixtures with a shift in ΔG. An important finding is that the relationship between G_u and ΔG appears to be strongly dependent upon paste constituents with little, if any, difference due to type of aggregate or percentage of fly ash used. The lack of effect due to aggregate type is, again, consistent with damage occurring in the paste. The lack of effect due to percentage of fly ash implies that response is similar for a very wide range of fly ash contents. These findings are examined further below.

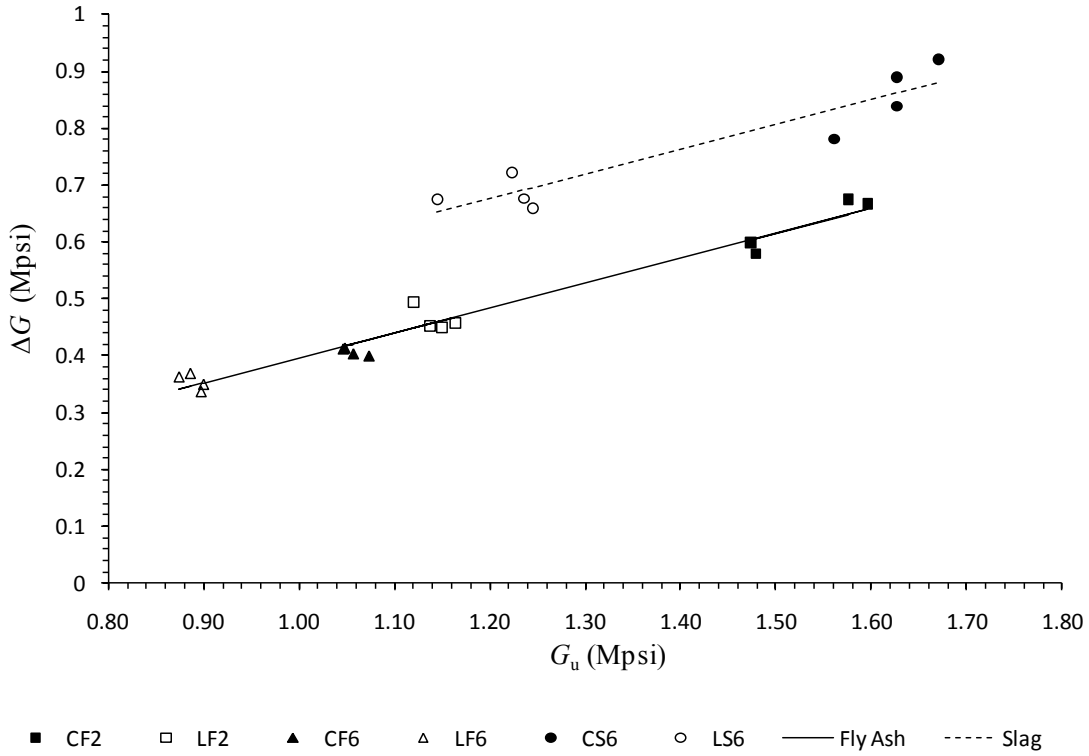

Fig. 5.1: Changes in *G* by SCM Type
(1.0 Mpsi = 6.89 GPa)

Analysis found an r^2 of almost 0.98 for the model shown in Equation 5.1, with G_u and SCM type both statistically significant.

$$\Delta G = 0.055 + 0.437\, G_u - 0.096\, \text{SCM[F]} \qquad (5.1)$$

where

ΔG = change in shear modulus

G_u = initial undamaged shear modulus

SCM[F] = 1 for fly ash and -1 for slag cement.

P values for all parameters were < 0.0001. Similar analysis including %SCM and aggregate type showed that neither factor was statistically significant in predicting changes in shear modulus with damage due to elevated temperature exposures.

5.4 Relationship Between Initial Crack Density and Changes in Crack Density

Another important purpose of this study was to examine the relationship between initial crack density, $\in_u$, and changes in crack density, $\Delta\in$, with damage. Figure 5.2 shows a linear relationship between $\in_u$ and $\Delta\in$, with a statistically significant difference due to type of SCM. Analysis found an r^2 of almost 0.90 for the model shown in Equation 5.2 of $\Delta\in$ against $\in_u$ and SCM type, with both $\in_u$ and SCM type statistically significant factors.

$$\Delta\in = 0.288 - 0.536\ \in_u - 0.020\ \text{SCM[F]} \qquad (5.2)$$

where

$\Delta\in$ = change in crack density

$\in_u$ = initial undamaged crack density

SCM[F] = 1 for fly ash and -1 for slag cement.

P values for all parameters were < 0.0001. Analysis found that aggregate was not statistically significant, but %SCM was statistically significant at just under a 97% confidence interval. Based on the limited data available, the %SCM and SCM type do not appear to be cross-correlated, but additional studies should examine this possibility.

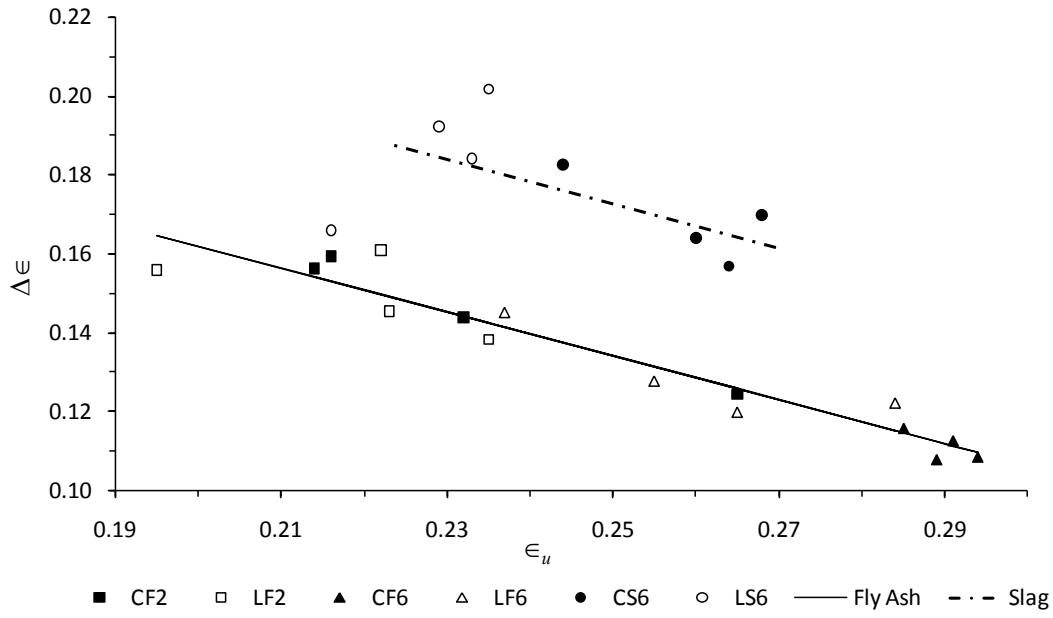

Fig. 5.2: Changes in ∈ by SCM Type

The measured $\Delta\in$ values were consistently higher for slag cement mixtures than for fly ash mixtures with the same initial crack density. As with Figure 5.1, the trends do not show a statistically significant effect due to aggregate type, and the slopes are approximately parallel, although there is a possible outlier in the LS6 mixture. This finding supports the conclusion that crack density and crack propagation are functions of the paste rather than aggregate type for this exposure.

5.5 Relationship Between Changes in Crack Density and Changes in Shear Modulus

Figure 5.3 shows the relationship between changes in crack density and changes in shear modulus. The relatively flat $\Delta\in$ - ΔG relationships for lightweight aggregate mixtures support the finding that $\Delta\in$ has only a minor effect on changes in stiffness

characteristics (*G* or *E*) of the mixtures under this type of exposure. A regressed value of the slope of each type of concrete must be used cautiously due to the limited degrees of freedom available for each group. Analysis indicates, however, that the slopes of the three lightweight mixtures are parallel but that the slopes of the conventional density mixtures increase with increased changes in stiffness (see Table 5.4).

Table 5.4: $\Delta G / \Delta \in$ Slopes by Group

	Slope	
	Conventional Aggregate	Lightweight Aggregate
20% Fly Ash	1.1	0.91
60% Fly Ash	2.8	1.1
60% Slag Cement	4.0	1.2

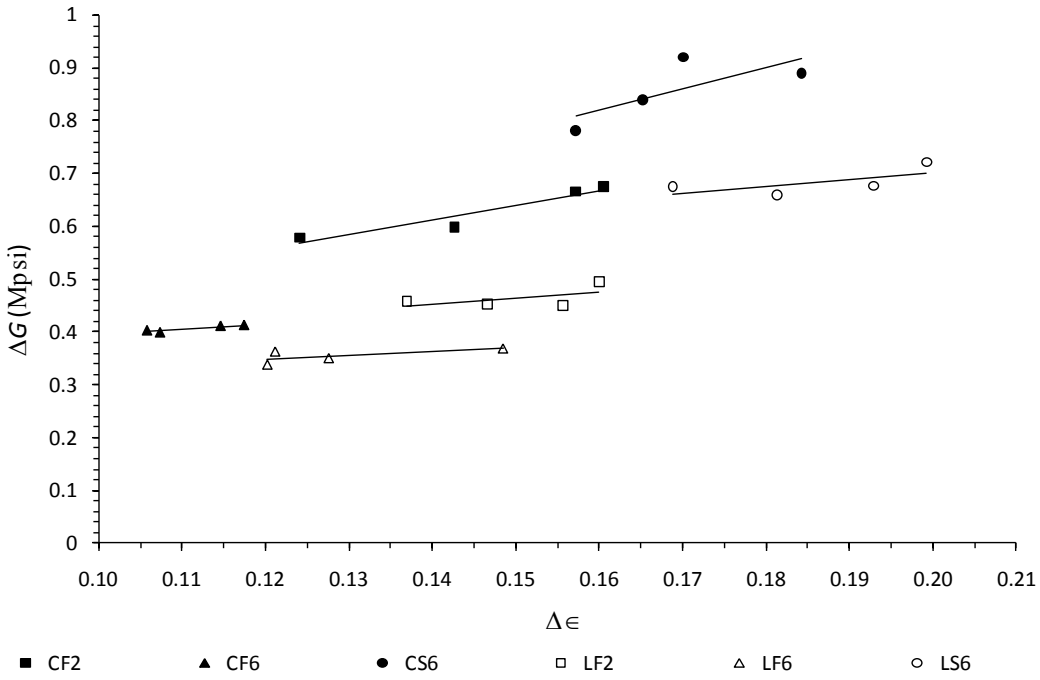

Fig. 5.3: Changes in *G* and ∈ by Aggregate and SCM
(1.0 Mpsi = 6.89 GPa)

The conventional aggregate mixtures experienced greater reduction in stiffness than the lightweight aggregate mixtures for roughly the same change in crack density. This is consistent with the fact that stronger concrete mixtures tend to have greater reduction in stiffness with exposure to elevated temperature, but it also demonstrates, from a microstructural perspective, how lightweight concrete mixtures improve performance in service when exposed to elevated temperatures, regardless of % SCM or SCM type.

5.6 Prediction Changes in Shear Modulus with Exposure to Elevated Temperatures

Two statistical models were examined using least squares regression. One model used $\in_u$, aggregate type, SCM type and %SCM to predict ΔG. The other model was similar except that $\in_u$ was not included. The model shown in Equation 5.3 based on composition only had an r^2 of over 0.94.

$$\Delta G = 0.659 + 0.65\ \text{Agg[C]} + 0.83\ \text{qSCM[20]} - 0.195\ \text{SCM[F]} \qquad (5.3)$$

where

ΔG = change in shear modulus

Agg[C] = 1 for conventional weight aggregate and -1 for lightweight aggregate

qSCM[20] = 1 for 20% SCM content and -1 for 60% SCM content

SCM[F] = 1 for fly ash and -1 for slag cement

All model factors were found to be strongly statistically significant.

The model including $\in_u$ found that $\in_u$ was not a statistically significant factor, and that % SCM was only marginally significant at a 95% confidence interval. This model

would therefore be rejected in favor of the model based on composition only. The relevance of this finding, in conjunction with those previously discussed, is that the crack density parameter is providing important information regarding the response of the mixtures to elevated temperature exposure but that the primary factors affecting the response are the constituent materials.

5.7 Discussion

Figures 5.1 and 5.2 indicate that SCM type has a strong influence on fundamental behavior of concrete exposed to elevated temperature. These figures, especially Figure 5.2, also indicate that a concrete mixture with enhanced sustainability provided by incorporating large amounts of SCM will, at the microstructural level, respond similarly to a conventional concrete mixture produced with the same raw materials. Clearly, mixture characteristics must be established to satisfy the design requirements, but these findings also imply that when material characteristics satisfy the design requirements, mixtures with enhanced sustainability, incorporating either fly ash or slag cement, can be used in elements exposed to elevated temperatures. These findings also imply that there may be a benefit in performance in service for ESC exposed to elevated temperatures that is largely related to reductions in initial stiffness. Additional research using a larger variety of SCM types would be beneficial. Figure 5.3 confirmed that lightweight concrete, whether with a conventional cementitious material system or one with enhanced sustainability, will be more resilient to exposures to elevated temperatures. Continued research with ESC mixtures is recommended to incorporate the results of this

investigation into design parameters that enable the EOR to incorporate the use of ESC material where appropriate in practice.

6.0 Conclusions and Recommendations

This study examined the effects of elevated temperature exposure on the mechanical properties and crack density parameter of mixtures with fly ash and slag cement employed in significant quantities to produce concrete with enhanced sustainability characteristics. The study involved quantitatively determining the changes in shear and elastic modulus, and crack density, as described by Recalde (2009), of conventional and lightweight aggregate concrete mixtures compared to mixtures typically found in commercial production.

6.1 Conclusions

1. No statistically significant difference in *E, G,* or $\in$ was found between disks exposed to 300 C (570 F) only and those exposed to both at 150 C and 300 C (300 F and 570 F).

2. Stiffer, stronger mixtures (those with smaller $\in_u$ and larger G_u) exhibited larger increases in $\Delta\in$. This is true for both slag cement and fly ash mixtures. Although the ESC (60% fly ash) mixture had a higher $\in_u$, the increase in $\in_u$ after thermal exposure was less than that of the conventional (20% fly ash) and routine sustainability (60% slag cement) mixtures. The ESC mixtures were found to respond similarly to conventional composition mixtures after extreme exposure events when expressed as $\Delta\in$ and ΔG, indicating that ESC mixtures could be appropriate for use in structures where the

potential for extreme exposure events exists provided that the initial design specifications are satisfied.

3. Lightweight aggregate mixtures were found to have reduced differences in crack density ($\Delta\in$) due to extreme exposure events for all %SCM and SCM types.

6.2 Recommendations

1. Additional studies to investigate the microstructural changes, including possible transition zone effects, using microscopic and nano-indentation techniques are recommended. Some of these studies are currently in progress.

2. Additional research is recommended to determine multiple exposure effects of a wider range of temperatures to better understand long-term durability of ESC mixtures, and to investigate changes in f_c and f_{ct} with respect to G or $\%\Delta\in$ after repeated extreme exposure events.

3. Incorporating the results of this study into structural analysis, such as the Modified Layered-Sectional Analysis (MLSA) technique (McCoy, Seracino and Leming, in review), can provide asset managers with analytical and forensic tools for evaluation of existing structures that have been damaged.

4. An improved understanding of the deterioration mechanisms at the microstructural level, based upon fundamental principles, could improve a more rapid assessment of concrete mixtures and enable more ESC materials to be placed into service. Additional

studies to examine the microstructural changes and relationship to changes in properties of concrete exposed to other damaging exposures are recommended.

5. An improved understanding of the effects of various constituents on changes in microstructure and elastic properties could also improve the industry's ability to better contribute to sustainable construction, infrastructure management, and development of design codes and specifications.

7.0 Acknowledgements

The authors would like to thank Godwin Amekuedi, Ken Vickers, Allen Avery, Gabriel Ballestas and David Emery of Argos USA for supplying all concrete mixture components, assisting with concrete mixing and specimen preparation, and conducting all fresh concrete and compressive strength tests. Additional thanks to James Crenshaw and F&R Lab in Richmond, VA for conducting the static modulus tests. Special thanks to Jerry Atkinson and Johnathan McEntire at the Constructed Facilities Laboratory (CFL) at North Carolina State University for support throughout the project with assistance in specimen preparation and testing.

Part II

MODIFIED LAYERED-SECTIONAL ANALYSIS FOR FORENSIC INVESTIGATION

Brad C. McCoy, Rudolf Seracino, and Michael L. Leming

1.0 Introduction

Evaluation of the effectiveness of construction materials with enhanced sustainability proposed for use in structural elements later exposed to severe conditions requires two types of analysis. The characteristics of the proposed materials must be determined in both the damaged and undamaged state and the structural analysis of the damaged member must be conducted. When this damage is localized, resulting in significant spatial variations in properties including elastic modulus (E) and moment of inertia (I), classical, closed-form solutions are not practical. A model that can easily include the effects of localized damage, including missing material, is needed.

This report examines the differences in predicted flexural behavior of precast double-tee beams exposed to a short, intense, localized fire and composed of either conventional lightweight aggregate concrete or a lightweight aggregate concrete with enhanced sustainability. Selected properties of the enhanced sustainability concrete mixtures were determined before and after exposure to 150 C (300 F) and 300 C (570 F). The full details are contained in a companion paper (McCoy, Leming and Seracino in review).

The structural analysis technique developed and used is a modified layered-sectional analysis (MLSA). The standard layered-sectional analysis approach was expanded to include variations in properties and geometry in the longitudinal and transverse directions, as well as with depth, permitting evaluation of the structural effects of localized damage. The MLSA model was validated by comparing results to the findings of a forensic investigation of a fire damaged prestressed double-tee structural member fabricated with lightweight aggregate concrete.

1.1 Research Significance

The proposed MLSA methodology provides the engineer with an analytical tool capable of evaluating the structural behavior of elements with localized damage. The results of the MLSA analysis indicated the method was capable of assessing the likely structural behavior near ultimate load, and predicting the outcome of a load test, with acceptable accuracy. The study also clearly demonstrated that certain concrete mixtures with enhanced sustainability would provide acceptable structural performance when exposed to similar, short, intense, fires.

1.2 Subject Case Study

This case study examined a precast, prestressed, lightweight concrete double-tee structural beam forming part of a three level parking structure located in Raleigh, North Carolina. Two of the simply supported 58 ft (17.7 m) long members were subjected to a vehicle fire beneath them that burned for 30 to 45 minutes, destroying the vehicle. The fire damaged double-tees (shown schematically in Figure 1.1) experienced cracking and

spalling in some areas. Portions of cores and exposed concrete exhibited a pink discoloration, indicating that the concrete temperature exceeded 570 F (300 C) during the fire and that the concrete properties were significantly compromised in these areas (Dilek 2005).

1.2.1 Field Investigation Techniques

A field investigation of the damaged structural members was conducted to evaluate the level of distress and necessary repairs or rehabilitation for "continued safe operation of the structure" (Dilek 2005). Dilek's investigation was conducted using nondestructive evaluation techniques, laboratory analysis, and a load test conducted in general accordance with ACI 318-99 Chapter 20.

Pulse velocity tests were conducted on the structure in general accordance with ASTM C597-01. The pulse-velocity measurements were taken transversely through the double-tee stems at one-foot grid intervals and compared with values from unaffected areas of the structure to determine the spatial extent of the damage along the double-tee. Concrete cores were then taken from the stems of the double-tee at four selected locations in the damaged stems and from an unaffected area away from the fire site for reference (Dilek 2005).

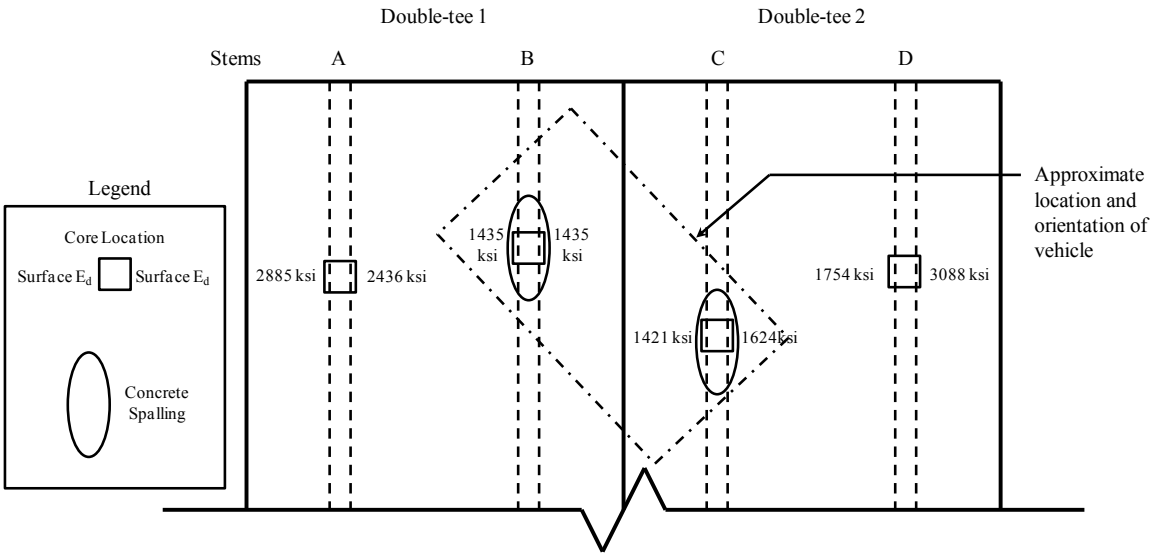

Fig. 1.1: Plan View of Site (Adapted from Dilek 2005)

1.2.2 Laboratory Testing of Concrete Core Samples

A quantitative analysis of the fire damage to the concrete was conducted by determining the dynamic elastic (Young's) modulus of elasticity (E_d) of one-inch thick concrete disks cut from the cores. The one-inch intervals permitted mapping of any damage gradients present in the stems. Dilek (2005) also determined the concrete splitting tensile strength (f_{ct}) of cores from both the fire damaged region and an undamaged region of the structure. The dynamic Young's modulus of the concrete disks was determined nondestructively using resonant frequency principles based upon the theory developed by Hutchinson (1979) using axisymmetric flexural vibration of a thick, free, circular plate, as described in detail by Leming, Nau, and Fukuda (1998) for the specific application of circular concrete disks.

The detailed results of the laboratory investigation are presented in Table 1.1 where E_d was taken as the average of two disks. Dilek found that E_d was reduced by 59% and 57% at the surface of stems B and C respectively (see Fig. 1.1). A significant loss in E_d was reported at both the surface and interior disks from the stems directly above the fire site, with greater damage in the surface disks. Areas farther away from the fire site (Stems A and D in Fig. 1.1) showed pronounced effects at the surfaces closest to the fire site, but minimal effects at the surfaces away (Dilek, 2005).

The conclusion of the laboratory investigation was that the two members were damaged significantly above the fire location, but generally unaffected elsewhere. A load test was ordered by the EOR due to the inability of available analytical models to readily predict the behavioral response of members with significant material variability through both the cross-section and along the member length.

Table 1.1: Laboratory Test Results From Field Evaluation (Dilek 2005)

Cores at stems	A	B[1]	C	D	Control[2]
E_d at surface, ksi (GPa)	2670 (18.4)	1440 (9.93)	1520 (10.5)	2420 (16.7)	3560 (24.5)
Loss with respect to control (%)	25	59	57	32	---
E_d at interior, ksi (GPa)	3240 (22.3)	2140 (14.8)	1700 (11.7)	2500 (17.2)	3430 (23.6)
Loss with respect to control (%)	6	38	50	27	---
f_{ct} , psi (GPa)	570 (3.93)	400 (2.76)	435 (3.00)	550 (3.79)	570 (3.93)
Loss with respect to control (%)	0	30	24	4	---

1. Cores at stems B and C were taken from stems directly above the fire and above the area of visible spalling.
2. Unaffected core was taken as reference about 60 ft (18 m) away from the fire site at a non-soot-stained concrete double-tee. It is assumed that the original concrete properties of the damaged area were the same as the control specimen.

Note: E_d was taken as the average of two discs. 1 ksi = 6.895 MPa

1.2.3 Load Testing of Damaged Members

Load test procedures outlined in ACI 318-99 at the time of the test stipulated that a flexural member must meet structural deformation limits over time to remain in service as the beam is subjected to a total load of 0.85 (1.4D + 1.7L) where D = dead load, and L = live load. A 44,800 lb (20,320 kg) test load per double-tee was applied as a uniform load in four equal increments of 11,200 lb (5,080 kg). Once the full load was applied it was maintained for 24 hours, then removed in four equal increments. Deflection measurements were taken after the application of each increment, after the 24 hour sustained load period, and after the removal of each load increment.

The results of the load test are shown in Figure 1.2. Both double-tee members satisfied the requirements for maximum deflection and recovery in accordance with ACI 318-99 Chapter 20, with a residual deflection for double-tees 1 and 2 of 0.4 in. (10 mm) and 0.2 in. (5 mm) respectively. Consequently, recommendations were made to repair the spalled areas, inject the visible cracks at the spalled areas with epoxy and restore the welded connections between the two double-tees that were cut to allow the members to deflect independently during the investigation. The double-tees were returned to service after the recommended repairs were made.

The laboratory tests of the field specimens and load test results from Dilek's investigation are the basis for the comparative analysis and validation of the application of the proposed MLSA to the forensic investigation of damaged structural members presented in this report. The results of the analysis are also compared with results of the

modified classical beam theory approach previously published (Reis, Mata and Dilek 2009).

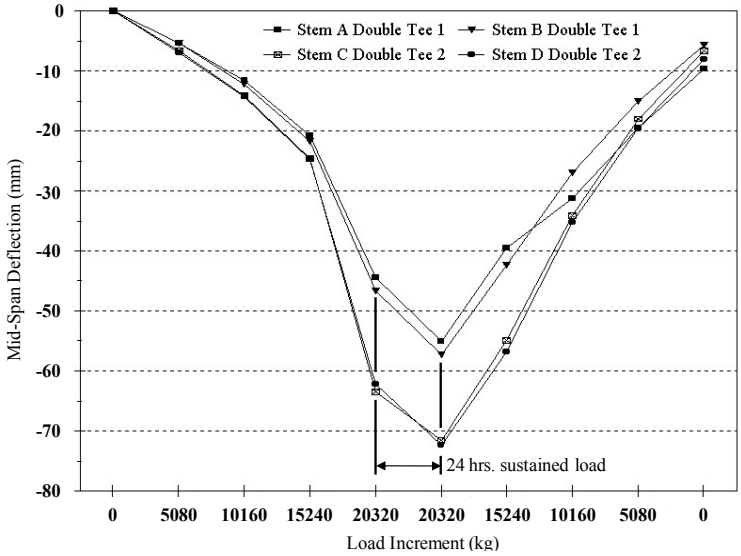

Fig. 1.2: Load Test Deflections and Rebound at Mid-Span (Dilek 2005)

1.2.4 Classical Beam Theory Analytical Model

Reis, Mata and Dilek (2009) developed an analytical model using the principles of classical beam theory to predict the behavior of the damaged members that were the subject of Dilek's (2005) field evaluation. The beam was divided longitudinally into 14 segments for the analysis. The variability of the mechanical properties (E, f_c, f_{ct}) proved too computationally challenging in the development of an accurate closed form analytical model. Consequently, measured mean values were used to define the modulus transversely and vertically through the cross-section, and longitudinally along the length of the member at each of the 14 analyzed sections. Additionally, to allow for the change in flexural rigidity due to damage gradients and cracking in the concrete, an effective

stiffness (EI_{eff}) was estimated using the secant stiffness, which was taken as the slope of the line between the balanced moment (where the angle of curvature, ϕ, is zero) and the applied moment on a moment-curvature (M-ϕ) diagram. The M-ϕ diagram used to determine EI_{eff} was developed using theoretical values for the balanced moment (M_b), cracking moment (M_{cr}) and corresponding curvature (ϕ_{cr}), and any point in the post-cracking range (M_x) and corresponding curvature (ϕ_x). For specific details, the reader is referred to Reis, Mata and Dilek (2009).

Reis, Mata and Dilek (2009) used EI_{eff} to predict the deflections of both damaged double-tees independently. In the initial analysis, the predicted deflections differed from the measured deflections by as much as 15%. A second analysis was conducted with adjusted EI_{eff} to better predict the deflections reported in the load test. The adjustments to EI_{eff} generally ranged between 6% and 15 % of the initial effective stiffness used, which improved the deflection prediction to within 6% of the measured deflection.

2.0 General Problem Statement

Reis, Mata and Dilek (2009) confirmed that classical beam theory, using mean values of material and geometric properties, was computationally inefficient for predicting the load deflection behavior of a fire-damaged member with significantly varying properties, both longitudinally and transversely along the member. Reis, Mata and Dilek (2009) noted that the need for substantial revisions to the model assumptions indicated a need for further research permitting damage gradients along the member as

well as through the section to be incorporated into the analysis. The proposed methodology for a MLSA approach is in part in response to their recommendation for further research in damaged member analysis with varying material and geometric properties.

Studies to establish a predictive behavioral model that allows for quantitative variability in the mechanical properties of material would be useful in several applications. The ability to estimate damage gradients in existing structures using resonant frequency techniques with thin disks sawn from cores (Leming, Nau, and Fukuda, 1998; Reis, Mata, and Dilek 2009) and apply those gradients to an analytical model to predict load–deflection behavior and flexural capacity of deteriorated or damaged structural members would also be useful in either forensic analysis or asset management. An analytical tool that could be used to help assess structural performance of reinforced and prestressed concrete beams would also be of value to the research engineer. For example, a better understanding of the fire resistance and flexural response of structural members produced using concrete mixtures with enhanced sustainability, for which limited information is available from the field, as compared with its conventional counterparts will allow design and construction engineers to develop infrastructure with more durable, longer lasting, service lives.

The layered-sectional analysis technique (Bentz 2000) is an effective analytical tool for design engineers. It provides a computationally efficient method to assess flexural capacity using discrete layers that allow for varied material properties vertically through a

member cross-section. With the use of sufficiently thin layers and appropriate constitutive models, the M-ϕ response can be accurately predicted. Because the proposed MLSA decretizes the member vertically into layers, and then horizontally into cells, the MLSA framework can conveniently incorporate differing material properties both vertically and transversely through the cross-section. The material properties needed to apply the MLSA technique in damaged and undamaged areas of a member can be estimated during the field investigations using non-destructive evaluation techniques and analysis of cores.

3.0 Development of the Modified Layered-Sectional Analysis

The layered-sectional analysis framework allows the user to incorporate constitutive models to accurately describe non-linear material behavior and provides the opportunity for the user to assign varying material properties to horizontal layers discretizing the cross-section. The method can be employed by the use of relatively simple spreadsheets to converge on a solution.

Bentz (2000) notes that the layered-sectional analysis uses the familiar concepts of axial load, moment and shear, and performs that analysis at one location along a member to calculate strength and deformation in terms of moments, shears, and curvatures. The application of strain (ε), stress (f), and force (F) to develop the M-ϕ response is illustrated in Figure 3.1. For a chosen maximum concrete compression strain, $\varepsilon_{c,max}$, the iterative solution adjusts the curvature, ϕ, to define a strain distribution such that:

$$\sum_{i=1}^{m} F_i = N \tag{3.1}$$

and

$$M = \sum_{i=1}^{m} F_i y_i \tag{3.2}$$

where

M = the moment corresponding to the given curvature

F = the axial force in each layer

N = the total applied axial force, typically equal to zero

y = the distance from the center of layer i to the centroid of concrete section

i = layer number

m = total number of layers

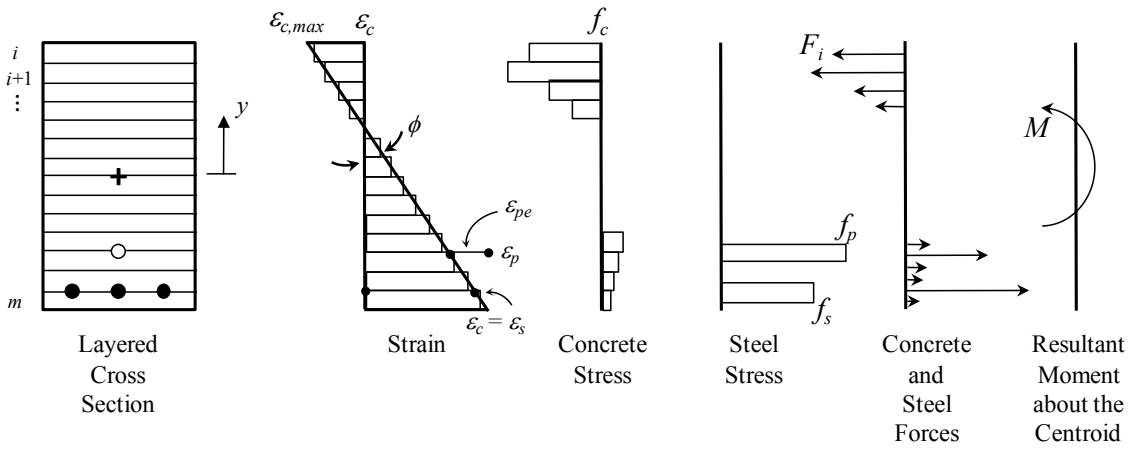

Fig. 3.1: Typical Layered-Sectional Analysis (Adapted from Collins and Mitchell 1997)

The layered-sectional analysis can be seen to lie between two extremes of analytical modeling. At one end of the spectrum are hand calculations, linear approximations, and graphical methods of analysis that tend to be idealized, and sometimes over-simplified, as described by Reis, Mata and Dilek (2009), in their behavioral prediction of a damaged member. At the other end is the finite-element method (FEM). FEM modeling can be expensive to develop and run even with commercial software programs. In addition, the results of FEM models must be assessed for strength capacity, unlike the MLSA described below, which includes a strength assessment in the results. The MLSA also implicitly models tension cracking in the section at the position of maximum moment.

3.1 Modified Layered-Sectional Analysis Model

The modification to the layered-sectional analysis framework described below allows for varying material properties in two directions by providing horizontal and vertical layers, creating discrete cells, each which may be defined with unique material properties. This modification provides an accurate and computationally efficient model for members that have sustained significant damage, but might still remain in service.

The fundamental assumption is that the strain is constant in each cell of a layer, whereas the stress may vary according to the appropriate constitutive model and mechanical properties. The individual cells (i, j) in each layer interact as illustrated in Figure 3.2 according to the selected constitutive models described later in this report. The total force F_i of layer i in Figure 3.2 is the summation of force components from each cell j in layer i, given by

$$F_i = \sum_{j=1}^{n} F_{ij} \tag{3.3}$$

where

F_i = total force in layer i

F_{ij} = resultant force of cell j in layer i

j = cell number (horizontally)

n = number of cells in layer i

and, as before: $M = \sum_{i=1}^{m} F_i y_i$ (3.2)

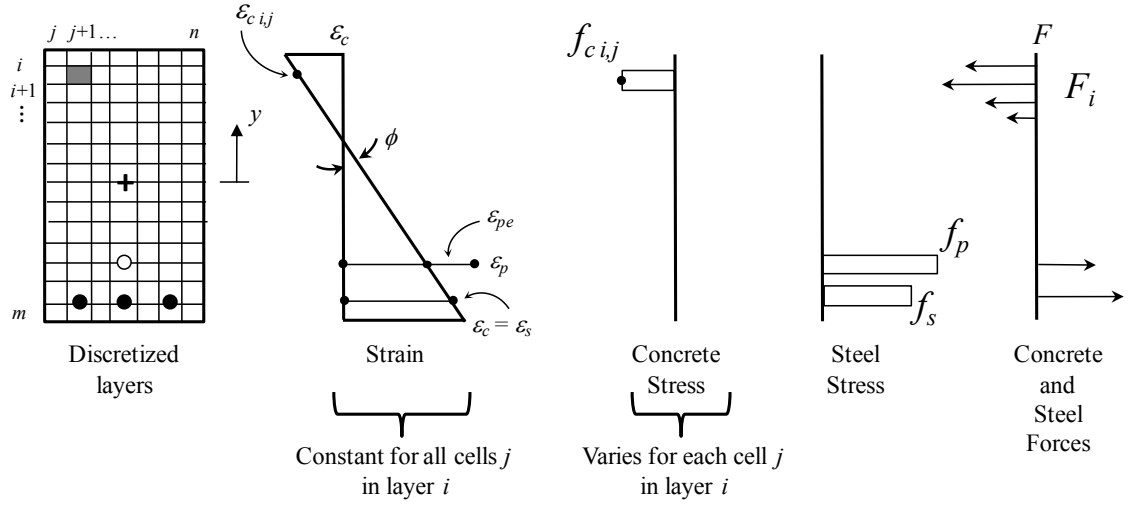

Fig 3.2: Modified Layered-Sectional Analysis

3.2 Constitutive Models for Undamaged Concrete

The constitutive models used in the MLSA framework in this paper are well-known and appropriate for illustrative purposes. Other models are available, and could easily be

incorporated into the framework as appropriate and necessary to enhance the predictive capabilities.

Hognestad's parabola was used to describe the constitutive relationship for concrete in compression given by

$$f_c = f'_c \left\{ 2\left(\frac{\varepsilon_c}{\varepsilon_0}\right) - \left(\frac{\varepsilon_c}{\varepsilon_0}\right)^2 \right\} \tag{3.4}$$

where

f_c = compressive stress

f'_c = ultimate compressive strength

ε_c = concrete strain

ε_o = strain at peak stress, which may be taken as

$$\varepsilon_0 = \frac{2f'_c}{E_t} \tag{3.5}$$

where

E_t = tangent elastic (Young's) modulus, and is effectively equal to the dynamic elastic (Young's) modulus, E_d, often available from simple tests.

Tension stiffening was not considered in this study [it is not typically considered in practice in the Prestressed and Precast Concrete Institute (PCI 2004) design methods] whereas uncracked concrete in tension is assumed to be elastic given by

$$f_c = \begin{cases} E_t \varepsilon_c & \varepsilon_c \le \varepsilon_{cr} \\ 0 & \varepsilon_c > \varepsilon_{cr} \end{cases} \tag{3.6}$$

where

ε_{cr} = concrete cracking strain, which may be taken as

$$\varepsilon_{cr} = \frac{f_{ct}}{E_t} \tag{3.7}$$

where

f_{ct} = concrete splitting tensile strength

The strain in the prestressing steel is related to the concrete strain at the same depth by the effective prestressing strain (as shown in Figures 3.1 and 3.2).

$$\varepsilon_p = \varepsilon_c + \varepsilon_{pe} \tag{3.8}$$

where

ε_p = strain in the prestressing steel

ε_c = strain in the concrete at the level of the prestressing steel

ε_{pe} = effective strain in the prestressing steel

and

$$\varepsilon_{pe} = \frac{f_{pi}}{E_{pe}} \tag{3.9}$$

where

f_{pi} = initial stress in the prestressing steel

E_{pe} = effective Young's modulus of elasticity for the prestressing steel

The stress in the prestressing steel after loading (f_p) is defined using the Ramberg-Osgood function (Collins and Mitchell 1997)

$$f_p = \varepsilon_p E_{pe}\left(0.03 + \frac{0.97}{\left[1+\left(121\varepsilon_p\right)^6\right]^{0.167}}\right) \tag{3.10}$$

where

f_p = stress in the prestressing steel after loading (psi).

Mild steel reinforcement was not included, but can be simply modeled assuming full compatibility with the concrete at the same depth (ie. $\varepsilon_s = \varepsilon_c$ as shown in Figures 3.1 and 3.2) and an elastic-plastic constitutive model given by

$$f_s = \begin{cases} E_s\varepsilon_s & f_s \le f_y \\ 0 & f_s > f_y \end{cases} \tag{3.11}$$

where

E_s = Elastic (Young's) modulus for mild steel

f_y = yield stress mild steel reinforcement

3.3 Constitutive Models for Fire Damaged Concrete:

Research conducted in a concurrent study (McCoy, Leming and Seracino in review) examined the effects of temperature exposure on conventional and lightweight concrete mixtures. The investigation used shear modulus (G) to estimate E_d and crack density ($\in$) (O'Connell and Budiansky 1974; Recalde 2009) to quantify changes in material properties associated with exposure to temperatures of 150 C (300 F) and 300 C (570 F).

McCoy, Leming and Seracino (in review) combined Kasami's findings (1975) and Neville's (1996) comparison of E, f_c and f_{ct} under moderate fire induced deterioration to develop the functional relationships used in this study.

McCoy, Leming and Seracino (in review) used the resonant frequency technique described by Leming, Nau, and Fukuda (1998) to determine G of replicate specimens before and after exposure to 150 C (300 F) and 300 C (570 F). The dynamic Young's modulus is given by the following

$$E_d = 2(1+\nu)\rho\left(\frac{\pi f d}{\Omega_0}\right)^2 \tag{3.12}$$

where

ν = Poisson's Ratio of the concrete specimen

ρ = the mass density of the disk (kg/m^3)

f = the fundamental cyclic natural frequency (Hz)

d = the diameter of the disk (mm)

Ω_0 = the dimensionless frequency parameter associated with the fundamental mode of vibration

After measuring f, d, and ρ, and obtaining Ω_0 iteratively, a reasonable estimate for ν must be made to determine E_d. Recalde (2009) showed that varying ν between 0.15 and 0.30 had a statistically insignificant effect on the calculated value of E_d.

McCoy, Leming and Seracino (in review) found that for mixtures similar to that used in the subject double-tee member, the measured E_d was approximately 15% higher than the measured secant Young's modulus, E_{cs}, which is consistent with Lydon and Balendran (1986). The secant modulus is often used to predict the concrete compressive stress within the elastic range. The correlation between E_d and E_{cs} therefore permits field values of E_d, which are easily obtained from cores, to be conveniently used to model elastic behavior within the MLSA technique. Further, field evaluation to develop an $E_d - E_{cs}$ correlation is possible when more accurate values for specific concrete mixtures are desired for analysis.

3.3.1 Concrete Temperature Gradient

A relationship between concrete temperature and compressive strength was developed for this study based upon findings reported by Neville (1996) and ACI 216.1-07. Figures 3.3 and 3.4 (Neville 1996) provide a general correlation for temperature effects on concrete properties, and Figure 3.5 provides the basis for temperature effects in semi-lightweight concrete after a 1-hour exposure, about the same duration of exposure to fire experienced by the semi-lightweight double-tees examined by Dilek (2005). The published temperature gradients were used to estimate gradients in material properties for use in the MLSA model. These proportions could also be established or confirmed in practice from measurements of disks sawn from cores.

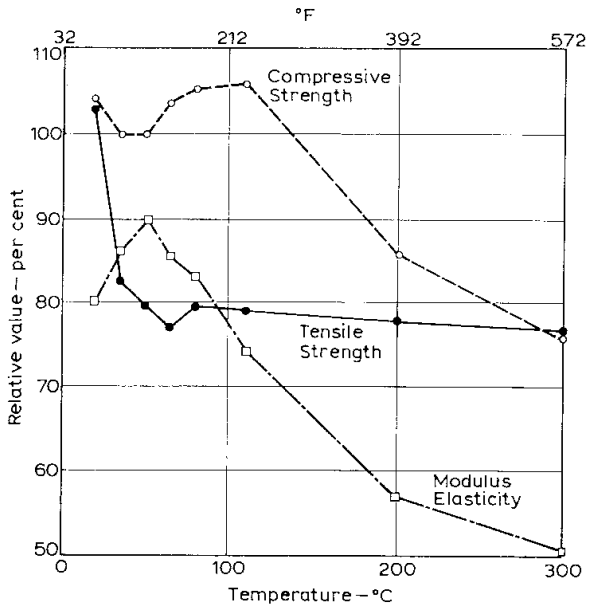

Fig. 3.3: Generalized Loss in Material Properties Due to Temperature Exposure (Neville 1996)

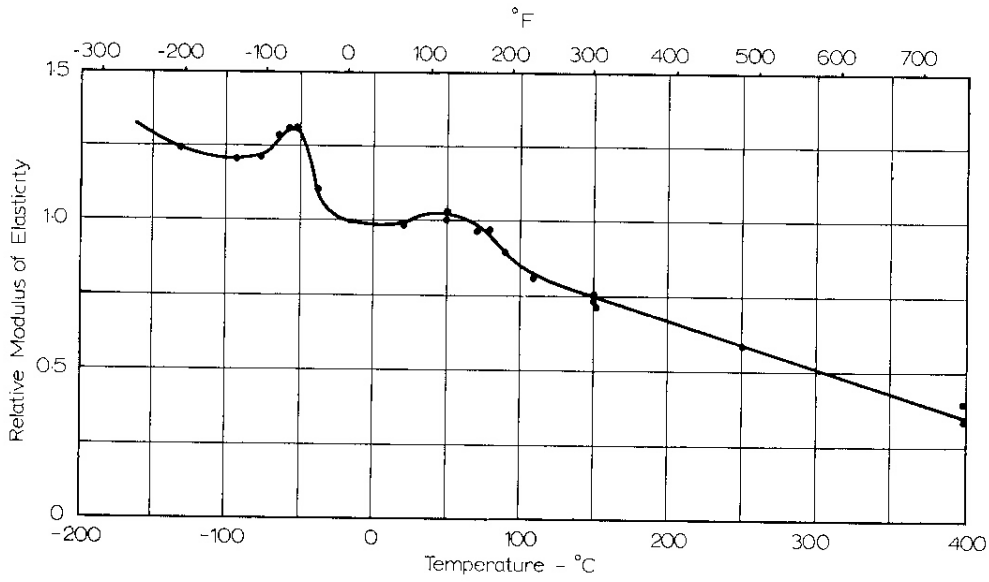

Fig. 3.4: Temperature Effects on Elastic (Young's) Modulus of Concrete (Neville 1996)

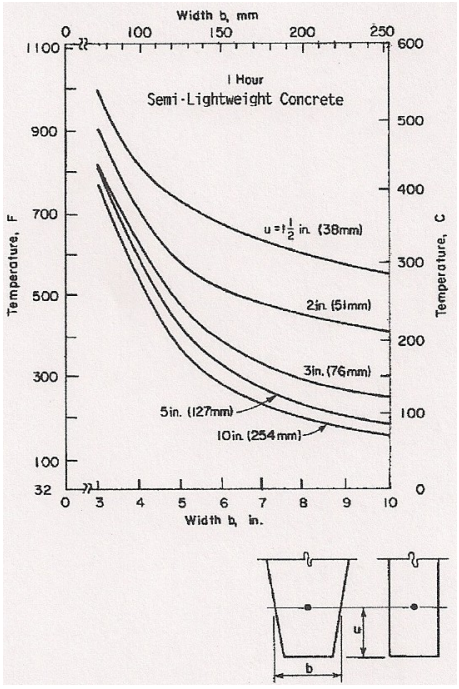

Fig. 3.5: Temperatures in Semi-Lightweight Concrete Rectangular and Tapered Units at 1 Hour of Fire Exposure (ACI 216.1 2007)

The material properties when subject to high temperature exposures, up to about 600 C (1100 F), vary widely depending upon stresses present at time of exposure, moisture content, aggregate type, length of exposure and cooling time. This variation prohibits the use of global generalizations for temperature effects (Neville 1996). Tests indicate that lightweight concrete exhibits a much lower loss in compressive strength than conventional weight concrete, with a residual strength of at least 50% reported in lightweight concrete after exposure to 600 C (1100 F), whereas similar conventional weight concrete had a residual strength of about 40% under identical exposure conditions (Neville 1996).

3.3.2 Double-Tee 1 Temperature Gradient Development

Figures 3.3 and 3.4 from Neville (1996) indicate that a 38% loss in *E* (interior of Stem B, Table 1.1) corresponds to a concrete temperature of approximately 170 C (330 F) and a 59% loss in *E* (surface of Stem B, Table 1.1) corresponds to a concrete temperature of approximately 340 C (640 F). The interior temperature of 170 C (330 F) is also in approximate agreement with Figure 3.5 which indicates that for a semi-lightweight concrete tapered stem, 5 in. (127 mm) wide at the mid-height and 22 in. (560 mm) tall, the interior concrete temperature is approximately 160 C (320 F). The concrete temperature at the surface location on Stem A (Figure 1.1), furthest from the fire, was set at 25 C (80 F) for this analysis, to correspond with no deterioration in material properties on the un-exposed side of Stem A consistent with published findings.

The pulse velocity results (Figure 3.6) from Dilek's (2005) investigation were used to reasonably estimate the temperature exposure along the length of the beam. The pulse velocity measurement of Stem B indicates that significant damage did not occur beyond approximately 10 ft (3.0 m) from the face of the support. The pulse velocity technique reports an average through velocity, and is therefore an indicator of a temperature gradient transversely through the stem of the double-tee in this study. The pulse velocity results were compared to likely surface temperatures as reported by Dilek (2005) to provide a calibration between pulse velocity and surface temperature. The surface temperatures were then used in conjunction with ACI 216.1-07 to estimate a transverse

temperature gradient through the section. The transverse gradient was selected to be consistent with ACI 216.1-07 and data reported by Dilek (2005).

Figures 3.7 and 3.8 were used to establish the relationship between temperature and material deterioration transversely through the cross-section and provide a starting point for deterioration along the length of the member. The developed temperature gradients were used in conjunction with the constitutive models described in Sections 3.3 and 3.4 to predict the material response at each of the 21 evaluated sections (Figure 3.8) along the member length.

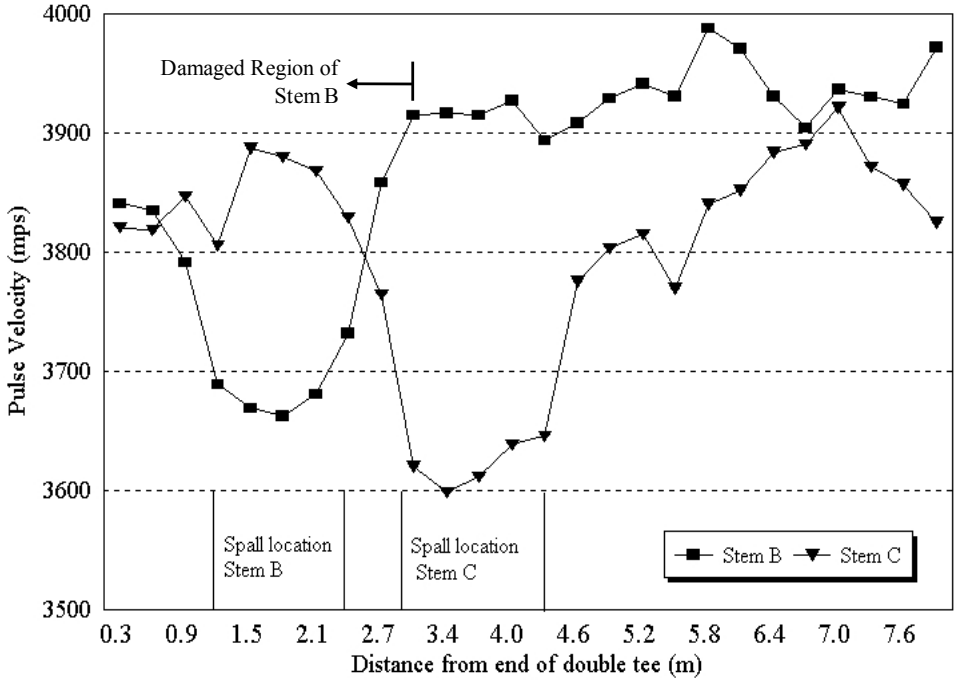

Fig. 3.6: Pulse Velocity Results Along the Length of Stems B and C (Dilek 2005)

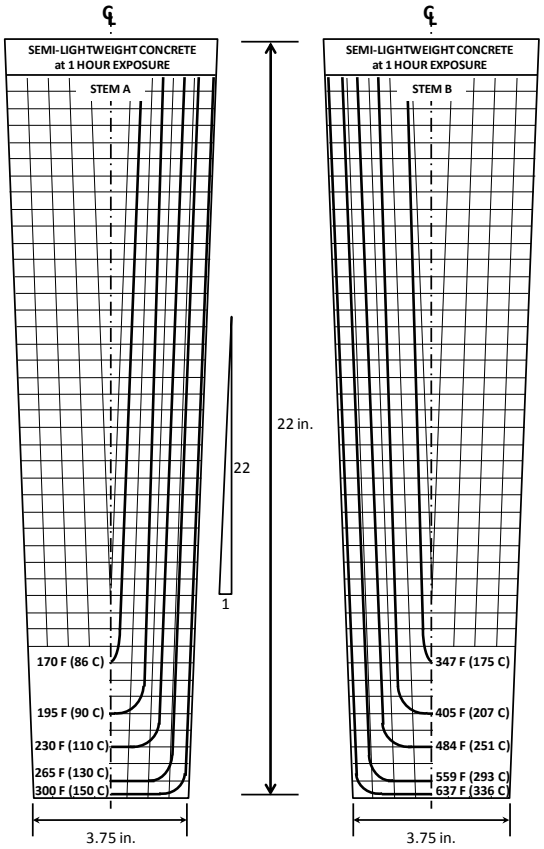

Fig. 3.7: Estimated Cross-Sectional Temperature Gradient for Stems A and B (adapted from ACI 216.1 2007)

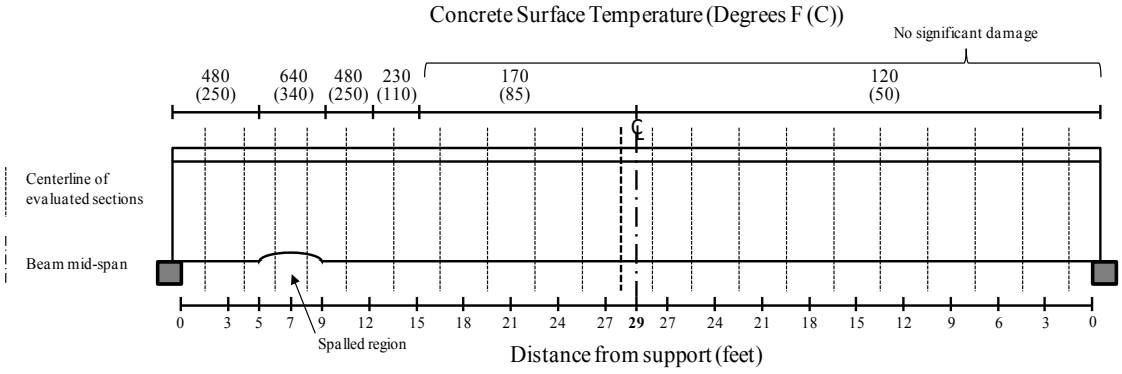

Fig. 3.8: Estimated Longitudinal Temperature Gradient at Evaluated Sections for Stem B

3.3.3 Compressive Strength Loss

Figure 3.3 shows an approximately linear relationship between changes in f_c and exposures between 100 C (210 F) and 300 C (570 F) (Kasami 1975; Neville 1996). Figure 3.4 (Neville 1996) also shows an approximately linear relationship between E and temperature in the region of interest with a loss of approximately 70% at 400 C (750 F) for the mixtures evaluated. These values are consistent with the findings in the concurrent experimental study (McCoy, Leming and Seracino in review). The relationship between f_c, and temperature can be estimated using Figure 3.9 (ACI 216.1-07). The relationship is essentially linear in the temperature region of interest in this study (Figures 3.3 and 3.4). The maximum deterioration for E in Dilek's (2005) investigation occurred in Stem B (Fig. 1.1), directly above the fire, and was found to be a 59% loss (see Table 1.1), indicating a concrete temperature of approximately 340 C (640 F) according to Figure 3.4. This approximate temperature was correlated with ACI 216.1-07 and indicates a similarity in response sufficient for the purposes of demonstrating the use of the MLSA model in this application. Cores and disks cut from cores would typically be available to the engineer of record in practice and would provide E and f_{ct} transversely through the cross-section.

The general linearity between temperature and mechanical properties allows Hognestad's parabolic model modified for damaged gradient parameters to be used to describe the constitutive behavior in the damaged areas of concrete in compression.

Equations 3.4 and 3.5 can be reformulated as in Equations 3.13 and 3.14 to estimate the strength and stiffness of damaged concrete in compression.

$$f_{c,dmg} = f'_{c,dmg}\left\{2\left(\frac{\varepsilon_c}{\varepsilon_0}\right) - \left(\frac{\varepsilon_c}{\varepsilon_0}\right)^2\right\} \tag{3.13}$$

where

$f_{c,dmg}$ = damaged concrete stress

$f'_{c,dmg}$ = damaged ultimate compressive strength (from Fig. 3.5)

ε_o = strain at peak stress $f'_{c,dmg}$, which may be taken as

$$\varepsilon_0 = \frac{2f'_{c,dmg}}{E_{d,dmg}} \tag{3.14}$$

where

$E_{d,dmg}$ = damaged dynamic elastic (Young's) modulus, and is equal to E_t as described previously.

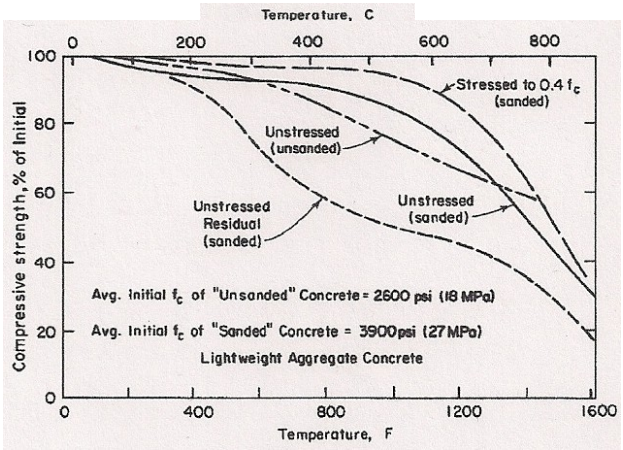

Fig. 3.9: Compressive Strength of Semi-Lightweight Concrete After Exposure to High Temperatures and Cooling (ACI 216.1 2007)

3.3.4 Concrete Tensile Strength Loss

Neville (1996) reports that losses in f_{ct} due to high temperature exposure are minimal between 100 C (212 F) and 300 C (510 F), with a maximum loss of approximately 25% at 300 C (510 F) (Fig. 3.3). This is consistent with the losses in f_{ct} that Dilek (2005) reported, with a maximum loss of 30% (Table 1.1) occurring directly above the fire in Stem B (Fig. 1.1). The corresponding loss in E_d was 59% (see Table 1.1) at this location.

For the purposes of this study, the total loss in f_{ct} is assumed to be 30% at the location in Stem B (Fig 1.1) above the fire, and 24% at the location in Stem C (Fig. 1.1) above the fire as reported by Dilek (Table 1.1). At all other damaged locations in the member, the loss in f_{ct} is conservatively assumed to be 20%, corresponding with Neville's findings (1996) for areas where the E_d deterioration is less than 25%. Equation 3.6 can therefore be re-written to model damaged concrete in tension as:

$$f_{c,dmg} = \begin{cases} E_{d,dmg}\varepsilon_c & \varepsilon_c \le \varepsilon_{cr,dmg} \\ 0 & \varepsilon_c > \varepsilon_{cr,dmg} \end{cases} \tag{3.15}$$

where

$f_{c,dmg}$ = damaged concrete stress

$E_{d,dmg}$ = damaged dynamic (Young's) modulus, and is equal to E_t as previously described

$\varepsilon_{cr,dmg}$ = damaged concrete cracking strain defined by

$$\varepsilon_{cr,dmg} = \frac{f_{ct,dmg}}{E_{d,dmg}} \tag{3.16}$$

where

$f_{ct,dmg}$ = damaged splitting tensile strength

3.3.5 Prestress Loss

Dilek's field investigation (2005) and the subsequent analytical study (Reis, Mata, and Dilek 2009) found no significant loss in the prestressing effects due to the fire exposure of the double-tee members after the members had cooled. For the purposes of this study, f_{pi} was taken as 160 ksi (1100 MPa) to correspond with the assumed value used by Reis, Mata, and Dilek (2009).

3.4 Application of MLSA to Example Case Study

The layer thickness used in the MLSA was 0.5 in. (13 mm) for this study. Each layer was also discretized in 0.5 in. (13 mm) transverse elements resulting in 2,564 0.25 in^2 (170 mm^2) cells for each cross-section evaluated. This thickness was found to be sufficiently thin to model the material property variation vertically and transversely through the cross-section because the disks cut from cores were 1.0 in. (25 mm) thick, and the temperature contours in ACI 216.1-07 are spaced at 0.5 in. (13 mm). This level of discretization also allows for a simplified geometrical representation of the tapered stem cross-section as illustrated in Figure 3.10, rather than tapered-stems, making the concrete area calculations uniform for all cells. Spalling was modeled by assigning an E value of zero to the discretized cells at the spalled location.

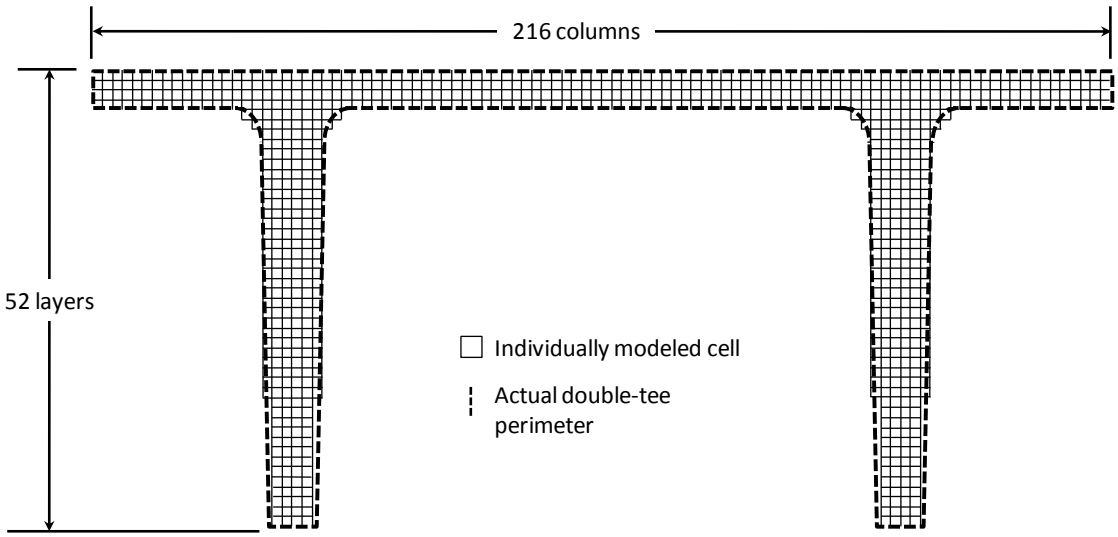

Fig. 3.10: Discretized Layers Superimposed on Double-Tee Cross-Section (not to scale)

3.5 Load Deflection

A standard beam analysis software was used to calculate the mid-span deflection. As discussed above, the MLSA technique generates the M-ϕ response at evaluated sections along the loaded member by incrementing $\varepsilon_{c,\max}$ (Figures 3.1 and 3.2). The MLSA calculated M-ϕ responses were used to determine an equivalent EI representative of the segment in question using a secant stiffness approach.

The MLSA technique was conducted at 21 points along the beam, creating 23 segments. The MLSA produced a M-ϕ relationship for each of the 23 segments, from which EI was calculated for the given moments and curvatures. The moment and EI for each segment were then entered into the beam analysis software to calculate deflection.

Figure 3.11 is a representation of the family of 21 M-ϕ responses and shows the response at the mid-span of the beam in comparison to the calculated flexural capacity, using ACI 318-99 and PCI (1992), as well as the responses at 6 ft (1.8 m) from the support for damaged (with spalling) and undamaged sections. There was a negligible difference in response between undamaged and damaged sections at x = 6 ft. as can be seen in Figure 3.11b, and therefore the damaged effect on deflection is expected to be insignificant. The mid-span deflection of the MLSA modeled beam compared with the actual mid-span deflection from the load test and to the calculations reported by Reis, Mata, and Dilek (2009) are reported in Figure 4.1.

The ultimate moment capacities (M_u) shown in Figure 3.11a were calculated using both PCI Table 4.10.3 (1992), and ACI 318-99. The MLSA calculated M_u is within 9% of the ACI prediction and 3% of the PCI prediction.

First cracking was not observed during the load test until after the application of the full load. During the load test, Dilek (2005) found that only "hairline" cracking occurred at the mid-span region of the member under full load, and did not correspond with any significant change in the deflection of the loaded member. This is confirmed in the model because the moment developed by the application of the full load was found to occur just beyond the cracking moment within the mid-span region of the member.

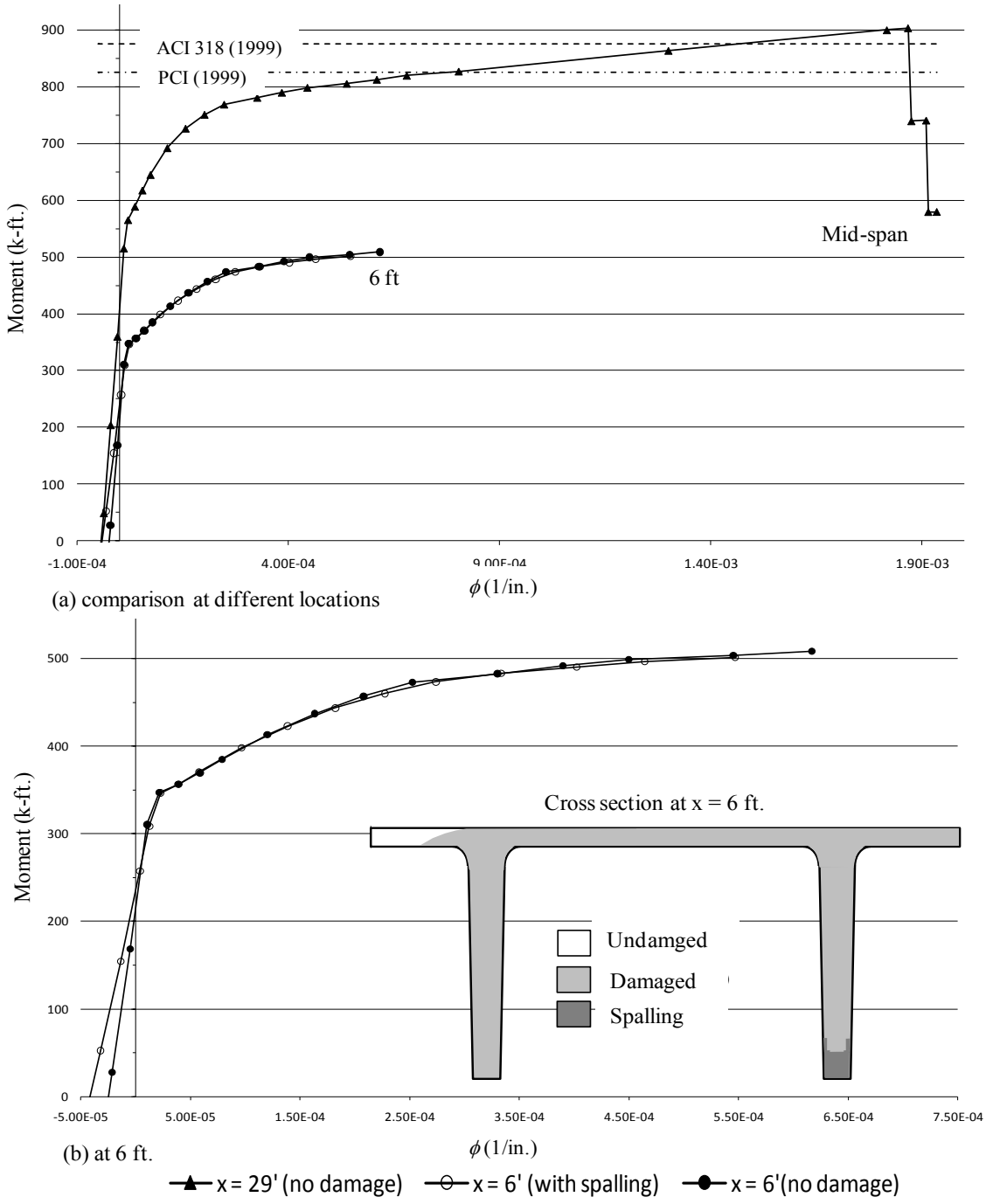

Fig. 3.11: Representative *M-ϕ* Responses for Double-Tee 1 from MLSA

4.0 Results and Discussion

4.1 Comparison of Results with Case Study

Figure 4.1 shows the results for the mid-span deflection at each applied load increment as a percentage of the load test deflection at full load. The comparative results include the deflections from the load test (Dilek 2005), those reported by Reis, Mata, and Dilek (2009), and the deflection calculated using the MLSA coupled with the beam analysis software. The full-load mid span deflection using Reis, Mata and Dilek's (2009) modified EI_{eff} is within 6% of the load test, and the MLSA full-load mid-span deflection is within 1% of the load test deflection.

Additional analyses were conducted using the MLSA framework to determine the undamaged deflection of the beam and the deflection of the beam if the same damage occurred at the mid-span. The results for these analyses are shown in Figure 4.1, which shows that the case study damage condition resulted in only a 1% deflection increase as compared with the undamaged deflection. This is largely because the damage occurred close to the support where the applied moment at full load is still well below M_{cr} of the damaged section (Figure 3.11b.). The dashed line in Figure 4.1 indicates that had the damage occurred at the mid-span, the predicted damaged deflection would be 12% higher than the undamaged section.

When M_{cr} is exceeded the differences between damaged and undamaged are reduced considerably. This can be seen by comparing the M-ϕ response of damaged and

undamaged sections in Figure 3.11b where the spalled section clearly has a reduced stiffness, however, the post-cracking responses show a negligible difference between damaged and undamaged responses. This is in part because the post-cracking capacity of the section is controlled primarily by the eccentricity and stress in the prestressing steel, and therefore the reduced stiffness due to damage is negligible with respect to the cracking due to load. Additionally, because the damage was close to a support where the applied moment was significantly less than the section capacity, the damage had little effect on the flexural behavior and deflection.

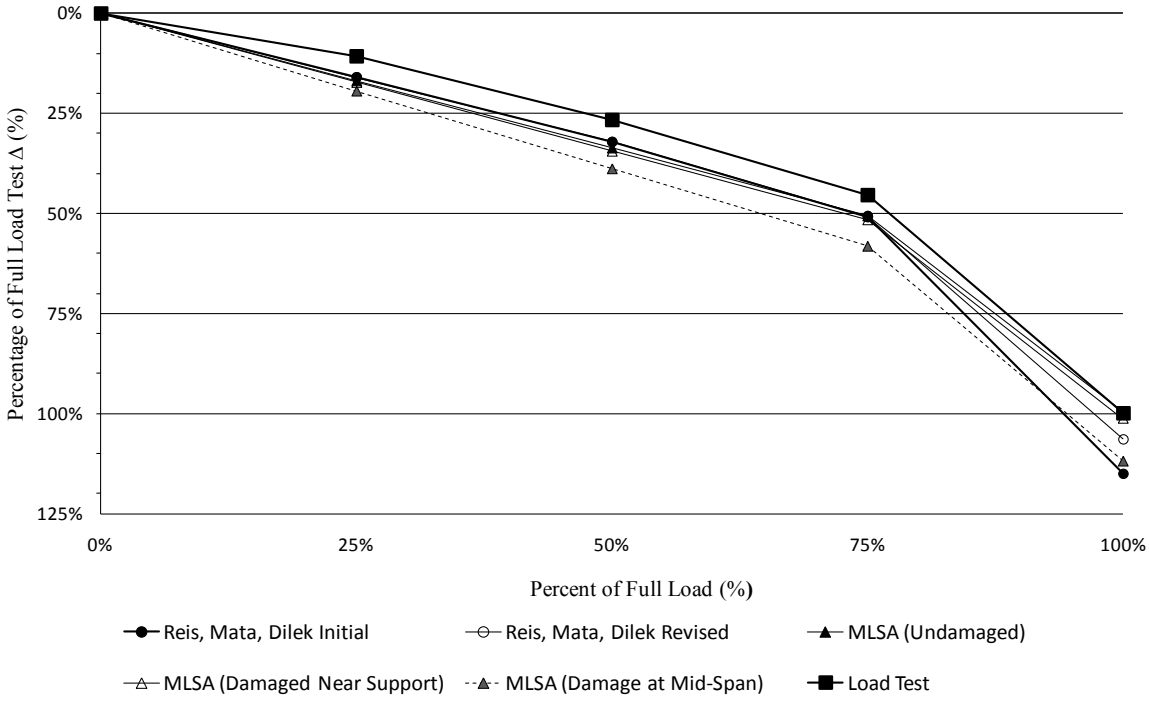

Fig. 4.1: Mid-Span Deflection Percentage Comparisons with Load Test Results

The deviation between the MLSA estimate and the ACI load test are largely due to the lack of data for tendon eccentricity and concrete unit weight. The prestressing tendon eccentricities and estimated unit weight of the concrete were not reported by Dilek (2005). Estimations were made for the eccentricities using the observed cracking between the third and forth load increments, and the reported tendon stress of 160 ksi (Dilek 2005). The actual tendon eccentricity data would likely be available to the investigating engineer, allowing for more accurate deflection calculations in the lower load increments. The unit weight of the concrete was estimated to be 115 pcf (1840 kg/m^3), a typical upper bound for commercial lightweight concrete. Unit weight could also be determined by the investigating engineer using cores.

4.2 Parametric Study Using Sustainable Concrete

A parametric study of two enhanced sustainability concrete (ESC) mixtures was also conducted using the MLSA framework to determine the performance of the mixtures under the more severe mid-span damaged condition. All geometric properties were kept identical to those of the subject double-tee, and only the material properties for the two ESC mixtures were adjusted for the comparison. The material property data was obtained from a concurrent study (McCoy, Leming and Seracino in review) that investigated the performance of ESC mixtures exposed to elevated temperatures up to 300 C (570 F). Figure 4.2 shows the deflection comparison of a 20% fly ash lightweight aggregate (LF2) mixture (conventional mixture) and a 60% fly ash lightweight aggregate

(LF6) mixture (ESC mixture) with deflection results for damage at mid-span and undamaged conditions.

The deflection comparisons for the parametric study of mixtures LF2 and LF6 with respect to the case study double-tee with damage relocated to the mid-span in Figure 4.2 shows that the LF2, case study, and LF6 mixtures experienced an approximate 10%, 12%, and 15% respective increase in deflection due to damage. The compressive strength of the case study mixture was 5700 psi (39.3 MPa) (Dilek 2005) and the compressive strength for mixtures LF2 and LF6 were 6900 psi (47.6 MPa) and 3800 psi (26.2 MPa) respectively. McCoy, Leming and Seracino (in review) found that the LF6 mixture experienced reduced changes in microstructure and elastic properties due to elevated temperature exposure to 300 C (570 F). The large difference in compressive strength between LF2 and LF6 and relatively small difference in percent change in deflection indicates that the MLSA results are consistent with the concurrent study (McCoy, Leming and Seracino in review), however, additional research is recommended to investigate ESC mixtures and conventional mixtures of similar compressive strengths to quantify ESC deflection behavior in extreme exposure events.

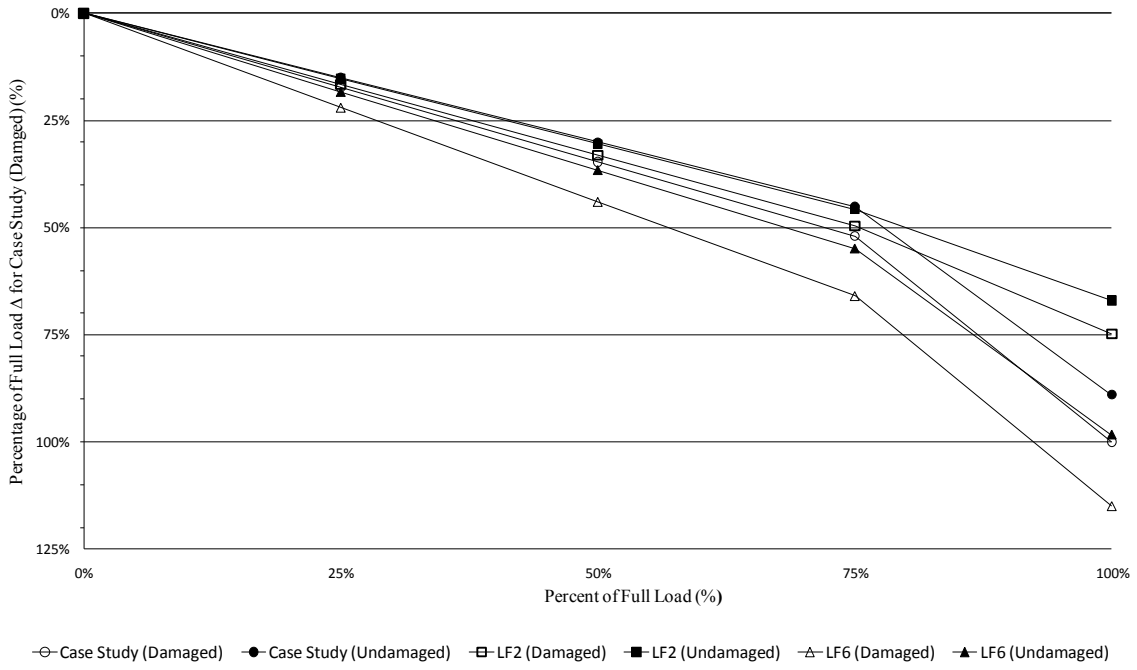

Fig. 4.2: Mid-Span Deflection Percentage Comparisons with Damage at Mid-Span

4.3 Discussion

The calculated deflections provided by Reis, Mata and Dilek (2009) require an accurate estimate of the member flexural rigidity (*EI*), which is difficult to determine in existing damaged members. After the initial calculations produced a mid-span deflection 15% greater than the load test, Reis, Mata and Dilek (2009) re-calculated a value of EI_{eff} to match predicted and measured load test responses. This technique would not be useful if the load test deflections were not available.

The MLSA technique does not require the investigating engineer to estimate EI_{eff} for the damaged member. Rather, the technique uses field data estimates of E_d and member geometry, including spalled sections, to calculate a family of M-ϕ responses, which can

then be used to determine either flexural capacity at a particular section, or member deflection under a given load condition, when coupled with a basic beam analysis program.

The data needed to conduct the analysis using the MLSA method is easily gathered using techniques that are standard practice for forensic investigations. The current tools available for the investigating engineer are visual observation, pulse velocity (ASTM C597-01), and drilled core samples (ASTM C42-01). The core samples provide splitting tensile strength (ASTM C496-04) and compressive strength (ASTM C39-10). Dynamic elastic (Young's) modulus can be estimated directly from disks sawn from cores samples (Leming, Nau and Fukuda 1998), and therefore can be measured at 1.0 in. (25 mm) increments through the cross-section, enabling the investigating engineer to estimate damage gradients for the subject member at various locations. The data gathered during the investigation provides sufficient input to allow the engineer to efficiently conduct a strength and deflection analysis using the MLSA framework, and thereby better determine if a load test is needed.

Based upon the analysis of the subject member in this paper using the MLSA framework, it is likely that the engineer of record could have made a recommendation for the member to remain in service with the recommended repairs (Dilek 2005) without ordering a load test to determine serviceability and deflection limits. The minimal deflection increase due to damage at full-load and a comparison of the M-ϕ to the applied

moment in the damaged region indicates that the serviceability of the member is satisfactory.

The MLSA framework may provide asset managers with analytical and forensic tools for evaluation of existing structures that are not only damaged due to potentially catastrophic events, but also structures that are worn beyond the limits of their design service life and need evaluation to determine if retrofitting or replacement is needed. The expense of load testing might be spared in cases where it is clear that the member can remain in service or must be replaced. The parametric study demonstrates that combined with an increased understanding of the structural response of ESC mixtures, the MLSA framework could enable advancement in applications of sustainable construction, infrastructure management, and development of design codes and specifications.

5.0 Conclusions and Recommendations

5.1 Conclusions

1. The MLSA provides a computationally efficient technique for the investigating engineer to determine the load-deflection response of damaged concrete members with varying material properties. The data needed for the investigating engineer to accurately model the damaged member is easily gathered using standard practices conducted during the field investigation phase of a forensic study.
2. The MLSA framework allows the engineer to incorporate a variety of constitutive models as appropriate for the materials present in the subject member.

3. A cost effective alternative to load testing is not currently available. The MLSA framework provides a tool for the engineer to help determine if a load test is needed. Additionally, the MLSA framework could also be used to assess the effectiveness of recommended repairs.

4. Although the MLSA is useful in determining a load-deflection response, it is more efficiently used to determine the strength capacity of a damaged member. For example, in the case study, the most damage was observed in the spalled area of the member. A strength analysis could be conducted for the spalled region of the member using the MLSA technique to determine the strength capacity of the member at that location. A comparison of the strength capacity with the applied moment could easily indicate if the damaged area has the capability to satisfy the strength limit state.

5.2 Recommendations

Future research is needed to determine the effects of various environmental exposures on additional ESC mixtures. The modified layered sectional-analysis technique, combined with damage gradients for ESC, would be a useful, inexpensive method for determining the serviceability of ESC structures subjected to damaging mechanisms.

6.0 Acknowledgements

The authors would like to thank Dr. Ufuk Dilek and MACTEC Engineering and Consulting Inc. for supplying the relevant data and figures for the background investigation of the subject member.

LIST OF REFERENCES

Part I

ACI Committee 201, “201.2R-08: Guide to Durable Concrete,” American Concrete Institute, Farmington Hills, 2008, 53 pp.

ACI Committee 216, “216.1-7: Code Requirements for Determining Fire Resistance of Concrete and Masonry Construction Assemblies,” American Concrete Institute, Farmington Hills, MI, 2007, 28 pp.

ACI Committee 318, "318-08: Building Code Requirements for Structural Concrete and Commentary," American Concrete Institute, Farmington Hills, MI, 2008, 465 pp.

ASCE, 2009, "2009 Report Card for America's Infrastructure," American Society of Civil Engineers, Reston, VA, www.infrastructurereportcard.org, 153 pp.

ASTM C469-02, “Standard Test Method for Static Modulus of Elasticity and Poisson’s Ratio of Concrete in Compression.” ASTM International, West Consohocken, PA, 2002, 5 pp.

ASTM C496-04, “Standard Test Method for Splitting Tensile Strength of Cylindrical Concrete Specimens.” ASTM International, West Consohocken, PA, 2004, 5 pp.

ASTM C1064-08, “Standard Test Method for Temperature of Freshly Mixed Hydraulic-Cement Concrete.” ASTM International, West Consohocken, PA, 2008, 3 pp.

ASTM C143-08, “Standard Test Method for Slump of Hydraulic-Cement Concrete.” ASTM International, West Consohocken, PA, 2008, 4 pp.

ASTM C31-09, “Standard Practice for Making and Curing Concrete Test Specimens in the Field.” ASTM International, West Consohocken, PA, 2009, 7 pp.

ASTM C138-09, “Standard Test Method for Density (Unit Weight), Yield, and Air Content (Gravimetric) of Concrete.” ASTM International, West Consohocken, PA, 2009, 4 pp.

ASTM C173-09, “Standard Test Method for Air Content of Freshly Mixed Concrete by the Volumetric Method.” ASTM International, West Consohocken, PA, 2009, 8 pp.

ASTM C231-09, “Standard Test Method for Air Content of Freshly Mixed Concrete by the Pressure Method.” ASTM International, West Consohocken, PA, 2009, 9 pp.

ASTM C39-10, “Standard Test Method for Compressive Strength of Cylindrical Concrete Specimens.” ASTM International, West Consohocken, PA, 2010, 7 pp.

Athena Sustainable Materials Institute, 1998, *Life Cycle Analysis of Brick and Mortar Products*. Merrickville, Ontario: The Athena Sustainable Materials Institute, September, http://www.epa.gov/climatechange/wycd/waste/downloads/clay-bricks-chapter10-28-10.pdf [accessed 02/04/11].

Athena Sustainable Materials Institute, 2001, *A Life Cycle Inventory for Road and Roofing Asphalt.* Prepared by: Franklin Associates Ottawa, Canada. March 2001, http://www.epa.gov/climatechange/wycd/waste/downloads/asphalt-concrete-chapter10-28-10.pdf [accessed 02/04/11].

Carrasquillo, R. L., Slate, F. O., and Nilson, A. H., 1981, "Microcracking and Behavior of High Strength Concrete Subject to Short-Term Loading." *ACI Journal,* ACI, Vol. 78, No. 3, pp. 179-186.

Dilek, U., 2005, “Evaluation of Fire Damage to a Precast Concrete Structure Nondestructive, Laboratory, and Load Testing.” *Journal of Performance of Constructed Facilities*, Vol . 19, No. 1, ASCE, pp. 42-48.

Dilek, U., and Leming, M. L., 2007, "Comparison of Pulse Velocity and Impact-Echo Findings to Properties of Thin Disks from a Fire Damaged Slab," *Journal of Performance of Constructed Facilities*, Vol. 21, No. 1, January/February, ASCE, pp. 13-21.

DilekU. and Leming M. L., 2008, "Elastic Dynamic Young's Modulus and Permeability of Concrete in Fire Damaged Structural Members," *Journal of Materials in Civil Engineering*, Vol. 20, No. 2, February, ASCE, pp. 102-110.

Dilek, U., Leming, M.L., and Sharpe, E.F., 2003, "Assessment of Cryogenic Fluid Spill Damage to Concrete," Forensic Engineering: Proceedings of the Third Congress, eds. P.A. Bosela et al., ASCE, pp 269-279.

Dilek, U., Leming, M. L., and Guth, D., 2004, "Relationship Between Elastic Modulus and Permeability of Damaged Concrete." *Journal of the Transportation Research Board,* Concrete TRB, National Research Council, pp. 53-60.

Hanle, L., Jayaraman, K. R., and Smith, J. S., 2004, "CO_2 Emissions Profile of the U. S. Cement Industry." Environmental Protection Agency, Washington D. C., 14 pp.

Holm, T. A., 1995, "Lightweight Concrete Aggregates." *Significance of Tests and Properties of Concrete and Concrete-Making Material (STP 169C)*. ASTM, West Consohocken, PA., pp. 522-532.

Holm, T. A., Ooi, O. S., and Bremner, T. W., 2003, "Moisture Dynamics in Lightweight Aggregate and Concrete," *Theodore Bremner Symposium on High-Performance Lightweight Concrete: Proceedings for the Sixth CANMET/ACI International Conference on Durability of Concrete, Thessaloniki, Greece, June 2003*, ed. J. P. Ries and T. A. Holm, American Concrete Institute, pp. 167-184.

Hutchinson, J. R., 1979, "Axisymmetric Flexural Vibrations of a Thick Free Circular Plate." *Journal of Applied Mechanics*, Vol. 46, March, pp. 139-144.

Leming, M. L., Nau, J. M., and Fukuda, J., 1998, "Nondestructive Determination of the Dynamic Modulus of Concrete Disks." *ACI Materials Journal*, Vol. 95, January-February, pp. 50-57.

Lepech, M. D., Li, V. C., Robertson, R. E., and Keoleian, G. A., 2008, "Design of Green Engineered Cementitious Composities for Improved Sustainability." *ACI Materials Journal*, November-December, pp. 567-575.

McCoy, B. C., Seracino, R., and Leming, M. L., in review, "Modified Layered-Sectional Analysis for Forensic Investigation." submitted to *ACI Structures Journal.*

Mehta, P.K., 2002, "Greening of the Concrete Industry for Sustainable Development." *Concrete International*, July, pp. 23-28.

Mehta, P. K., and Monteiro, P. J., 2006, *Concrete: Microstructure, Properties, and Materials.* 3rd ed., The MacGraw Hill Companies., 659 pp.

Malhotra, V. M., 2002, "High-Performance High-Volume Fly Ash Concrete." *Concrete* International, July, pp. 30-34.

NIST, 2010, "*NIST/SEMATECH e-Handbook of Statistical Methods*, http://www.itl.nist.gov/div898/handbook/, National Institute of Standards and Technology, Gaithersburg, MD.

O'Connell, R. J., and Budiansky, B., 1974, "Seismic Velocities in Dray and Saturated Cracked Solids." *Journal of Geophysical Research*, Vol. 79, No. 35, pp. 5412-5426.

Phan, L. T., and Carino, N. J., 2002, "Effects of Test Conditions and Mixture Proportions on Behavior of High-Strength Concrete Exposed to High Temperatures." *ACI Materials Journal,* Vol. 99, No.1, pp. 54-66.

Recalde, J. J., 2009, "Estimating Crack Growth in Temperature Damaged Concrete," dissertation, presented to North Carolina State University at Raleigh, NC, in partial fulfillment of the requirements for the degree of Doctor of Philosophy, 211 pp.

Recalde, J. J., and Leming, M. L., 2009, "Changes in Fluid Penetrability and Mechanical Properties of Concrete Due to High Temperature Exposure." *Journal of ASTM International,* Vol. 6, No. 6, 13 pp.

SAS Institute Incorporated, 2010, JMP ® 9.0.0, Copyright © 2010, All Rights Reserved, Statistical Analysis Software.

Schonlin, K., and Hilsdorf, H. K., 1988, "Permeability as a Measure of Potential Durability of Concretes- Development of a Suitable Test Apparatus." American Concrete Institute, Detroit, MI, pp. 99-115.

U. S. Census Bureau, 2008, "2008 Value of Construction Put in Place – Seasonally Adjusted Annual Rate." *U.S. Census Bureau: Manufacturing, Mining and Construction Statistics*, http://www.census.gov/const/C30/totsa2008.pdf [accessed 04/12/10].

U. S. Green Building Council, 2008, "LEED 2009 for New Construction and Major Renovations Rating System." *U.S. Green Building Council,* http://www.usgbc.org/ShowFile.aspx?DocumentID=5546 [accessed 04/12/10].

U. S. Census Bureau, 2009, "2009 Value of Construction Put in Place – Seasonally Adjusted Annual Rate." *U.S. Census Bureau: Manufacturing, Mining and Construction Statistics*, http://www.census.gov/const/C30/totsahist.pdf [accessed 04/12/10].

U. S. Census Bureau, 2010, "2010 Value of Construction Put in Place – Seasonally Adjusted Annual Rate." *U.S. Census Bureau: Manufacturing, Mining, and Construction Statistics,* http://www.census.gov/const/C30/totsahist.pdf [accessed 02/09/11].

Vaysburd, A. M., 1992, “Durability of Lightweight Concrete and Its Connections with the Composition of Concrete, Design and Construction Methods,” *Structural Lightweight Aggregate Concrete Performance* (*SP-136*), ed. T. A. Holm and A. M. Vaysburd, American Concrete Institute, pp. 295-317.

Zia, P., Ahmad, S. H., Leming, M. L., Schemmel, J. J., and Elliot, R. P., 1993, "Mechanical Behavior of High-Performance Concretes, Volume 5, Very High Strength Concrete." *Rep. No. SHRP-C-365,* Strategic Highway Research Program, National Research Council, Washington, D. C.

Part II

ACI Committee 216, “216.1-7: Code Requirements for Determining Fire Resistance of Concrete and Masonry Construction Assemblies,” American Concrete Institute, Farmington Hills, MI, 2007, 28 pp.

ACI Committee 318, "318-99: Building Code Requirements for Structural Concrete and Commentary," American Concrete Institute, Farmington Hills, MI, 1999, 391 pp.

ACI Committee 318, "318-08: Building Code Requirements for Structural Concrete and Commentary," American Concrete Institute, Farmington Hills, MI, 2008, 465 pp.

ASCE 7-95, *Minimum Design Loads for Buildings and Other Structures*, Reston, VA, 1995, 214 pp.

ASTM C39-01, “Standard Test Method for Compressive Strength of Cylindrical Concrete Specimens.” ASTM International, West Consohocken, PA, 2001, 7 pp.

ASTM C42-01, “Standard Test Method for Obtaining and Testing Drilled Cores and Sawed Beams of Concrete.” ASTM International, West Consohocken, PA, 2001, 6 pp.

ASTM C496-01, “Standard Test Method for Splitting Tensile Strength of Cylindrical Concrete Specimens.” ASTM International, West Consohocken, PA, 2001, 5 pp.

ASTM C597-01, “Standard Test Method for Pulse Velocity Through Concrete.” ASTM International, West Consohocken, PA, 2001, 4 pp.

Bentz, E. C., 2000, *Sectional Analysis of Reinforce Concrete Members*, Doctoral thesis, University of Toronto, 187 pp.

Collins, M. P., Mitchell, D., 1997, *Prestressed Concrete Structures,* Response Publications, Toronto, 766 pp.

Dilek, U., 2005, “Evaluation of Fire Damage to a Precast Concrete Structure Nondestructive, Laboratory, and Load Testing.” *Journal of Performance of Constructed Facilities*, Vol . 19, No. 1, pp. 42-48.

Hutchinson, J. R., 1979, “Axisymmetric Flexural Vibrations of a Thick Free Circular Plate.” *Journal of Applied Mechanics*, Vol. 46, March, pp. 139-144.

Kasmi, H., 1975, "Effects of Elevated Temperature Exposure on the Properties of Concrete." *Takenaka Technical Research Report*, No. 13, April, pp. 24-32.

Leming, M. L., Nau, J. M., and Fukuda, J., 1998, "Nondestructive Determination of the Dynamic Modulus of Concrete Disks." *ACI Materials Journal*, Vol. 95, January-February, pp. 50-57.

Lydon, F. D., and Balendran, R. V., 1986, "Some Observations on Elastic Properties of Plain Concrete." *Cement and Concrete Research*, Vol. 16, No. 3, pp. 314-24.

McCoy, B. C., Leming, M. L., and Seracino, R., in review, "Crack Density and Elastic Properties of Sustainable Concretes." submitted to *ACI Materials Journal.*

Neville, A. M., 1996, *Properties of Concrete*, Fourth Edition, John Wiley and Sons, Inc., Essex, England, 884 pp.

PCI, 1992, *PCI Design Handbook: Fourth Edition*, Precast/Prestressed Concrete Institute, Chicago, IL.

Recalde, J. J., 2009, *Estimating Crack Growth in Temperature Damaged Concrete*, Doctoral thesis, North Carolina State Universtiy, 211 pp.

Reis, E. M., and Mata, L. A., and Dilek, U., 2009, "An Analytical Model for Estimating Load-Test Deflections in Fire-Damaged Precast, Prestressed Concrete Members." *PCI Journal*, Summer, pp. 2-15.

APPENDICES

APPENDIX A:

Test Schedule and Detailed Test Data

Appendix A contains the data and charts for E_d, G, and $\in$. Table A.1 is the overall experimental test matrix, and Figure A.1 shows the rate of heat gain for exposures to 150 C and 300 C. All specimens were exposed in the same oven for a given exposure condition. Figure A.1 shows the consistency of heat gain through 250 C. When the 300 C exposure group reached a temperature of 290 C, the 60 minute time began for that exposure condition because the rate of heat gain had slowed considerably.

Table A.1 Experimental Test Matrix

Cylinder ID per mixture	Tests								
	7 day f_c	28 day f_c	56 day		Temperature Rise	Exposure			Ut wt
			f_c	E_c		*No*	*300 C*	*150 C + 300 C*	
A	X								
B	X								
C		X							
D		X							
E		X							
F			X						
G			X						
H			X						
I						X			
K							X		
L								X	
M				X					
W	Extra cylinder for future tests if needed								X
Z					X				

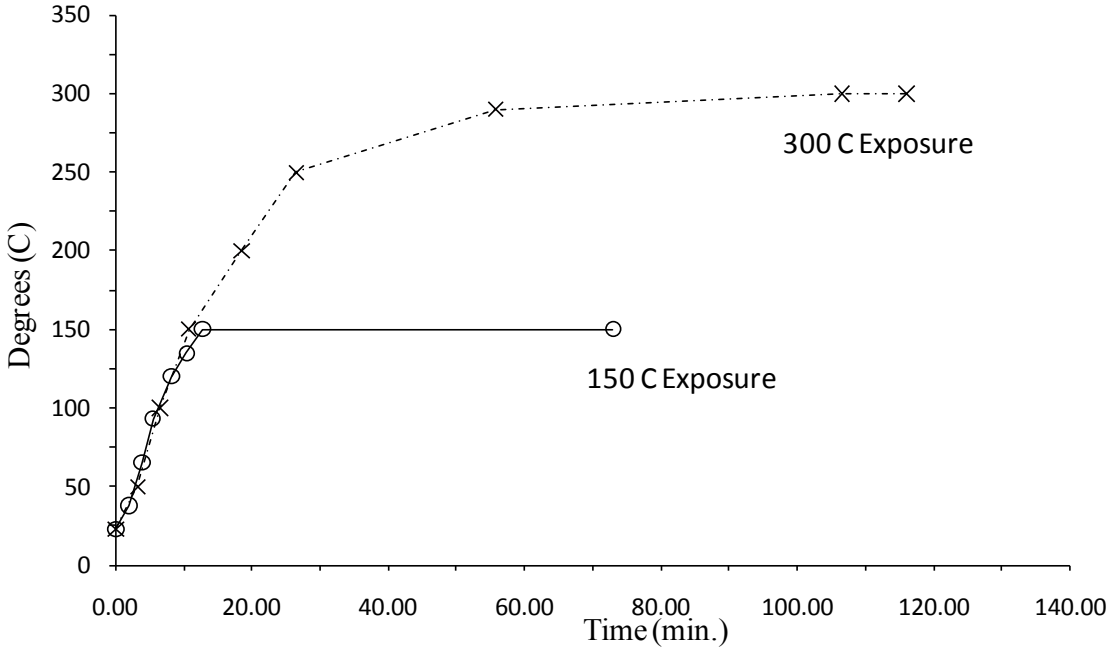

Fig. A.1: Rate of Heat Gain for 150 C and 300 C Exposure Conditions

Table A.2 is summary data from the resonant frequency testing for undamaged, 150 C + 300 C, and 300 C only exposure conditions.

Table A.2: E_d and G for All Specimens at Undamaged and Damaged Condition

	Undamaged								150 C + 300 C								300 C							
	$E_{d,wet}$ (Mpsi)	$E_{d,wet}$ AVG (Mpsi)	G_{wet} (Mpsi)	G_{wet} AVG (Mpsi)	$E_{d,dry}$ (Mpsi)	$E_{d,dry}$ AVG (Mpsi)	G_{dry} (Mpsi)	G_{dry} AVG (Mpsi)	$E_{d,wet}$ (Mpsi)	$E_{d,wet}$ AVG (Mpsi)	G_{wet} (Mpsi)	G_{wet} AVG (Mpsi)	$E_{d,dry}$ (Mpsi)	$E_{d,dry}$ AVG (Mpsi)	G_{dry} (Mpsi)	G_{dry} AVG (Mpsi)	$E_{d,wet}$ (Mpsi)	$E_{d,wet}$ AVG (Mpsi)	G_{wet} (Mpsi)	G_{wet} AVG (Mpsi)	$E_{d,dry}$ (Mpsi)	$E_{d,dry}$ AVG (Mpsi)	G_{dry} (Mpsi)	G_{dry} AVG (Mpsi)
CF2 I1	4.68	4.80	1.87	1.92	3.69	3.80	1.48	1.52																
CF2 I2	4.97		1.99		3.80		1.52																	
CF2 K1	4.79		1.92		3.94		1.58										3.57	3.49	1.43	1.40	2.25	2.22	0.900	0.888
CF2 K2	4.60		1.84		3.68		1.47										3.41		1.36		2.19		0.875	
CF2 L1	4.89		1.96		3.70		1.48		3.31	3.39	1.33	1.36	2.25	2.29	0.900	0.915								
CF2 L2	4.84		1.94		3.99		1.60		3.47		1.39		2.32		0.930									
CF6 I1	3.59	3.67	1.43	1.47	2.57	2.64	1.03	1.06																
CF6 I2	3.72		1.49		2.70		1.08																	
CF6 K1	3.61		1.44		2.62		1.05										2.63	2.67	1.05	1.07	1.59	1.61	0.635	0.645
CF6 K2	3.71		1.49		2.64		1.06										2.71		1.08		1.64		0.654	
CF6 L1	3.66		1.46		2.62		1.05		2.25	2.40	0.898	0.959	1.59	1.64	0.635	0.655								
CF6 L2	3.73		1.49		2.68		1.07		2.55		1.02		1.69		0.674									
CS6 I1	5.29	5.36	2.12	2.14	3.81	4.03	1.52	1.61																
CS6 I2	5.63		2.25		4.15		1.66																	
CS6 K1	5.33		2.13		4.07		1.63										3.67	3.50	1.47	1.40	1.97	1.96	0.788	0.784
CS6 K2	5.16		2.06		3.90		1.56										3.33		1.33		1.95		0.780	
CS6 L1	5.56		2.22		4.18		1.67		3.65	3.58	1.46	1.43	1.88	1.86	0.75	0.743								
CS6 L2	5.18		2.07		4.07		1.63		3.52		1.41		1.84		0.74									
LF2 I1	3.38	3.48	1.35	1.39	2.64	2.81	1.06	1.12																
LF2 I2	3.50		1.40		2.80		1.12																	
LF2 K1	3.50		1.40		2.84		1.14										2.71	2.71	1.08	1.09	1.71	1.74	0.684	0.695
LF2 K2	3.65		1.46		2.91		1.16										2.72		1.09		1.76		0.705	
LF2 L1	3.44		1.38		2.80		1.12		2.46	2.47	0.985	0.988	1.56	1.66	0.63	0.663								
LF2 L2	3.39		1.36		2.88		1.15		2.48		0.991		1.75		0.70									
LF6 I1	2.91	2.90	1.17	1.16	2.21	2.22	0.886	0.888																
LF6 I2	2.81		1.12		2.21		0.882																	
LF6 K1	2.92		1.17		2.25		0.900										2.14	2.13	0.858	0.853	1.38	1.40	0.550	0.560
LF6 K2	2.97		1.19		2.25		0.898										2.12		0.848		1.42		0.569	
LF6 L1	3.01		1.20		2.19		0.874		1.90	1.89	0.759	0.757	1.28	1.28	0.51	0.514								
LF6 L2	2.79		1.11		2.22		0.886		1.89		0.754		1.29		0.52									
LS6 I1	3.67	3.73	1.47	1.49	2.99	3.02	1.20	1.21																
LS6 I2	3.68		1.47		3.01		1.21																	
LS6 K1	3.89		1.56		3.11		1.24										2.90	2.79	1.16	1.12	1.46	1.43	0.585	0.572
LS6 K2	3.84		1.54		3.09		1.24										2.67		1.07		1.40		0.559	
LS6 L1	3.84		1.54		3.06		1.22		2.61	2.55	1.04	1.02	1.26	1.22	0.502	0.486								
LS6 L2	3.49		1.39		2.86		1.15		2.50		0.999		1.17		0.470									

Statistical analysis of the data in Figures A.2 through A.5 and Table A.2 confirmed that damage due to exposure conditions of 150 C + 300 C and 300 C only could be considered similar at a 95% confidence interval. This allowed for Groups K and L to be combined giving 4 replicate specimens per exposure condition.

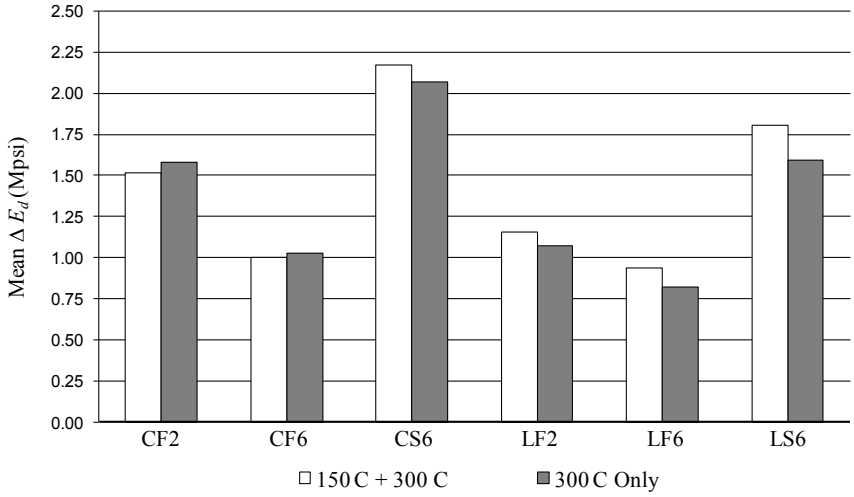

Fig. A.2: Mean Δ E_d Comparison of 150 C + 300 C and 300 C Only

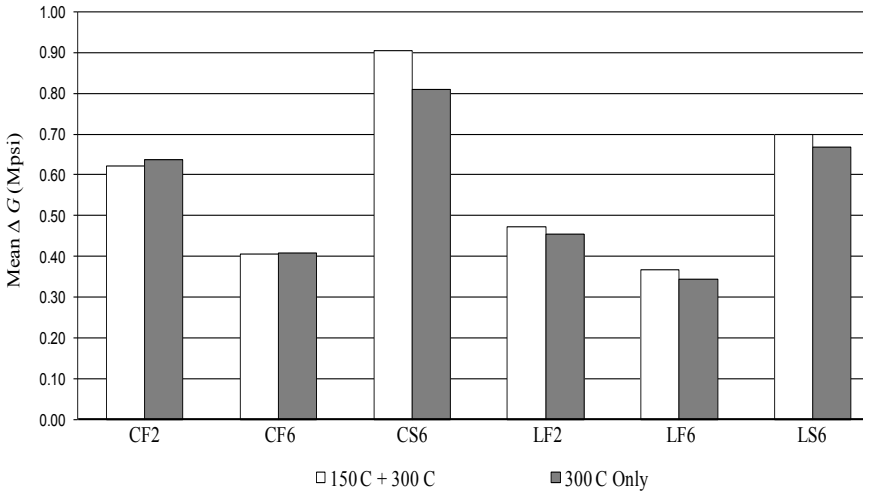

Fig. A.3: Mean ΔG Comparison of 150 C + 300 C and 300 C Only

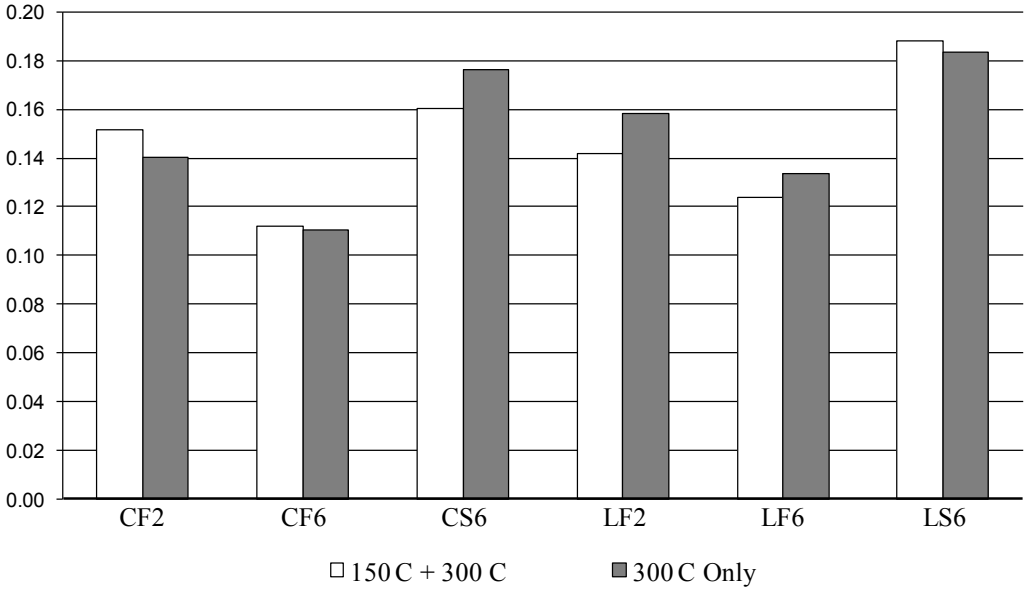

Fig. A.4 Mean Δ∈ Comparison of 150 C + 300 C and 300 C Only

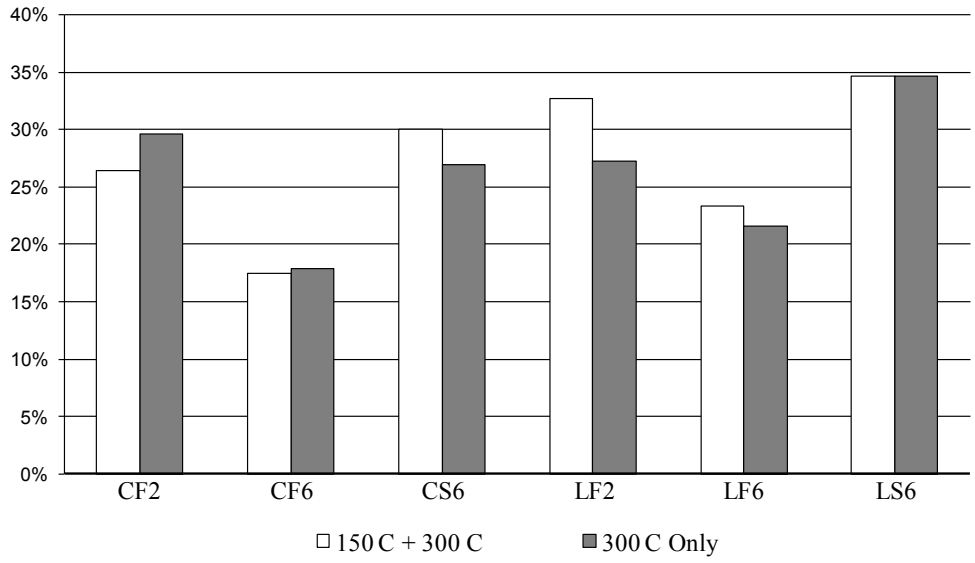

Fig. A.5 Mean Δ $\overline{L}$ Comparison of 150 C + 300 C and 300 C Only

Table A.3: Summary Data for G and $\in$

Mixture	Specimen	Exposure	G_0 (Mpsi)	G_u (Mpsi)	G_{dmg} (Mpsi)	ΔG (Mpsi)	Crack Density Parameter ε_u	Crack Density Parameter ε_{dmg}
CF2	I1	---	2.35	1.48	---	---	0.239	---
	I2	---	2.35	1.52	---	---	0.229	---
	K1	300 C	2.35	1.58	0.90	0.68	0.215	0.375
	K2		2.30	1.47	0.88	0.60	0.234	0.376
	L1	150 C	2.53	1.48	1.21	0.27	0.265	0.325
		300 C (2)			0.90	0.58		0.389
	L2	150 C	2.37	1.60	1.25	0.35	0.213	0.298
		300 C (2)			0.93	0.67		0.371
CF6	I1	---	1.89	1.03	---	---	0.288	---
	I2	---	1.89	1.08	---	---	0.273	---
	K1	300 C	1.89	1.05	0.64	0.41	0.282	0.400
	K2		1.99	1.06	0.65	0.40	0.298	0.403
	L1	150 C	1.93	1.05	0.87	0.18	0.289	0.340
		300 C (2)			0.64	0.41		0.403
	L2	150 C	1.97	1.07	0.91	0.16	0.289	0.334
		300 C (2)			0.67	0.40		0.397
CS6	I1	---	2.81	1.52	---	---	0.290	---
	I2	---	2.81	1.66	---	---	0.262	---
	K1	300 C	2.73	1.63	0.79	0.84	0.258	0.424
	K2		2.65	1.56	0.78	0.78	0.264	0.421
	L1	150 C	2.87	1.67	1.24	0.43	0.267	0.349
		300 C (2)			0.75	0.92		0.437
	L2	150 C	2.61	1.63	1.18	0.45	0.242	0.339
		300 C (2)			0.74	0.89		0.427
LF2	I1	---	1.70	1.06	---	---	0.244	---
	I2	---	1.70	1.12	---	---	0.223	---
	K1	300 C	1.73	1.14	0.68	0.45	0.222	0.368
	K2		1.83	1.16	0.71	0.46	0.237	0.374
	L1	150 C	1.71	1.12	0.93	0.19	0.224	0.288
		300 C (2)			0.63	0.49		0.384
	L2	150 C	1.63	1.15	0.94	0.21	0.196	0.271
		300 C (2)			0.70	0.45		0.351
LF6	I1	---	1.50	0.89	---	---	0.261	---
	I2	---	1.50	0.88	---	---	0.265	---
	K1	300 C	1.49	0.90	0.55	0.35	0.255	0.383
	K2		1.53	0.90	0.56	0.34	0.264	0.385
	L1	150 C	1.58	0.87	0.74	0.13	0.285	0.330
		300 C (2)			0.51	0.36		0.406
	L2	150 C	1.38	0.89	0.74	0.15	0.232	0.293
		300 C (2)			0.52	0.37		0.380
LS6	I1	---	1.81	1.20	---	---	0.220	---
	I2	---	1.81	1.21	---	---	0.217	---
	K1	300 C	1.95	1.24	0.59	0.66	0.237	0.418
	K2		1.91	1.24	0.56	0.68	0.229	0.422
	L1	150 C	1.93	1.22	0.85	0.37	0.239	0.345
		300 C (2)			0.50	0.72		0.438
	L2	150 C	1.70	1.15	0.83	0.32	0.211	0.319
		300 C (2)			0.47	0.68		0.380

"G_0" is the shear modulus of the uncracked solid,"$\in_u$" is the undamaged crack density parameter, "$\in_{dmg}$" is the damaged crack density parameter after heat exposure to 150 C and / or 300 C +/- 10 C for 60 +/- 2 min.

APPENDIX B:

Statistical Model Results

SINGLE FACTOR ANOVA RESULTS

Anova: Single Factor

E_d

SUMMARY

Groups	*Count*	*Sum*	*Average*	*Variance*
150 + 300	12	19.87945	1.656621	0.142996
300	12	20.70946	1.725788	0.092599

ANOVA

Source of Variation	*SS*	*df*	*MS*	*F*	*P-value*	*F crit*
Between Groups	0.028704	1	0.028704	0.243676	0.626456	4.300949
Within Groups	2.591549	22	0.117798			
Total	2.620254	23				

Fig. B.1: E_d ANOVA for 150 C + 300 C and 300 C Only Exposures

Anova: Single Factor

G

SUMMARY

Groups	*Count*	*Sum*	*Average*	*Variance*
150+300	12	77.96339	6.49695	2.199236
300	12	81.23138	6.769282	1.42625

ANOVA

Source of Variation	*SS*	*df*	*MS*	*F*	*P-value*	*F crit*
Between Groups	0.444989	1	0.444989	0.245478	0.62519	4.300949
Within Groups	39.88035	22	1.812743			
Total	40.32534	23				

Fig. B.2: *G* ANOVA for 150 C + 300 C and 300 C Only Exposures

Anova: Single Factor

API

SUMMARY

Groups	*Count*	*Sum*	*Average*	*Variance*
150C + 300C	12	4.151564	0.345964	0.02404
300C	12	3.320103	0.276675	0.011301

ANOVA

Source of Variation	*SS*	*df*	*MS*	*F*	*P-value*	*F crit*
Between Groups	0.028805	1	0.028805	1.630093	0.215003	4.300949
Within Groups	0.388761	22	0.017671			
Total	0.417567	23				

Fig. B.3: API ANOVA for 150 C + 300 C and 300 C Only Exposures

ONEWAY ANALYSIS RESULTS (t-TEST)

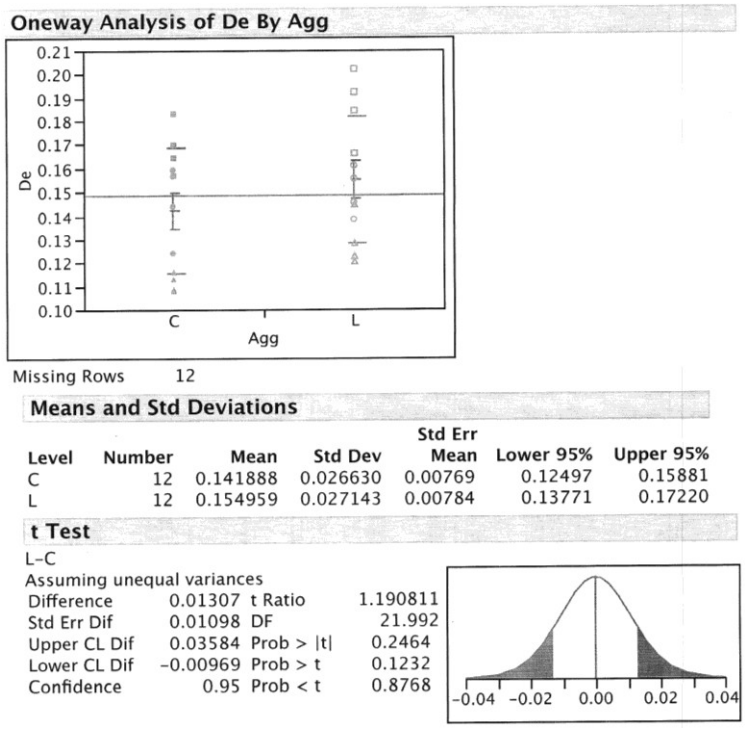

Fig. B.4: Δ∈ by Aggregate Type

Oneway Analysis of De By SCM

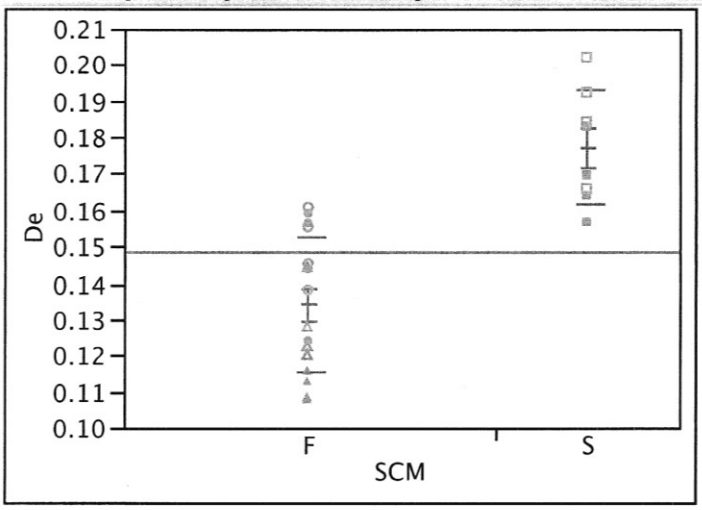

Missing Rows 12

Means and Std Deviations

Level	Number	Mean	Std Dev	Std Err Mean	Lower 95%	Upper 95%
F	16	0.134012	0.018724	0.00468	0.12403	0.14399
S	8	0.177246	0.015595	0.00551	0.16421	0.19028

t Test

S-F

Assuming unequal variances

Difference	0.043234	t Ratio	5.977647
Std Err Dif	0.007233	DF	16.68299
Upper CL Dif	0.058515	Prob > |t|	<.0001*
Lower CL Dif	0.027952	Prob > t	<.0001*
Confidence	0.95	Prob < t	1.0000

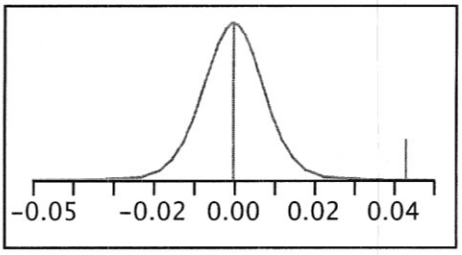

Fig. B.5: $\Delta\epsilon$ by SCM Type

Oneway Analysis of De By qSCM

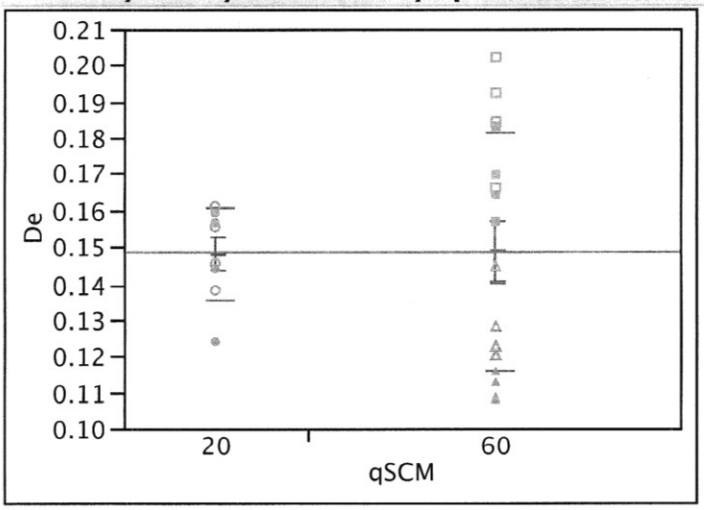

Missing Rows 12

Means and Std Deviations

Level	Number	Mean	Std Dev	Std Err Mean	Lower 95%	Upper 95%
20	8	0.147966	0.012625	0.00446	0.13741	0.15852
60	16	0.148652	0.032467	0.00812	0.13135	0.16595

t Test

60-20
Assuming unequal variances

Difference	0.00069	t Ratio	0.07411
Std Err Dif	0.00926	DF	21.27505
Upper CL Dif	0.01994	Prob > |t|	0.9416
Lower CL Dif	-0.01856	Prob > t	0.4708
Confidence	0.95	Prob < t	0.5292

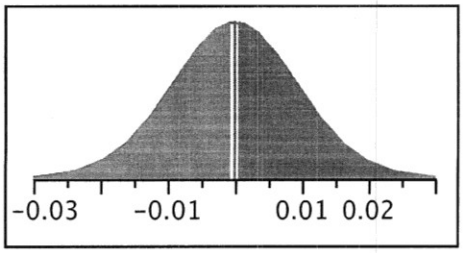

Fig. B.6: $\Delta\epsilon$ by %SCM

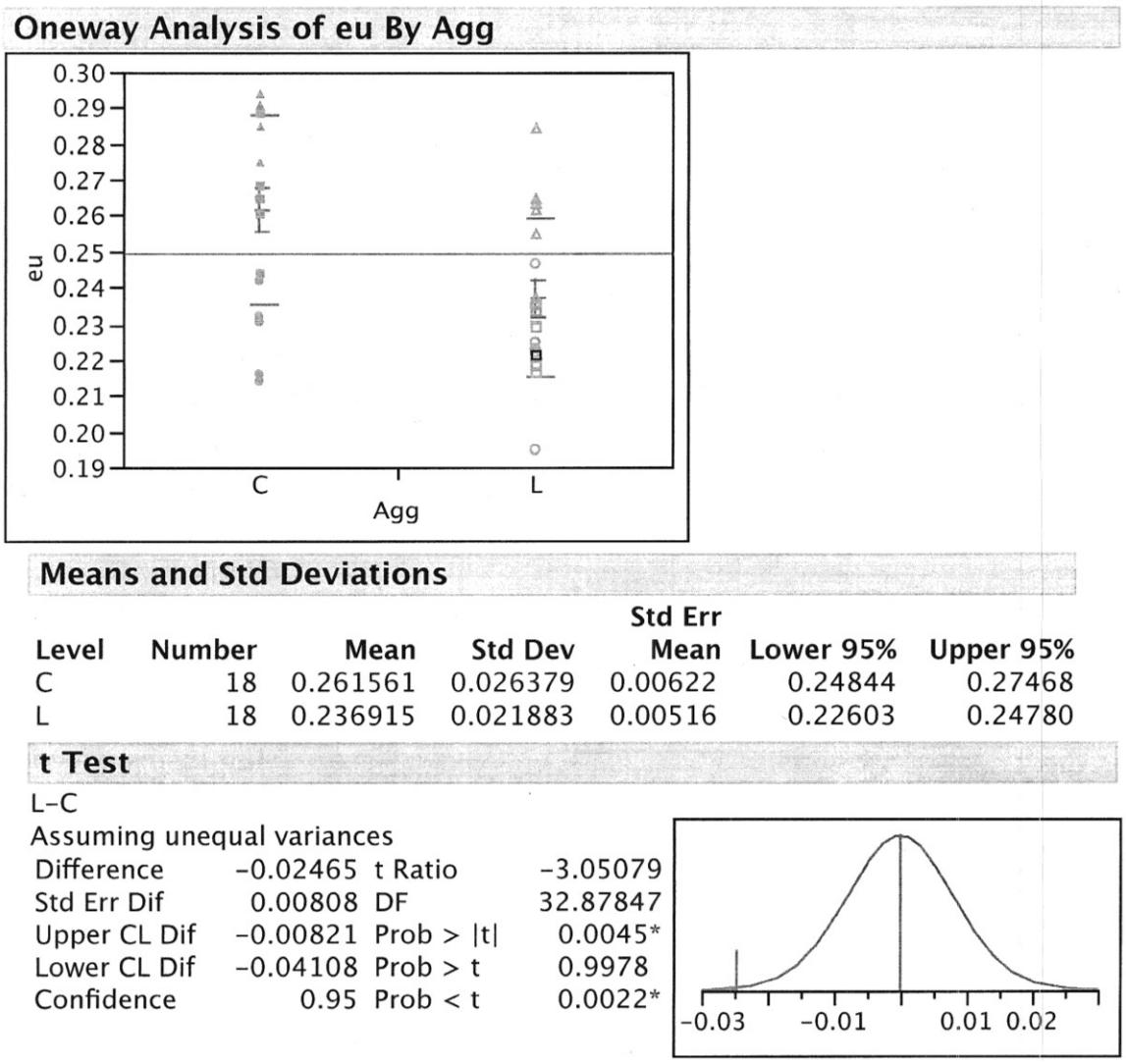

Fig. B.7: $\in_u$ by Aggregate Type

Oneway Analysis of eu By SCM

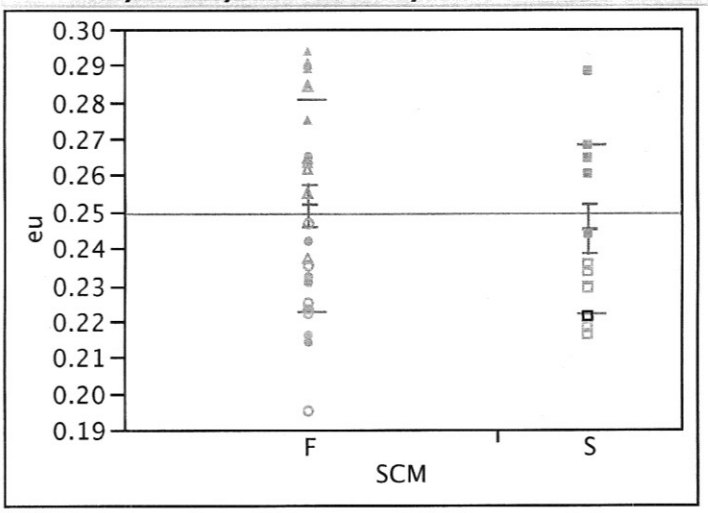

Means and Std Deviations

Level	Number	Mean	Std Dev	Std Err Mean	Lower 95%	Upper 95%
F	24	0.251448	0.028895	0.00590	0.23925	0.26365
S	12	0.244820	0.023126	0.00668	0.23013	0.25951

t Test

S-F

Assuming unequal variances

Difference	-0.00663	t Ratio	-0.744
Std Err Dif	0.00891	DF	27.00516
Upper CL Dif	0.01165	Prob > |t|	0.4633
Lower CL Dif	-0.02491	Prob > t	0.7684
Confidence	0.95	Prob < t	0.2316

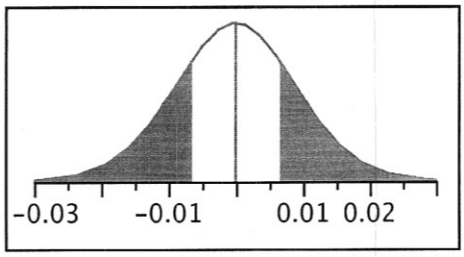

Fig. B.8: $\in_u$ by SCM Type

Oneway Analysis of eu By qSCM

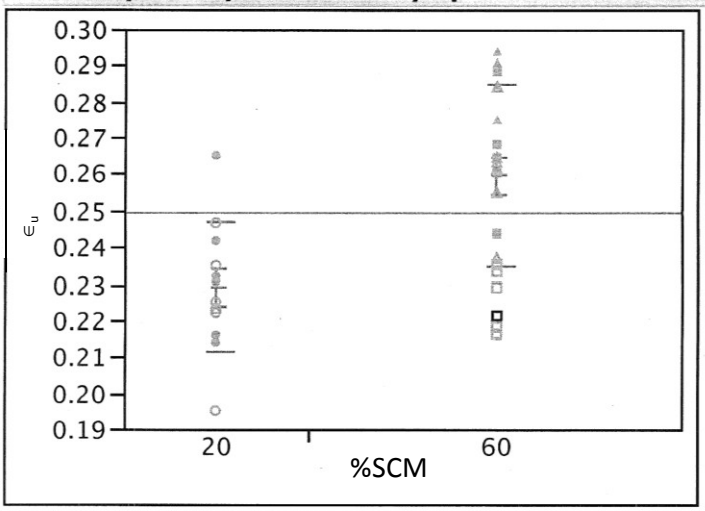

Means and Std Deviations

Level	Number	Mean	Std Dev	Std Err Mean	Lower 95%	Upper 95%
20	12	0.228838	0.017749	0.00512	0.21756	0.24011
60	24	0.259439	0.025092	0.00512	0.24884	0.27003

t Test

60-20
Assuming unequal variances

Difference	0.030601	t Ratio	4.22394
Std Err Dif	0.007245	DF	29.75699
Upper CL Dif	0.045402	Prob > |t|	0.0002*
Lower CL Dif	0.015800	Prob > t	0.0001*
Confidence	0.95	Prob < t	0.9999

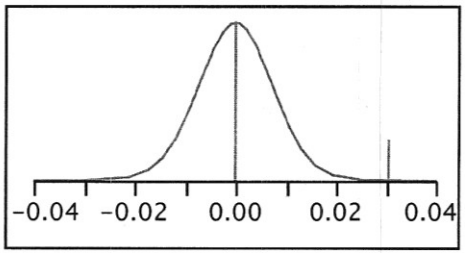

Fig. B.9: ϵ_u by %SCM

LEAST SQUARES FIT RESULTS

Response DG

Whole Model

Regression Plot

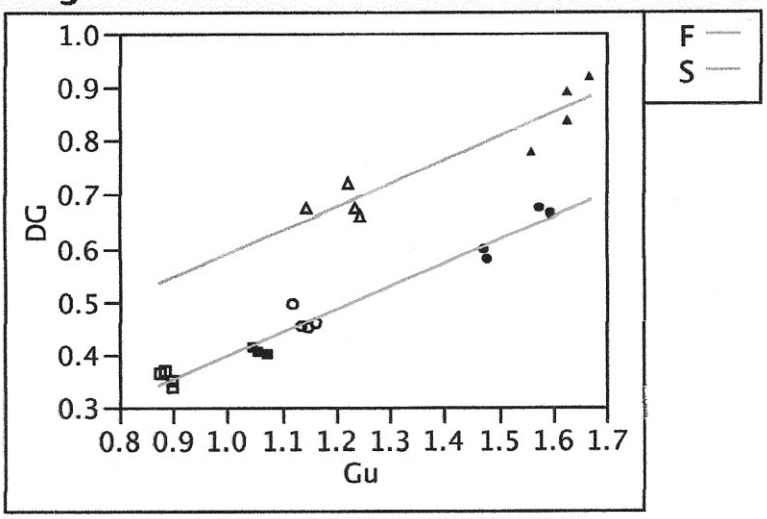

Summary of Fit

RSquare	0.979749
RSquare Adj	0.97782
Root Mean Square Error	0.026987
Mean of Response	0.565972
Observations (or Sum Wgts)	24

Analysis of Variance

Source	DF	Sum of Squares	Mean Square	F Ratio
Model	2	0.73989989	0.369950	507.9830
Error	21	0.01529372	0.000728	**Prob > F**
C. Total	23	0.75519361		<.0001*

Parameter Estimates

Term	Estimate	Std Error	t Ratio	Prob>|t|
Intercept	0.0550595	0.031597	1.74	0.0960
Gu	0.4371157	0.024151	18.10	<.0001*
SCM[F]	−0.096028	0.006645	−14.45	<.0001*

Fig. B.10: ΔG vs. G_u by SCM Type

Response De

Whole Model

Regression Plot

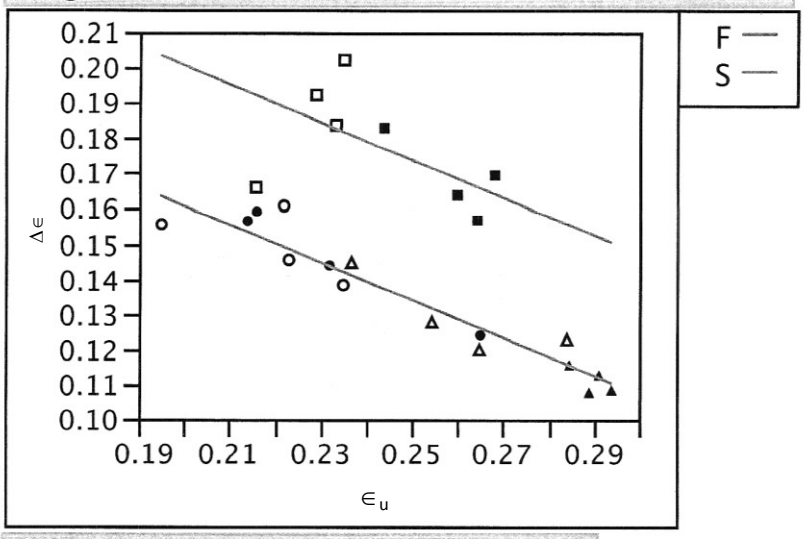

Summary of Fit

RSquare	0.896051
RSquare Adj	0.886151
Root Mean Square Error	0.009154
Mean of Response	0.148423
Observations (or Sum Wgts)	24

Analysis of Variance

Source	DF	Sum of Squares	Mean Square	F Ratio
Model	2	0.01516998	0.007585	90.5113
Error	21	0.00175983	0.000084	Prob > F
C. Total	23	0.01692981		<.0001*

Parameter Estimates

Term	Estimate	Std Error	t Ratio	Prob>|t|
Intercept	0.288072	0.016928	17.02	<.0001*
eu	-0.536446	0.068093	-7.88	<.0001*
SCM[F]	-0.01993	0.001993	-10.00	<.0001*

Fig. B.11: $\Delta\in$ vs. $\in_u$ by SCM Type

Response DG

Whole Model

Regression Plot

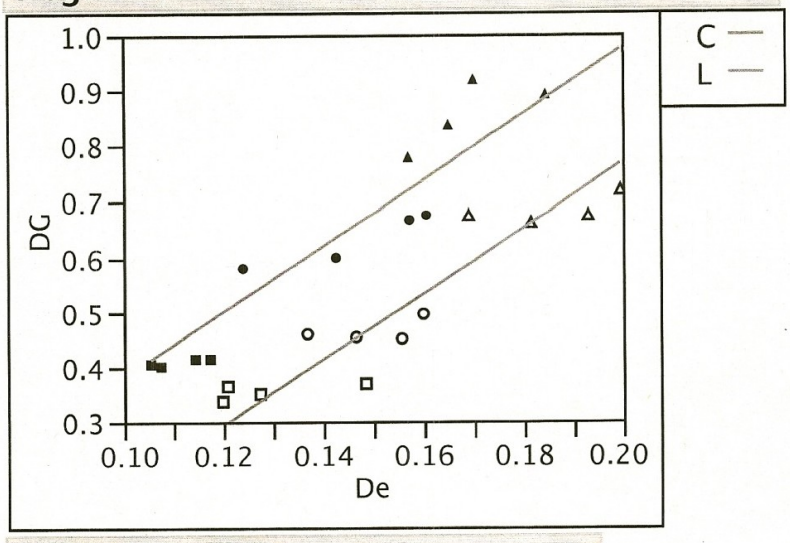

Summary of Fit

RSquare	0.893467
RSquare Adj	0.883321
Root Mean Square Error	0.061896
Mean of Response	0.565972
Observations (or Sum Wgts)	24

Analysis of Variance

Source	DF	Sum of Squares	Mean Square	F Ratio
Model	2	0.67474074	0.337370	88.0612
Error	21	0.08045287	0.003831	Prob > F
C. Total	23	0.75519361		<.0001*

Parameter Estimates

Term	Estimate	Std Error	t Ratio	Prob>|t|
Intercept	-0.323176	0.07381	-4.38	0.0003*
Agg[C]	0.1032391	0.013012	7.93	<.0001*
De	5.9854269	0.489532	12.23	<.0001*

Fig. B.12: ΔG vs. $\Delta \in$ by Aggregate Type

Response DG

Whole Model

Actual by Predicted Plot

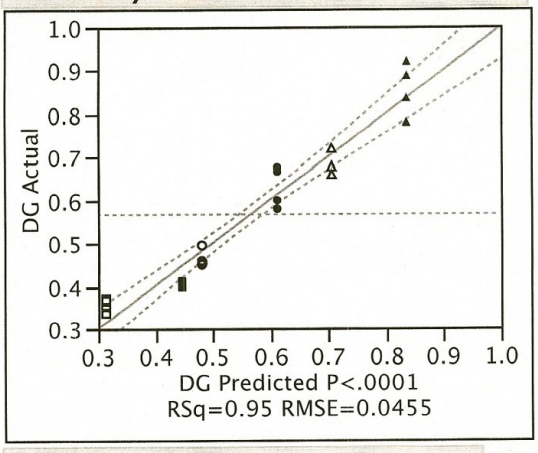

Summary of Fit

RSquare	0.945208
RSquare Adj	0.936989
Root Mean Square Error	0.045485
Mean of Response	0.565972
Observations (or Sum Wgts)	24

Analysis of Variance

Source	DF	Sum of Squares	Mean Square	F Ratio
Model	3	0.71381515	0.237938	115.0059
Error	20	0.04137846	0.002069	Prob > F
C. Total	23	0.75519361		<.0001*

Lack Of Fit

Source	DF	Sum of Squares	Mean Square	F Ratio
Lack Of Fit	2	0.01896850	0.009484	7.6179
Pure Error	18	0.02240996	0.001245	Prob > F
Total Error	20	0.04137846		0.0040*
				Max RSq
				0.9703

Parameter Estimates

Term	Estimate	Std Error	t Ratio	Prob>|t|
Intercept	0.6586168	0.011371	57.92	<.0001*
Agg[C]	0.0651956	0.009285	7.02	<.0001*
qSCM[20]	0.0830915	0.011371	7.31	<.0001*
SCM[F]	-0.194843	0.011371	-17.13	<.0001*

Fig. B.13: ΔG Prediction with Composition Only

Response DG

Whole Model

Actual by Predicted Plot

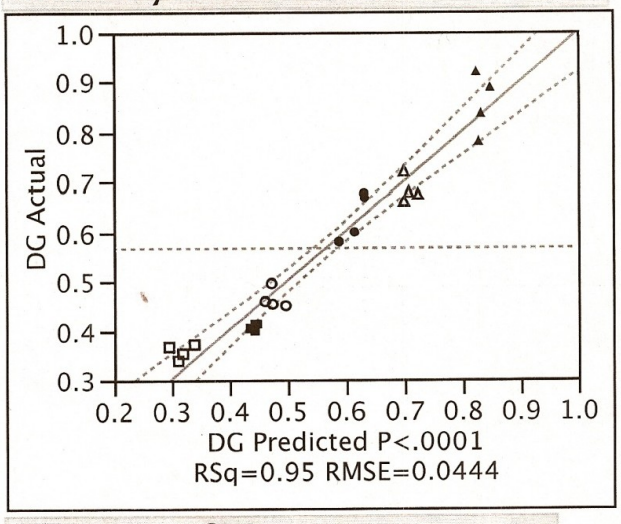

Summary of Fit

RSquare	0.9504
RSquare Adj	0.939958
Root Mean Square Error	0.044401
Mean of Response	0.565972
Observations (or Sum Wgts)	24

Analysis of Variance

Source	DF	Sum of Squares	Mean Square	F Ratio
Model	4	0.71773591	0.179434	91.0159
Error	19	0.03745769	0.001971	Prob > F
C. Total	23	0.75519361		<.0001*

Parameter Estimates

Term	Estimate	Std Error	t Ratio	Prob>|t|
Intercept	0.8569066	0.141045	6.08	<.0001*
eu	-0.845291	0.599397	-1.41	0.1746
qSCM[20]	0.0625544	0.018311	3.42	0.0029*
SCM[F]	-0.181791	0.014453	-12.58	<.0001*
Agg[C]	0.0752682	0.011539	6.52	<.0001*

Fig. B.14: ΔG Prediction with Composition and $\in_u$

Response DG

Whole Model

Actual by Predicted Plot

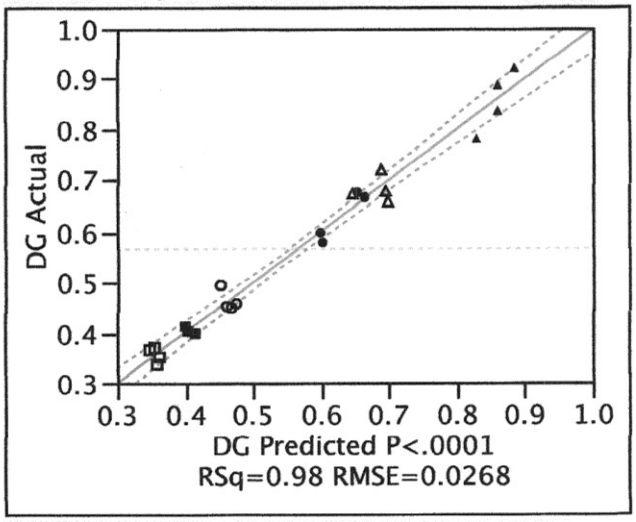

Summary of Fit

RSquare	0.981902
RSquare Adj	0.978092
Root Mean Square Error	0.026821
Mean of Response	0.565972
Observations (or Sum Wgts)	24

Analysis of Variance

Source	DF	Sum of Squares	Mean Square	F Ratio
Model	4	0.74152613	0.185382	257.7102
Error	19	0.01366748	0.000719	**Prob > F**
C. Total	23	0.75519361		<.0001*

Parameter Estimates

Term	Estimate	Std Error	t Ratio	Prob>|t|
Intercept	-0.068671	0.11737	-0.59	0.5654
Gu	0.5282676	0.085113	6.21	<.0001*
qSCM[20]	-0.013069	0.016882	-0.77	0.4484
SCM[F]	-0.077552	0.020052	-3.87	0.0010*
Agg[C]	-0.019651	0.014726	-1.33	0.1978

Fig. B.15: ΔG Prediction with All Parameters

Figure B.16 is an overlay plot of ΔG vs. G_u showing that lower initial shear modulus results in lower ΔG due to damage as described in relation to $\in$ in Part I: Section 5.3. Figure B.17 shows that lightweight aggregate mixtures experience less change in shear modulus with the same change in crack density as their conventional weight counterpart.

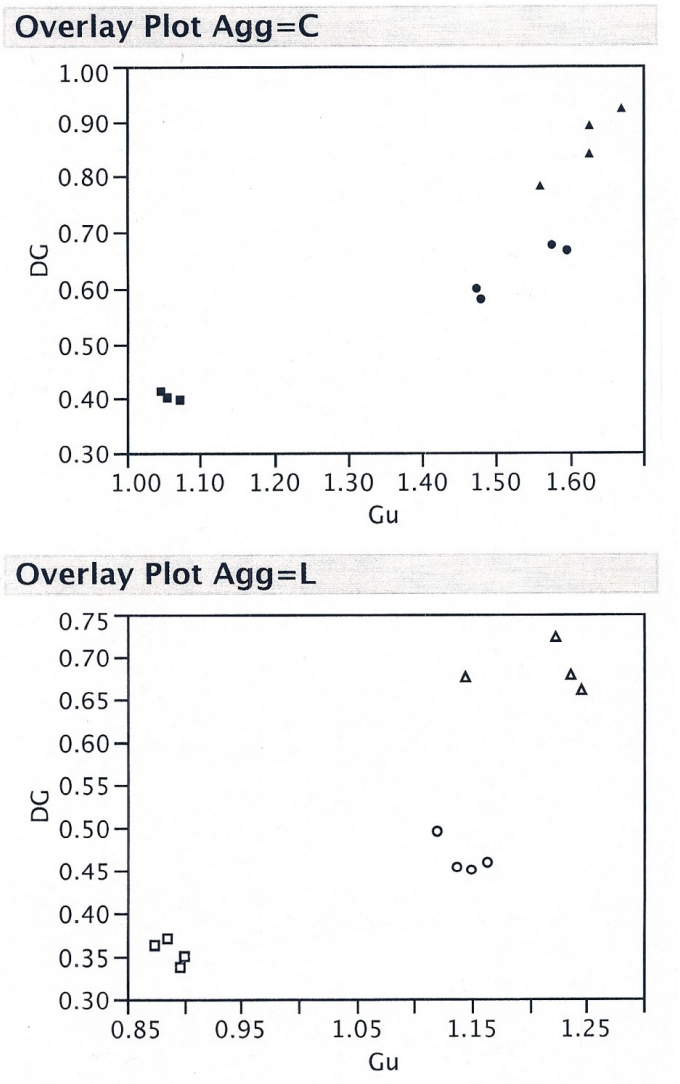

Fig. B.16: Overlay of ΔG vs. G_u by Aggregate Type

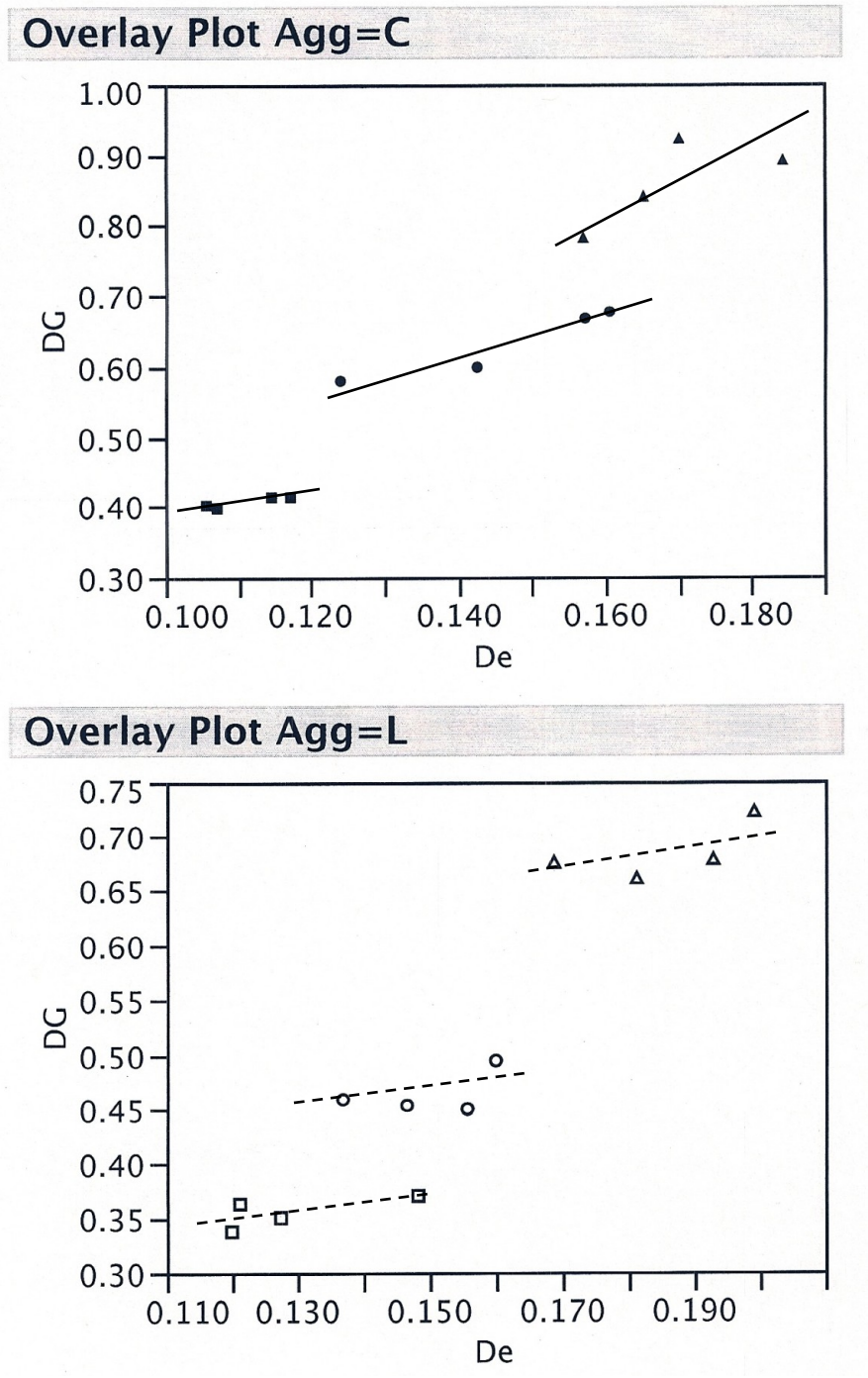

Fig. B.17: Overlay of ΔG vs. $\Delta\in$ by Aggregate Type

APPENDIX C:

Crack Density Parameter vs. Dynamic Shear Modulus Charts

Appendix C contains the family of G vs. $\in$ charts. The charts show initial (uncracked), undamaged and damaged conditions for each specimen in Groups K and L.

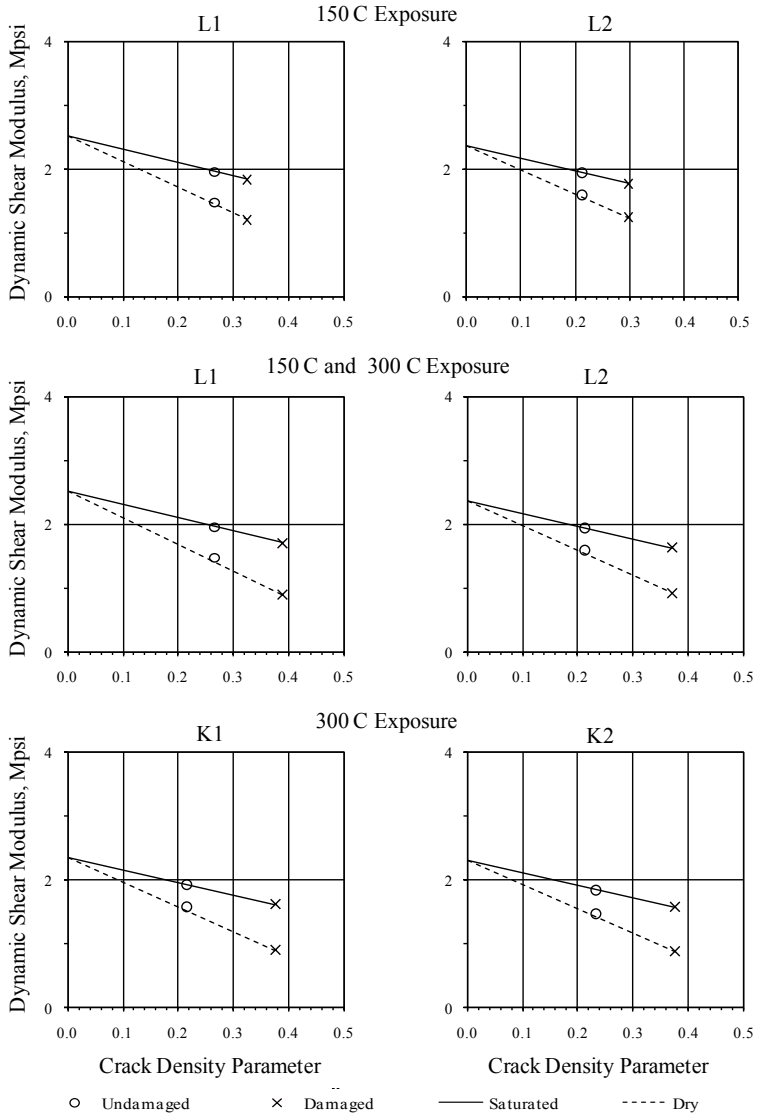

Fig. C.1: Mixture CF2 G vs. $\in$

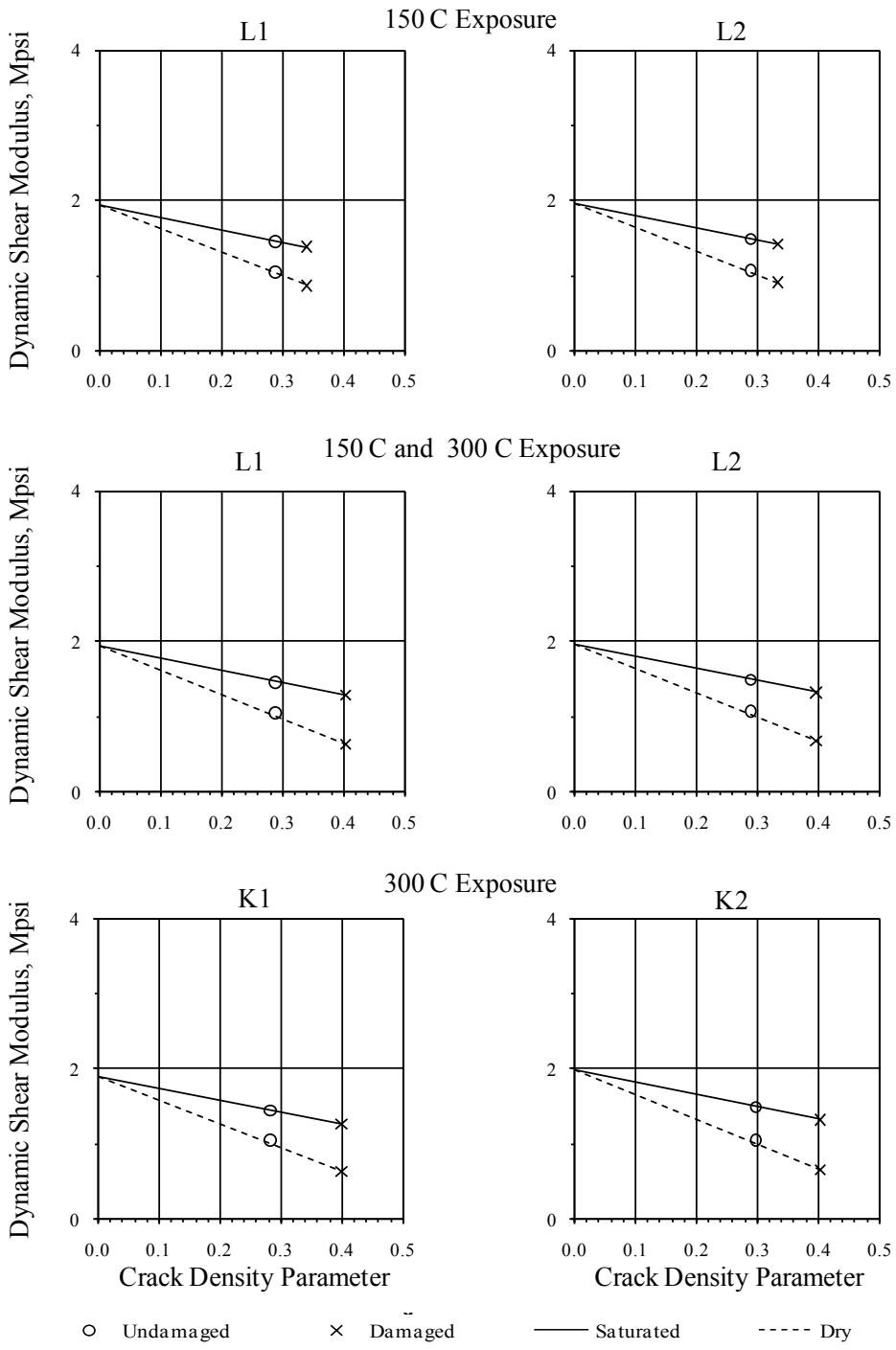

Fig. C.2: Mixture CF6 *G* vs. ∈

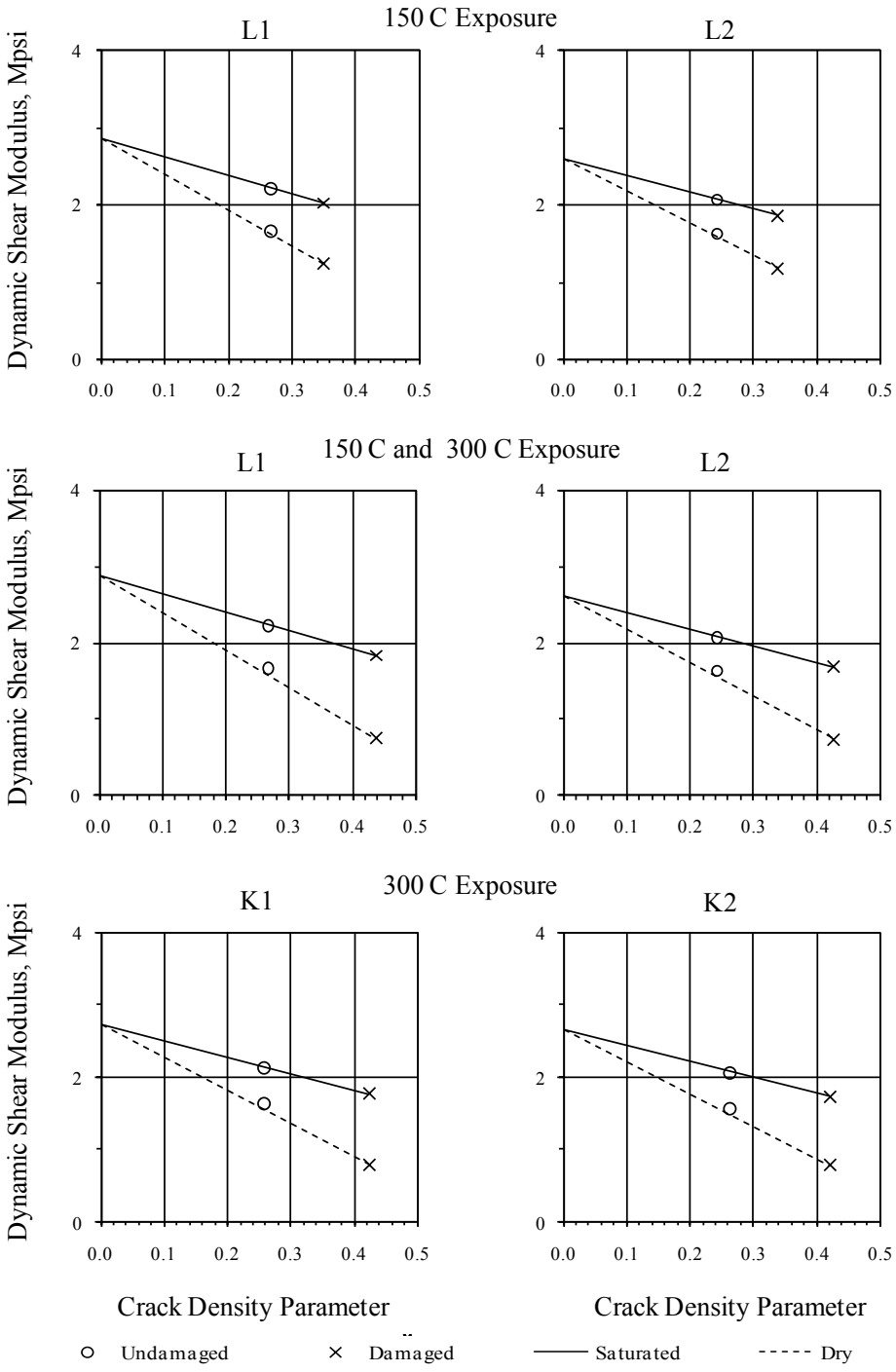

Fig. C.3: Mixture CS6 *G* vs. ∈

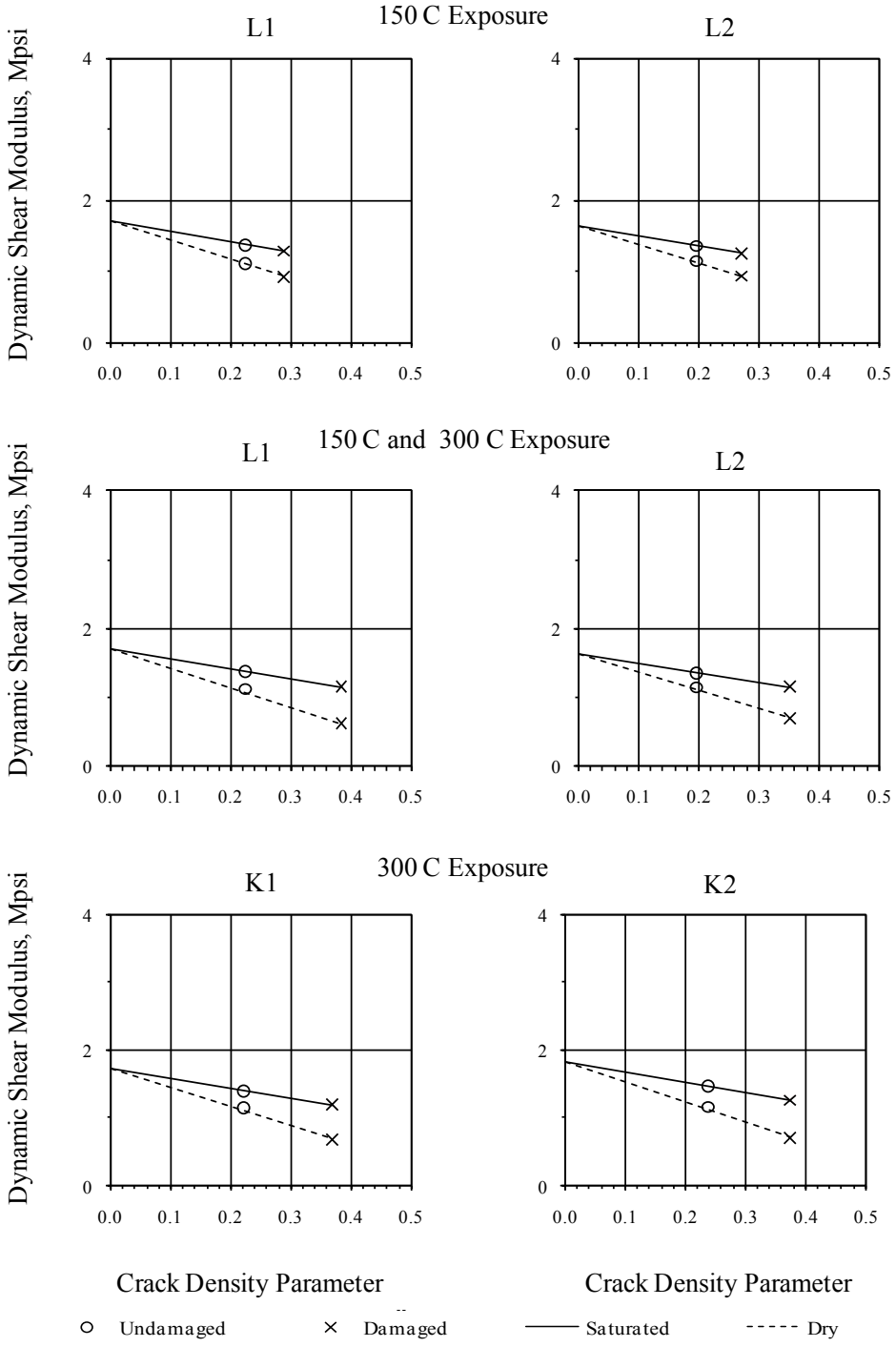

Fig. C.4: Mixture LF2 *G* vs. ∈

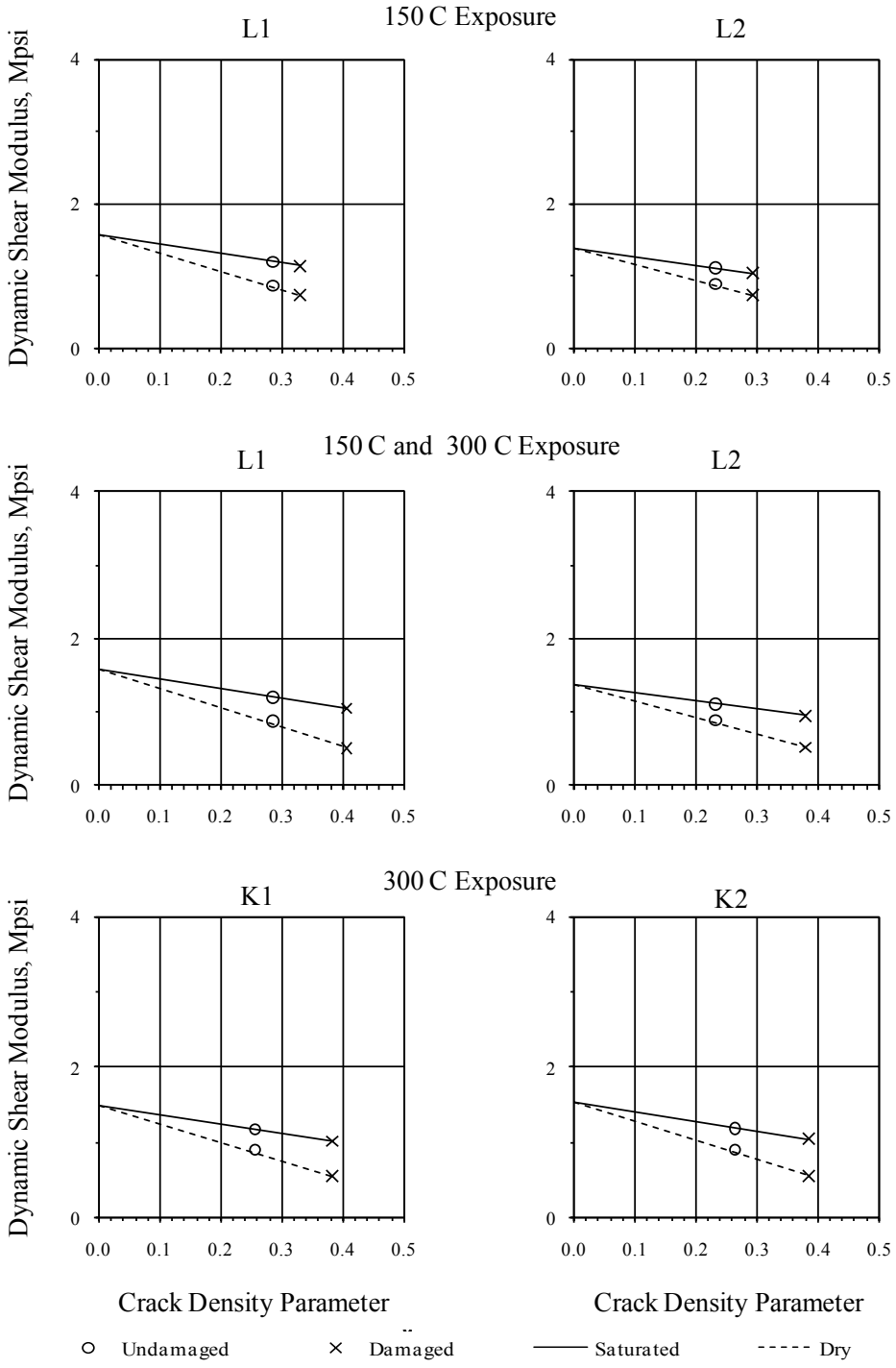

Fig. C.5: Mixture LF6 *G* vs. ∈

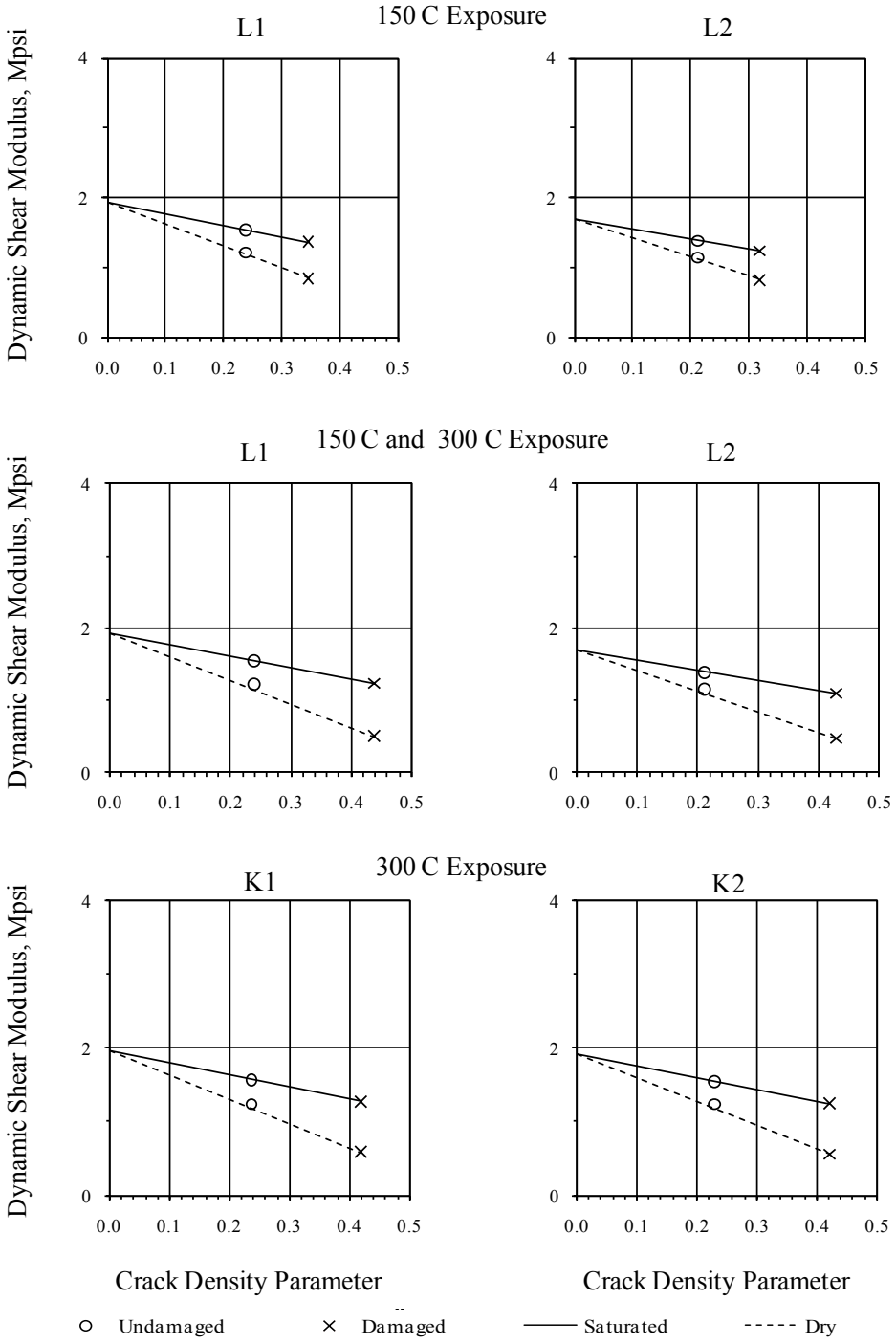

Fig. C.6: Mixture LS6 *G* vs. ∈

APPENDIX D:

Detail Temperature Rise and Splitting Tensile Test Results

Appendix D contains results for temperature rise during initial 24 hours of curing (Figure D.1) and the splitting tensile strength test results for damaged and undamaged specimens (Figure D.2). The two conventional type mixtures (20% fly ash) showed significant levels of heat of hydration over the routine and enhanced sustainability mixtures as expected with reduced amounts of portland cement (Figure D.1).

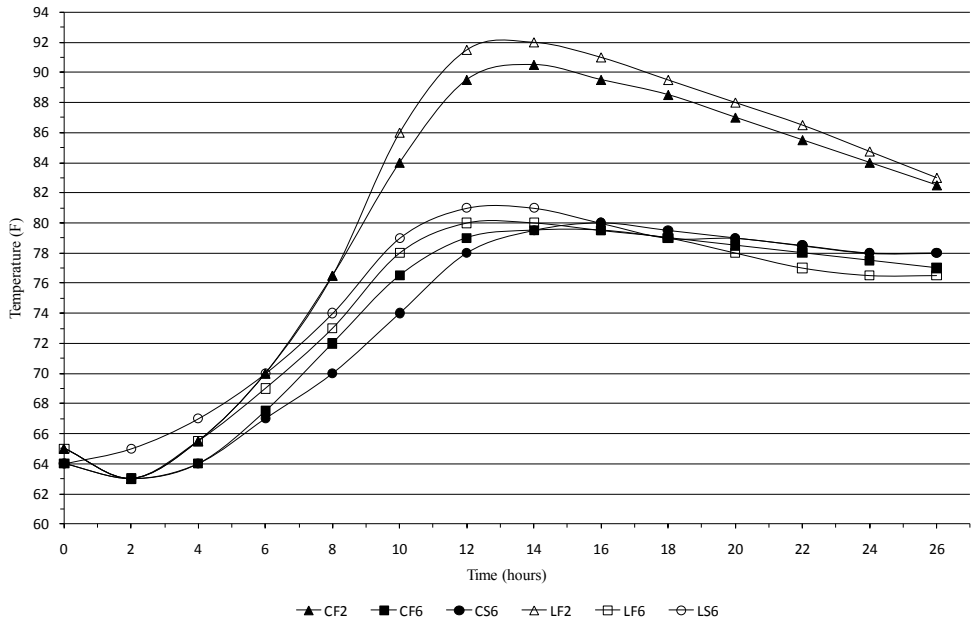

Fig. D.1: Mixture Temperature Rise

Table D.2 shows the results for the splitting tensile strength tests conducted on the damaged and undamaged specimens. The results for f_{ct} are inconsistent within mixture type and across mixtures of like aggregate, and in some cases show signs of additional internal curing after damaged, which is inconsistent with the results for E_d, G and $\in$ (Part

I: Section 5). Further research is being conducted to look at transition zone effects and identify potential sources of the inconsistency for f_{ct} results.

Table D.2: f_{ct} Results

	P_{max} (lbf)	$f_{ct,u}$ (psi)	$f_{ct,dmg}$ (psi)	$AVG\, f_{ct}$ (psi)	$\%\Delta f_{ct}$
CF2 I1	3516	594.93	---	582.33	2.2%
CF2 I2	3407	569.73	---		
CF2 K1	3453	---	561.46	569.23	
CF2 K2	3325	---	598.80		
CF2 L1	3273	---	562.66		
CF2 L2	3303	---	554.02		
CF6 I1	1839	293.41	---	276.35	-3.6%
CF6 I2	1682	259.29	---		
CF6 K1	1757	---	293.83	286.39	
CF6 K2	1787	---	275.90		
CF6 L1	1733	---	282.19		
CF6 L2	1768	---	293.63		
CS6 I1	3179	517.40	---	546.05	-1.3%
CS6 I2	3590	574.70	---		
CS6 K1	3790	---	584.64	553.00	
CS6 K2	3294	---	538.35		
CS6 L1	3290	---	540.98		
CS6 L2	3393	---	548.02		
LF2 I1	3953	683.69	---	680.21	26.3%
LF2 I2	3744	676.74	---		
LF2 K1	3122	---	481.09	501.42	
LF2 K2	2650	---	426.53		
LF2 L1	3493	---	564.04		
LF2 L2	3236	---	534.02		
LF6 I1	2774	437.47	---	407.53	7.4%
LF6 I2	2474	377.59	---		
LF6 K1	2336	---	373.41	377.25	
LF6 K2	2194	---	352.07		
LF6 L1	2278	---	394.08		
LF6 L2	2457	---	389.42		
LS6 I1	3041	525.31	---	547.59	12.7%
LS6 I2	3324	569.86	---		
LS6 K1	3363	---	527.77	478.05	
LS6 K2	2928	---	444.63		
LS6 L1	2642	---	445.03		
LS6 L2	3176	---	494.76		

APPENDIX E:

Moment – Curvature Charts from MLSA Results

Appendix E contains the family of M-ϕ charts from the MLSA results at the evaluated sections. The charts are organized from x = 1.5 ft. to x = 29 ft. (mid-span) (Part II: Figure 3.10) by damaged and undamaged conditions. The order of mixtures is the case study mixture (5700 psi), LF2 mixture (6940 psi), and LF6 mixture (3740 psi).

CASE STUDY MIXTURE (f_c = 5700 psi) – DAMAGED CONDITIONS

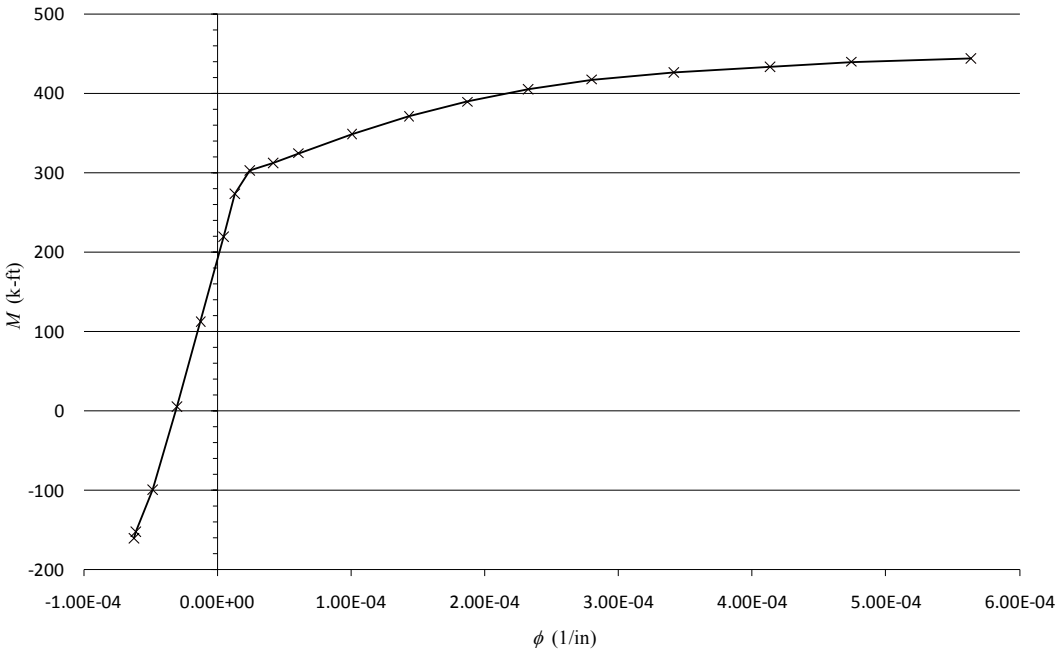

Fig. E.1: Damaged Condition at x = 1.5 ft

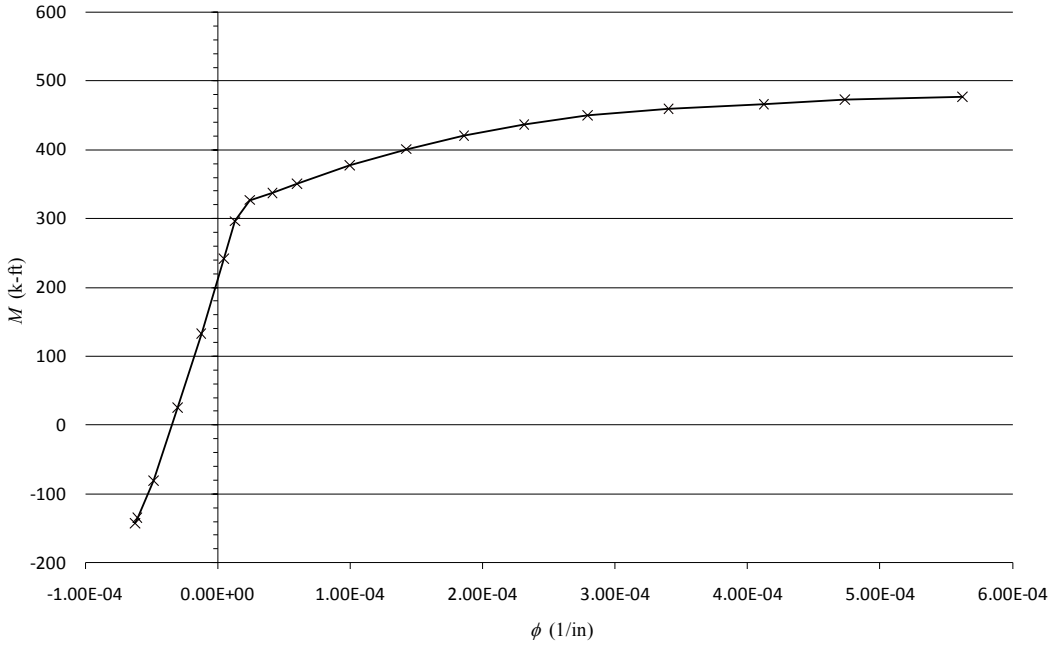

Fig. E.2: Damaged Condition at x = 4 ft

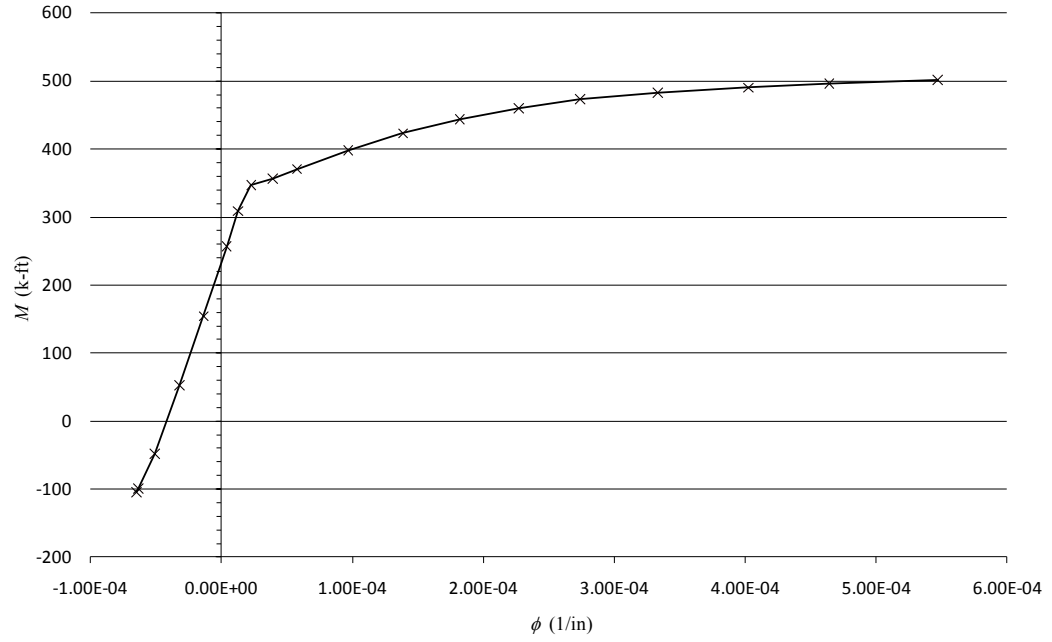

Fig. E.3: Damaged Condition at x = 6 ft (Spalling)

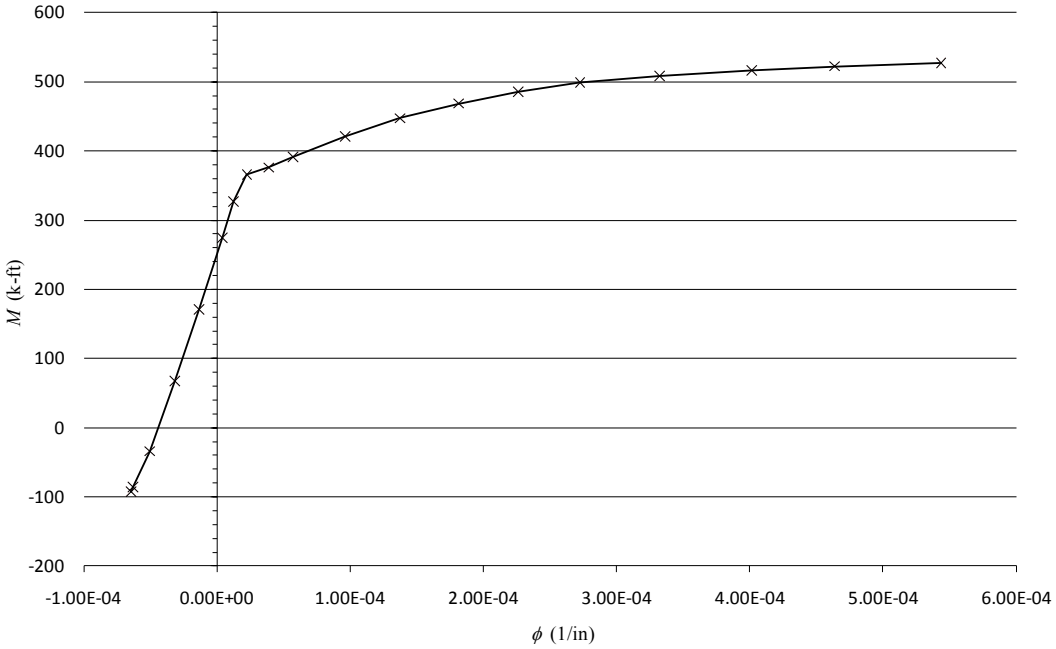

Fig. E.4: Damaged Condition at x = 8 ft (Spalling)

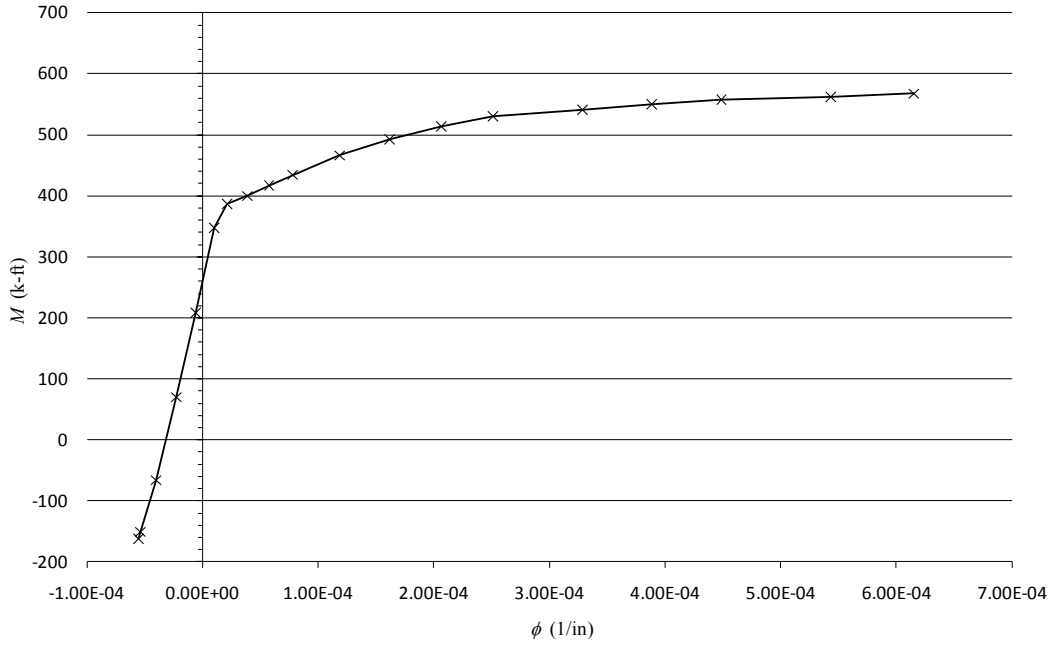

Fig. E.5: Damaged Condition at x = 10.5 ft

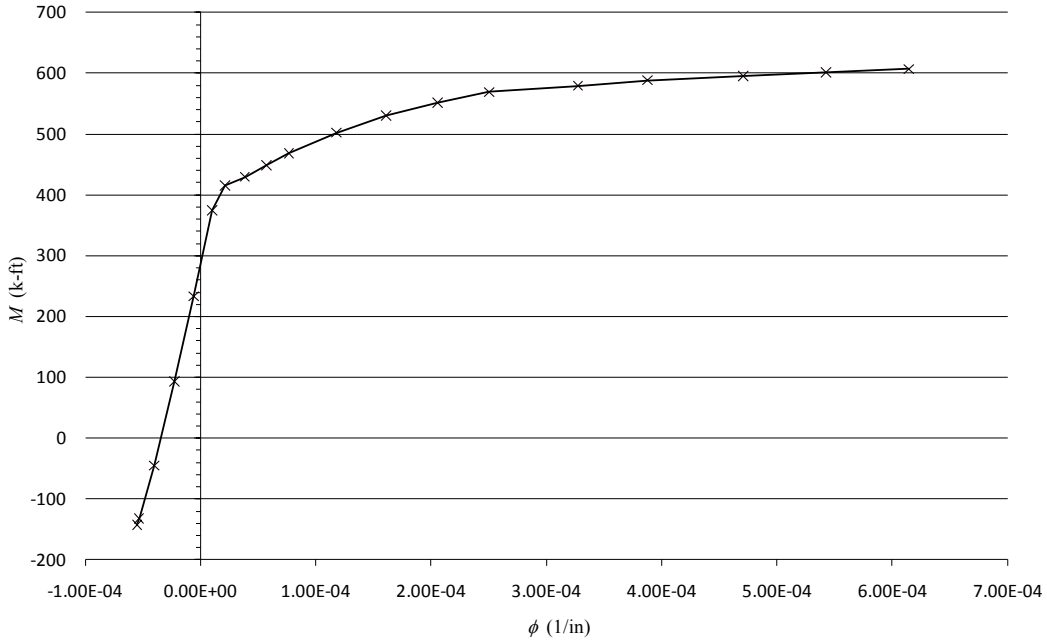

Fig. E.6: Damaged Condition at x = 13.5 ft

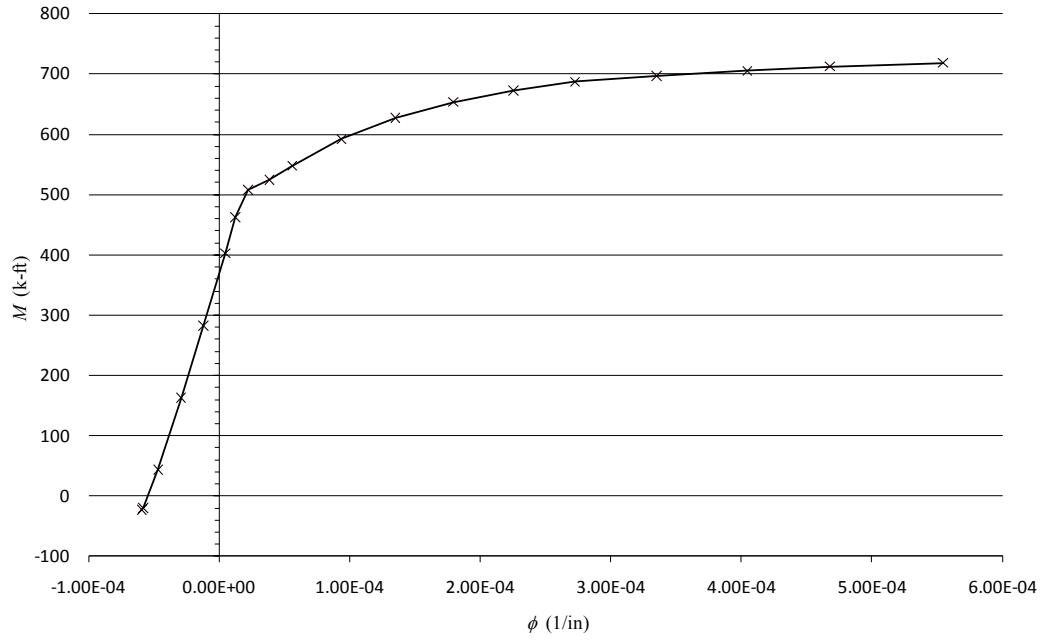

Fig. E.7: Damaged Condition at x = 22.5 ft

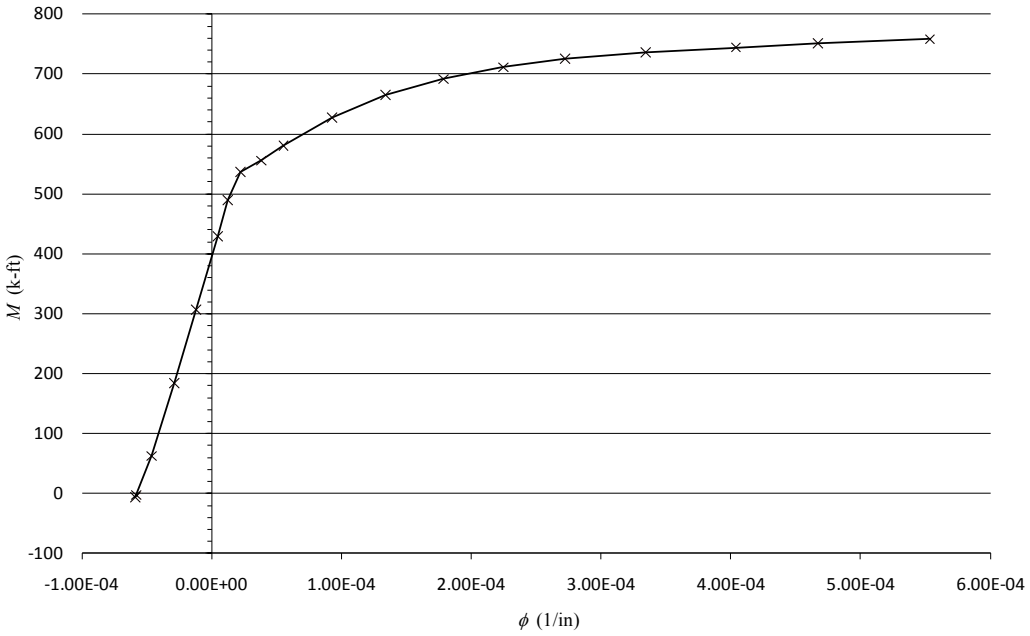

Fig. E.8: Damaged Condition at x = 25.5 ft

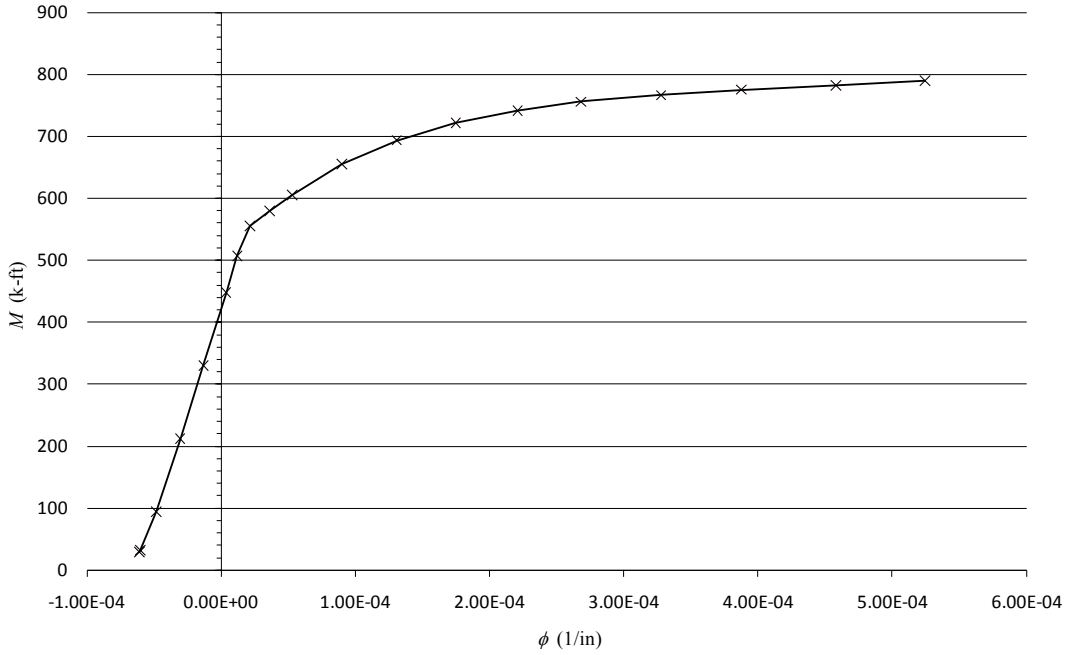

Fig. E.9: Damaged Condition at x = 28 ft (Spalling)

CASE STUDY MIXTURE (f_c = 5700 psi) – UNDAMAGED CONDITIONS

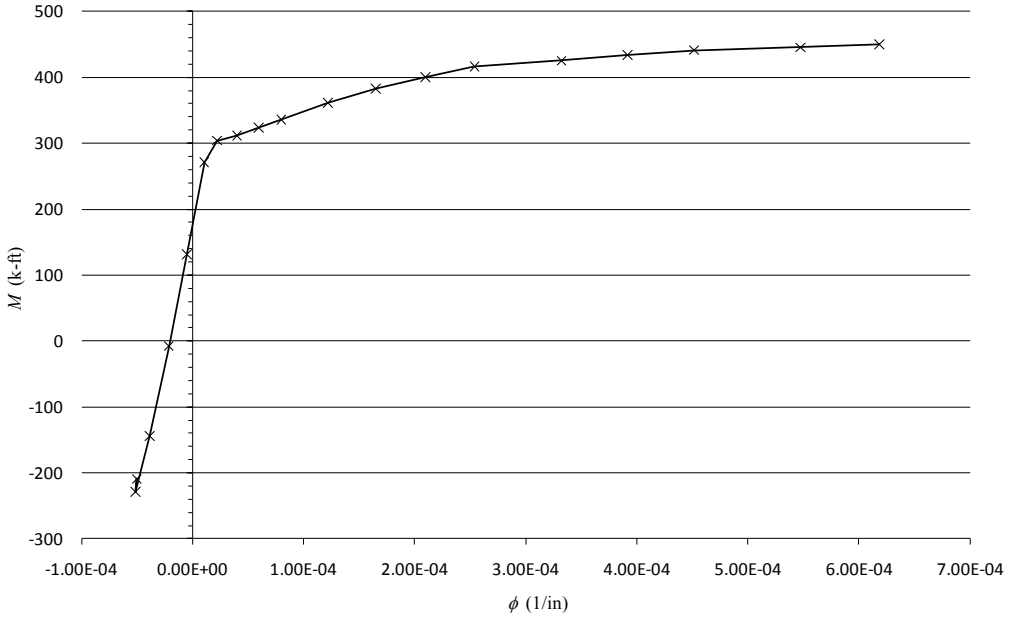

Fig. E.10: Undamaged Condition at x = 1.5 ft

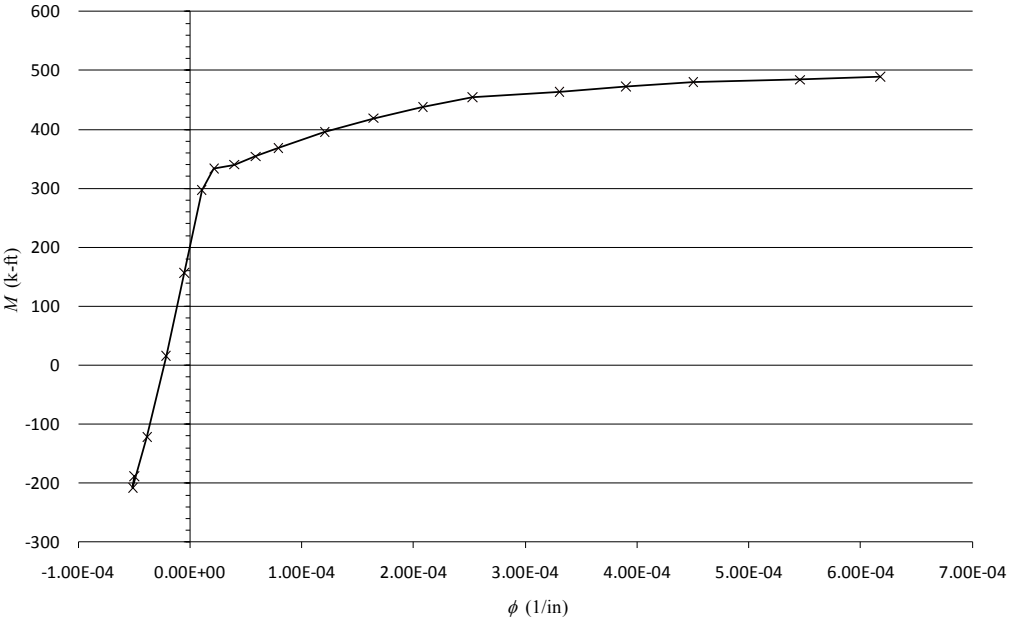

Fig. E.11: Undamaged Condition at x = 4.5 ft

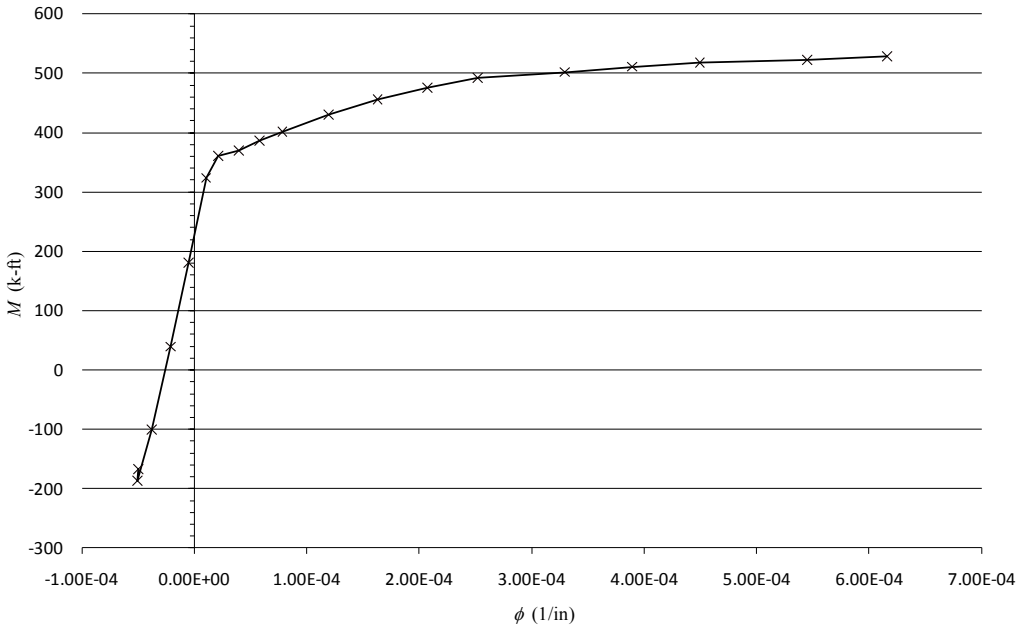

Fig. E.12: Undamaged Condition at x = 7.5 ft

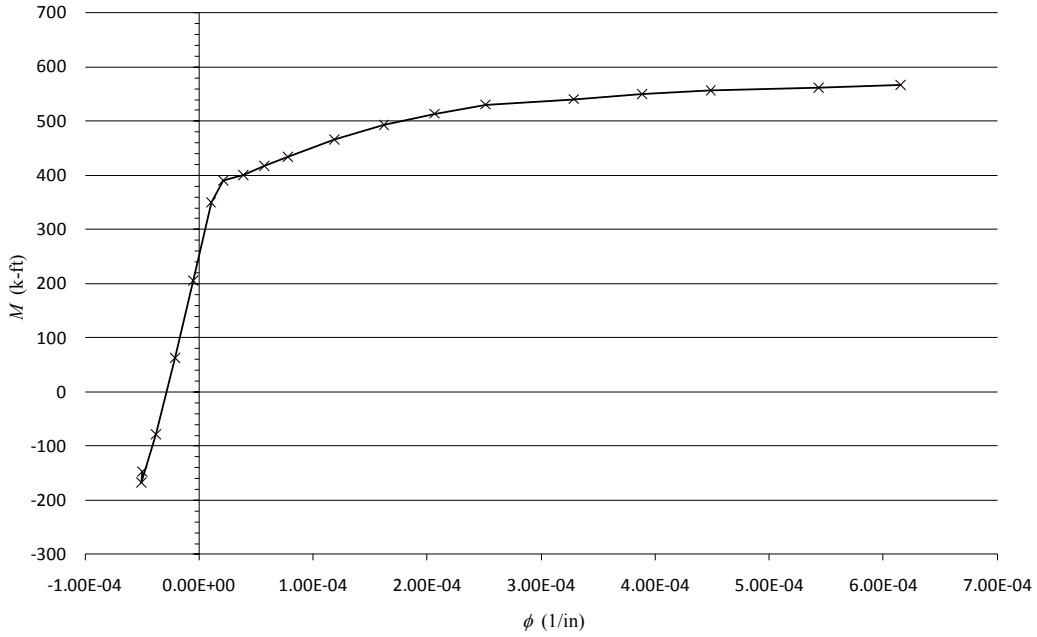

Fig. E.13: Undamaged Condition at x = 10.5 ft

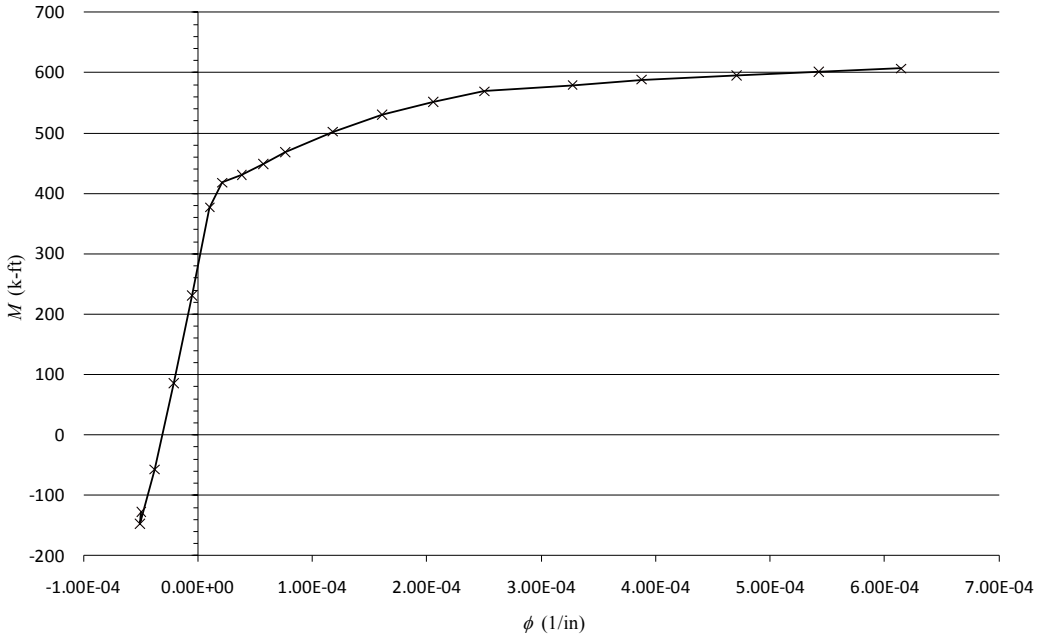

Fig. E.14: Undamaged Condition at x = 13.5 ft

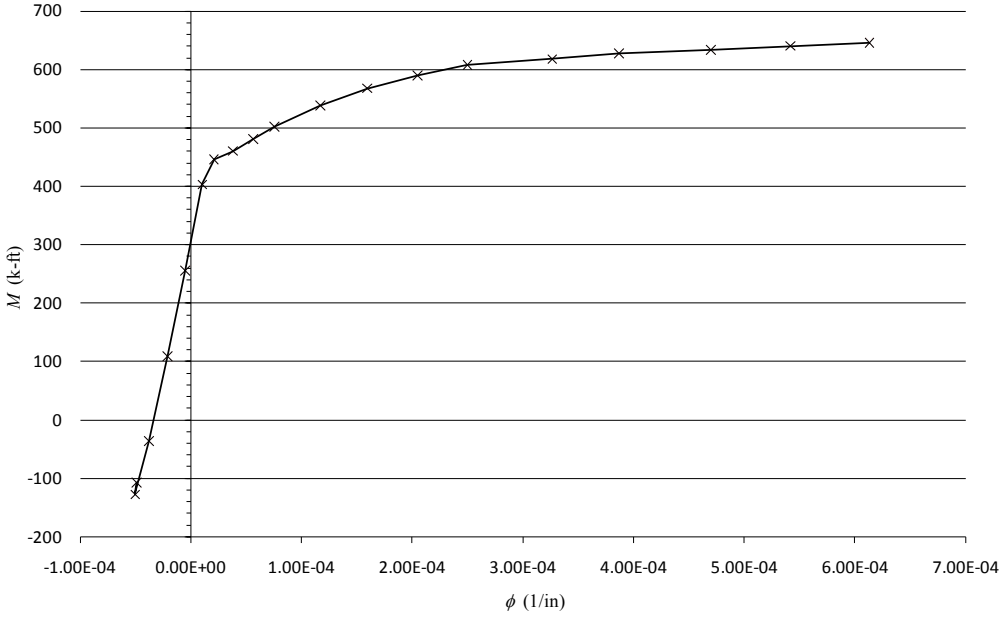

Fig. E.15: Undamaged Condition at x = 16.5 ft

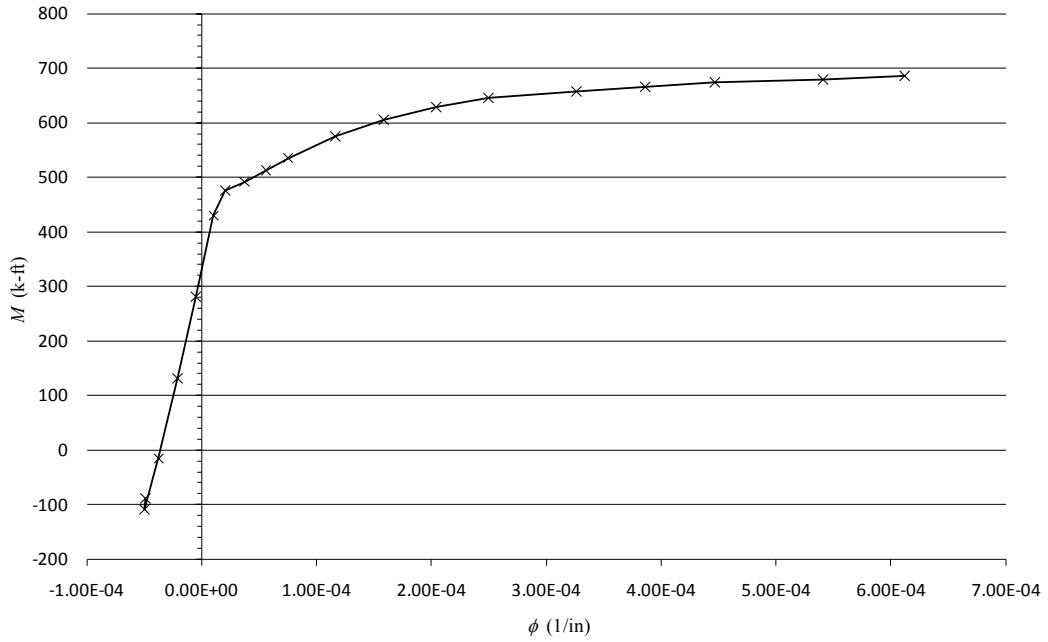

Fig. E.16: Undamaged Condition at x = 19.5 ft

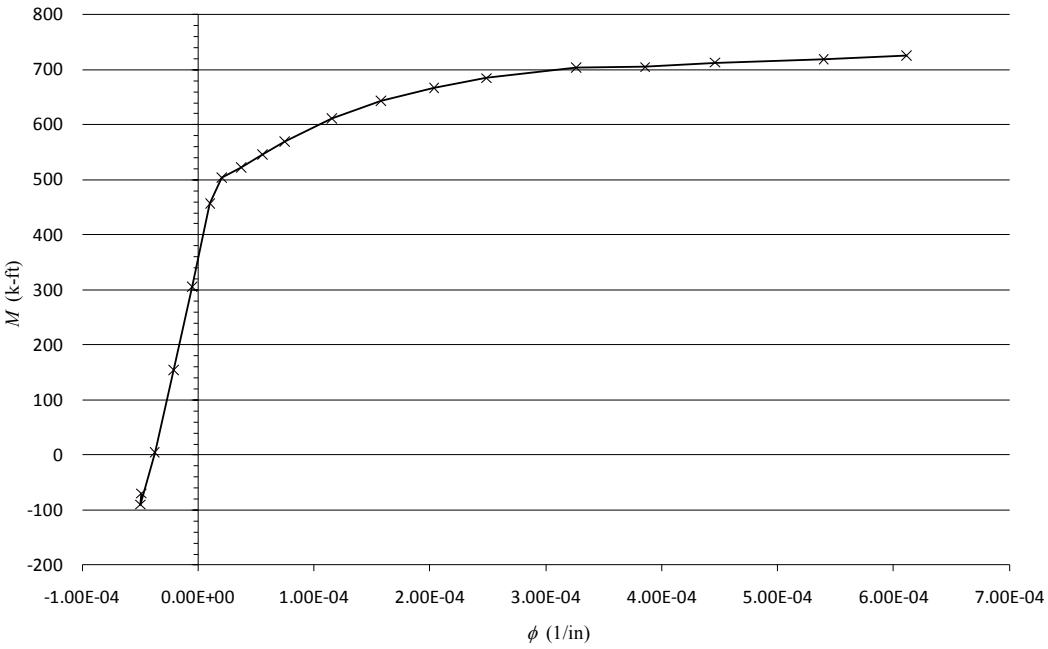

Fig. E.17: Undamaged Condition at x = 22.5 ft

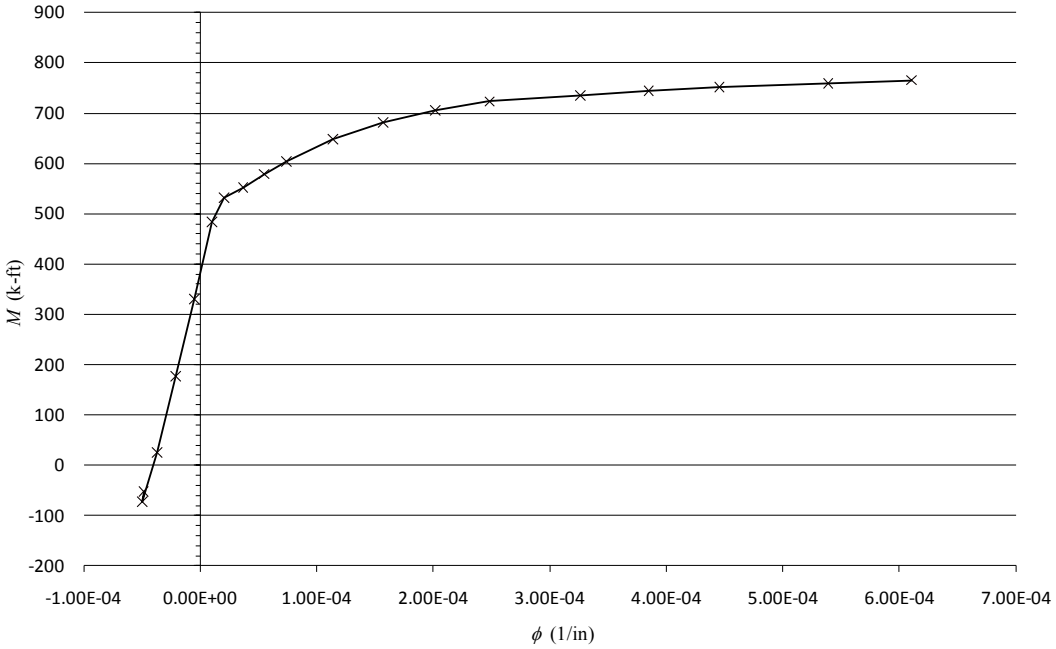

Fig. E.18: Undamaged Condition at x = 25.5 ft

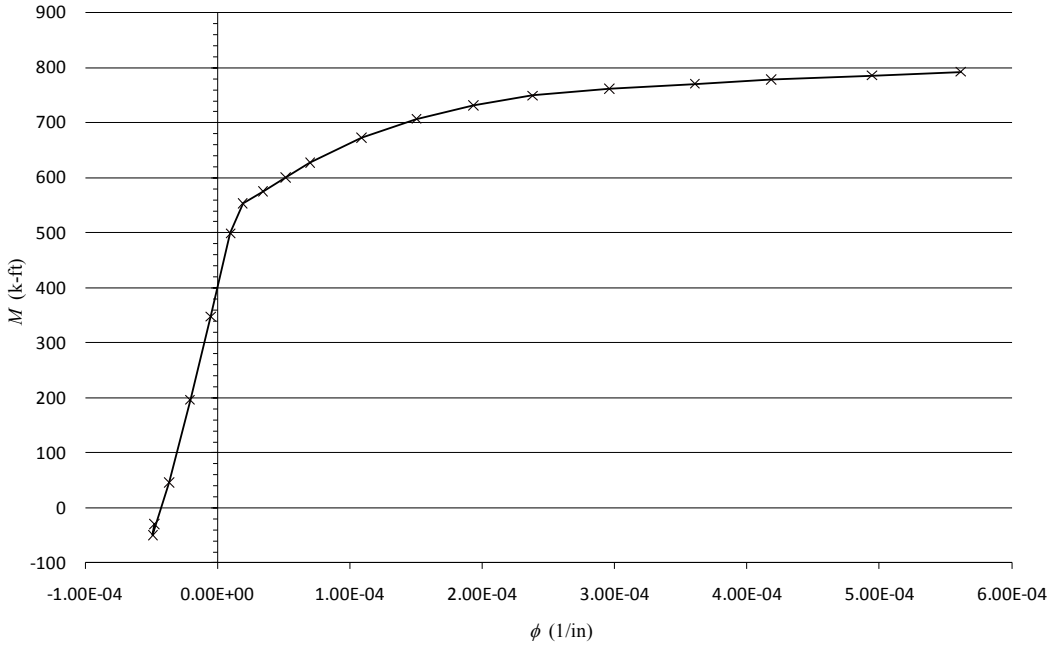

Fig. E.19: Undamaged Condition at x = 28 ft

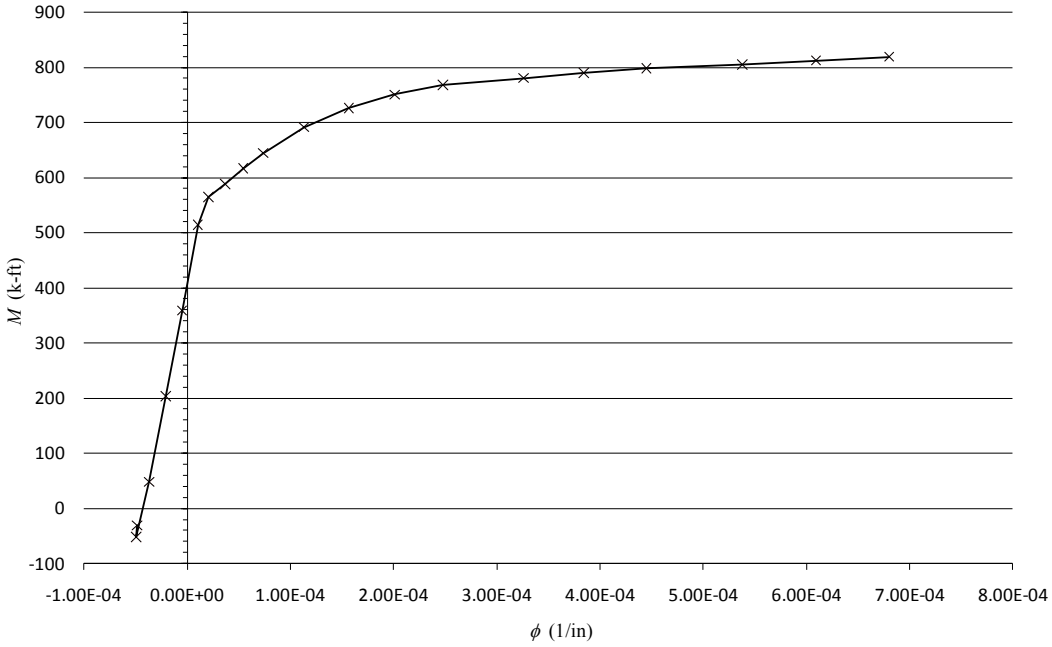

Fig. E.20: Undamaged Condition at x = 29 ft (Mid-Span)

LF2 MIXTURE (f_c = 6940 psi) – DAMAGED CONDITIONS

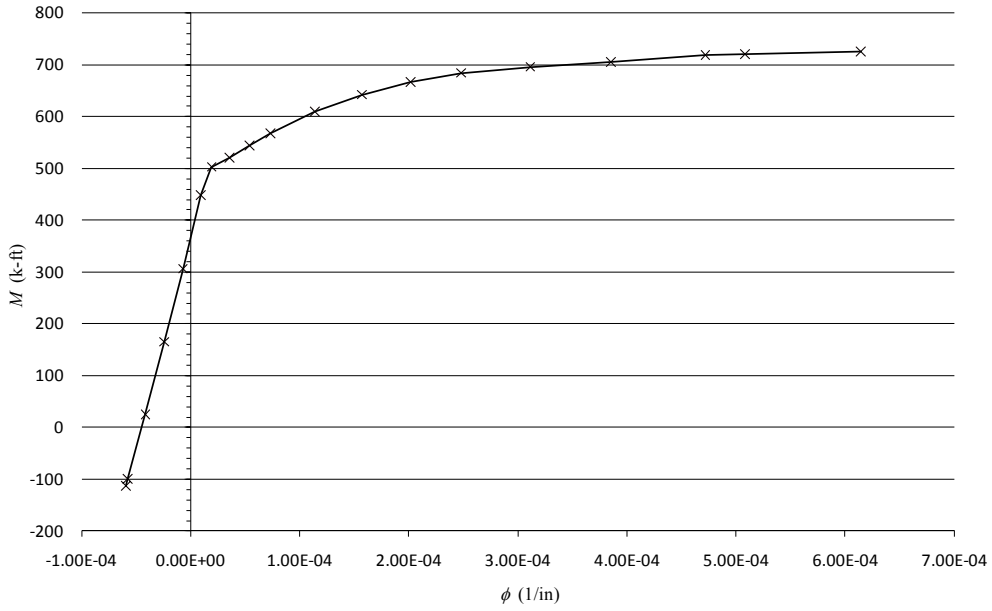

Fig. E.21: LF2 Damaged Condition at x = 22.5 ft

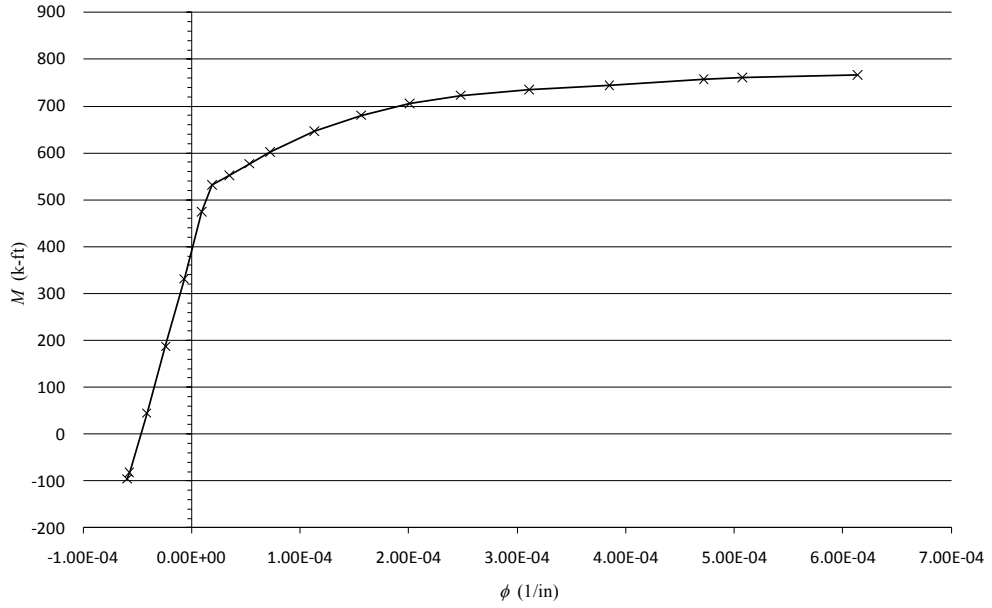

Fig. E.22: LF2 Damaged Condition at x = 25.5 ft

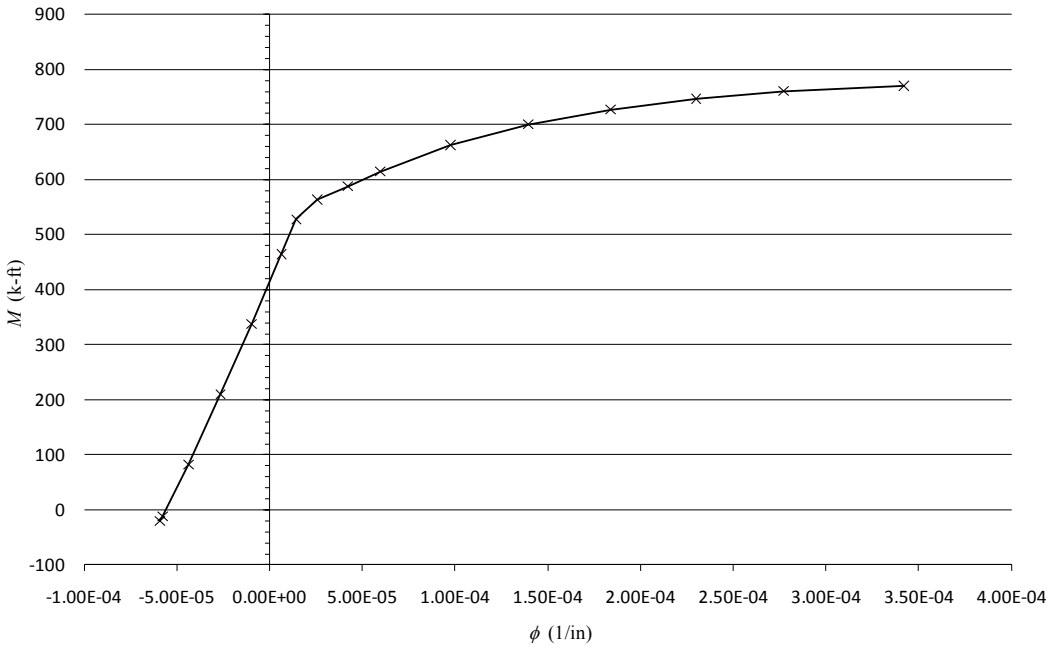

Fig. E.23: LF2 Damaged Condition at x = 28 ft (Spalling)

LF2 MIXTURE (f_c = 6940 psi) – UNDAMAGED CONDITIONS

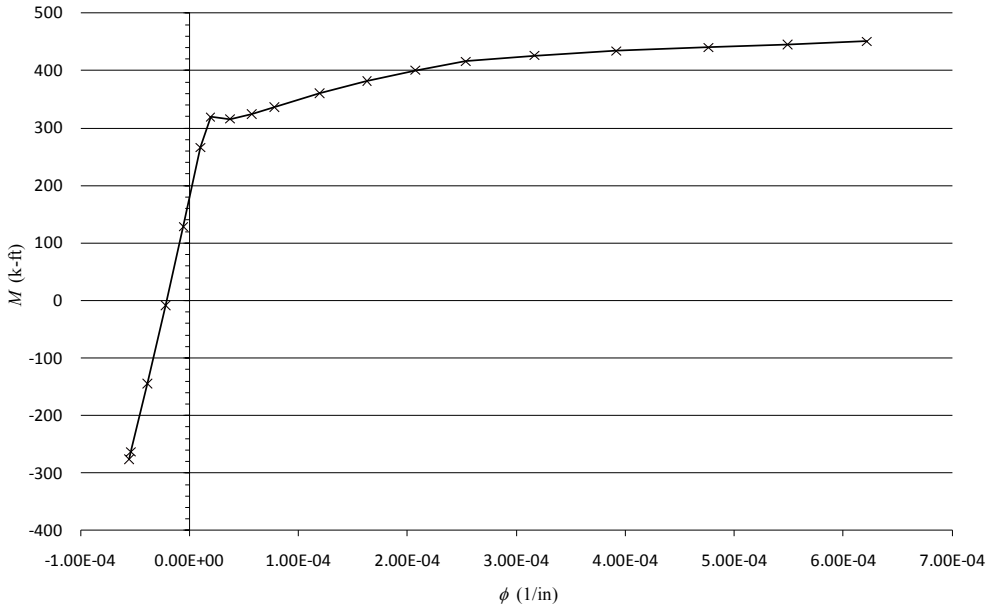

Fig. E.24: LF2 Undamaged Condition at x = 1.5 ft

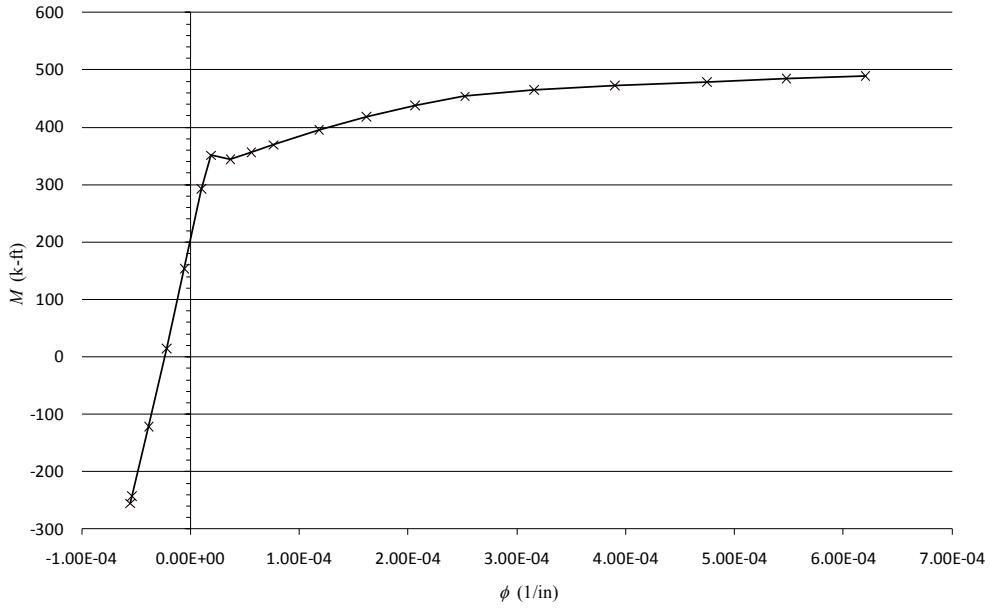

Fig. E.25: LF2 Undamaged Condition at x = 4.5 ft

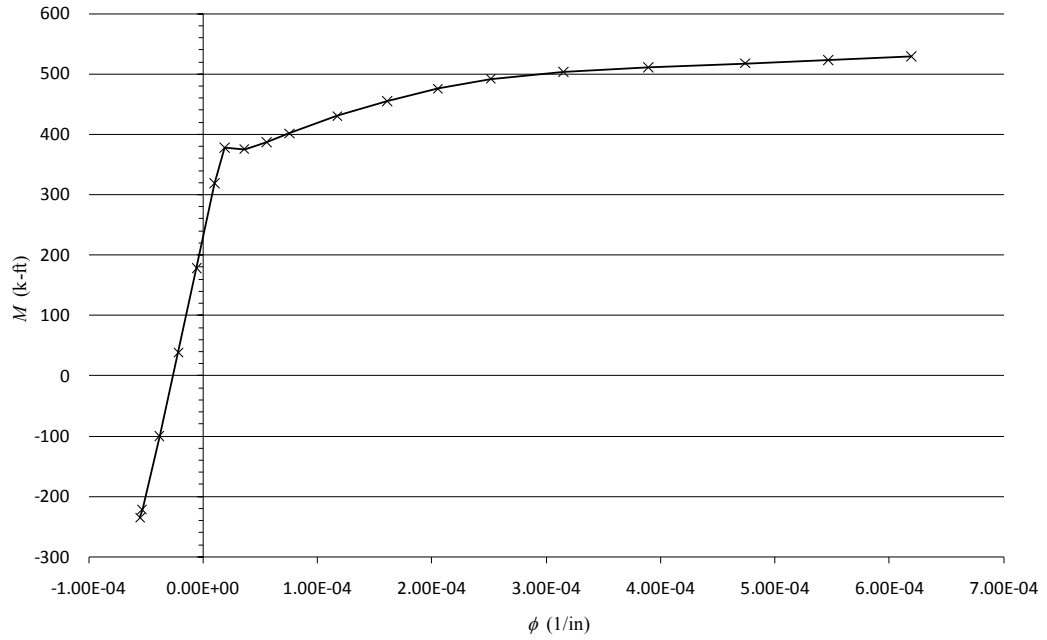

Fig. E.26: LF2 Undamaged Condition at x = 7.5 ft

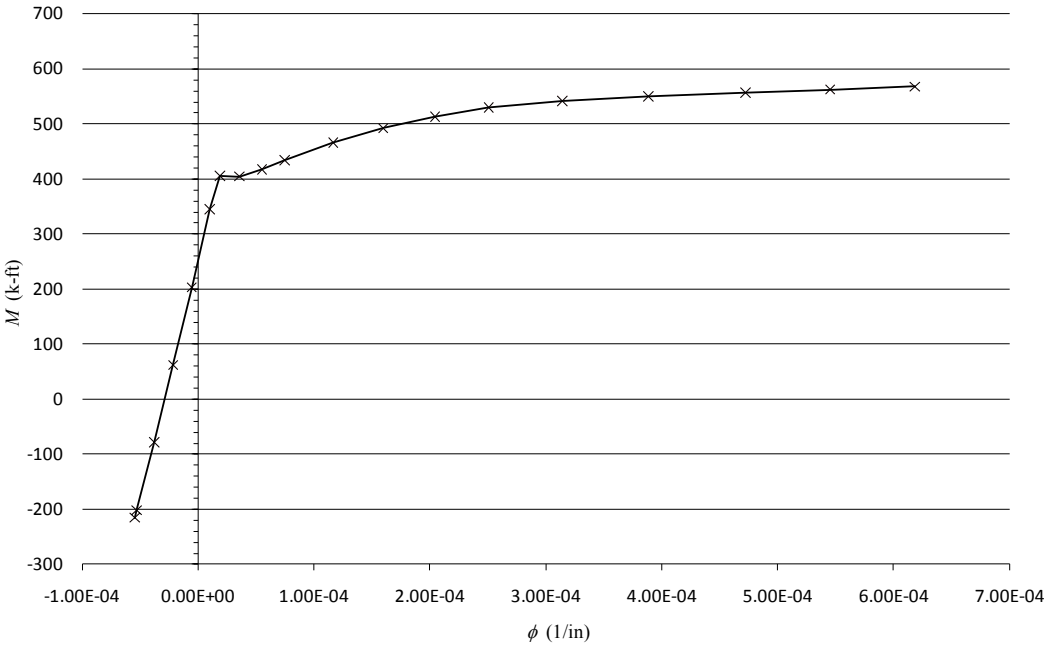

Fig. E.27: LF2 Undamaged Condition at x = 10.5 ft

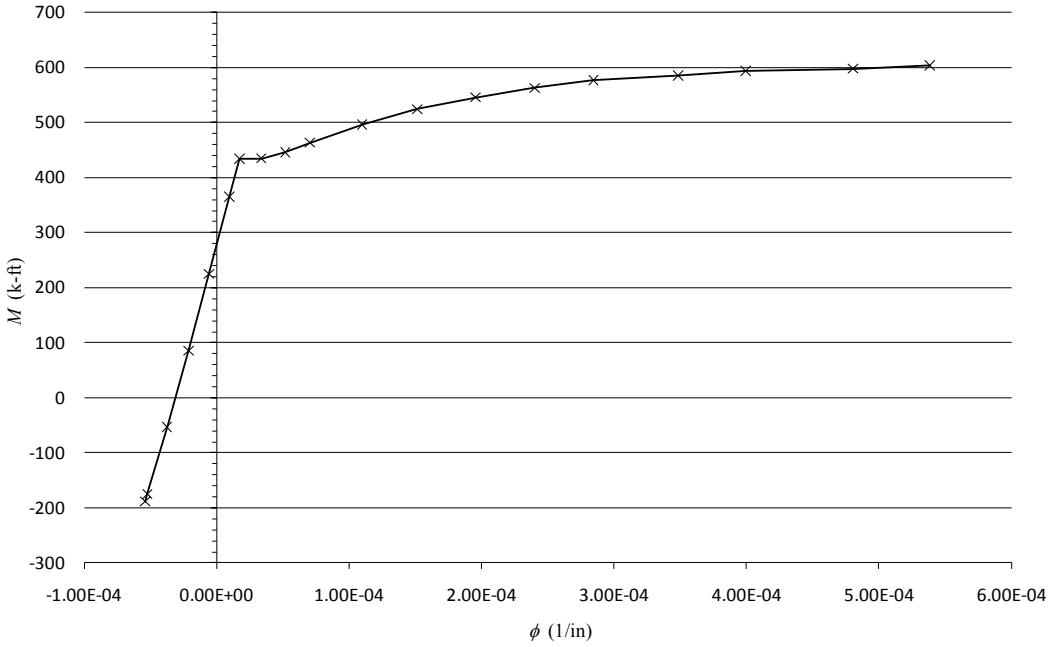

Fig. E.28: LF2 Undamaged Condition at x = 13.5 ft

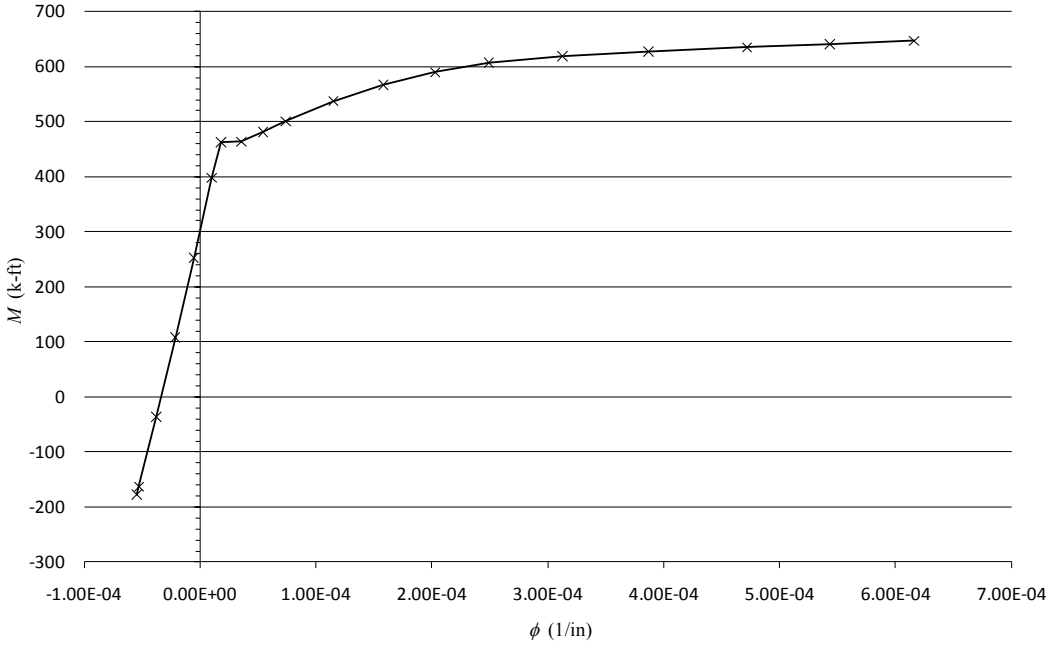

Fig. E.29: LF2 Undamaged Condition at x = 16.5 ft

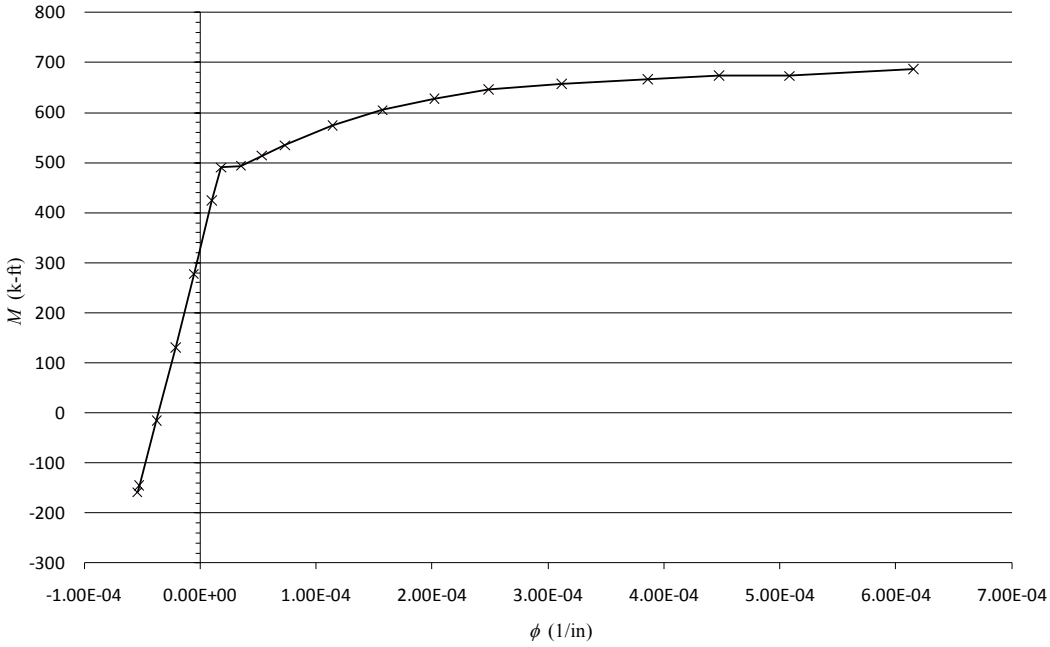

Fig. E.30: LF2 Undamaged Condition at x = 19.5 ft

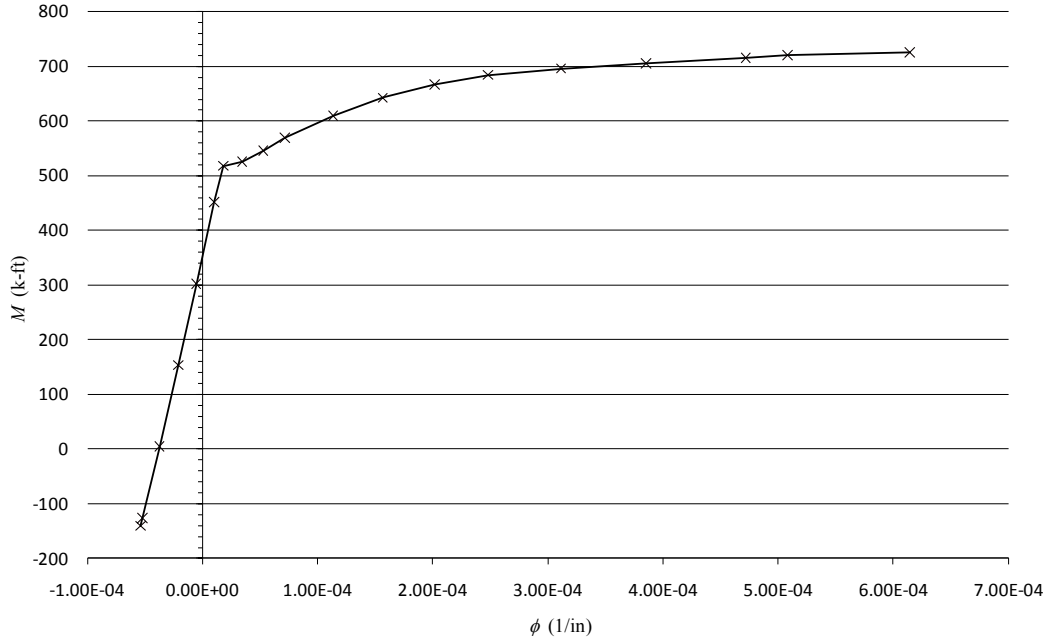

Fig. E.31: LF2 Undamaged Condition at x = 22.5 ft

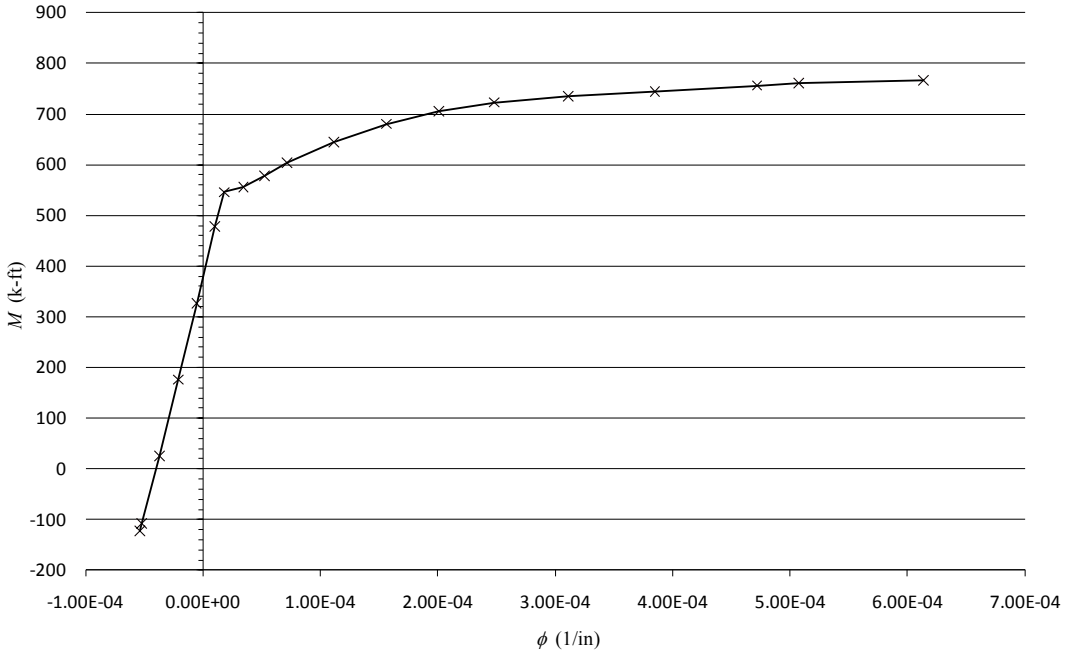

Fig. E.32: LF2 Undamaged Condition at x = 25.5 ft

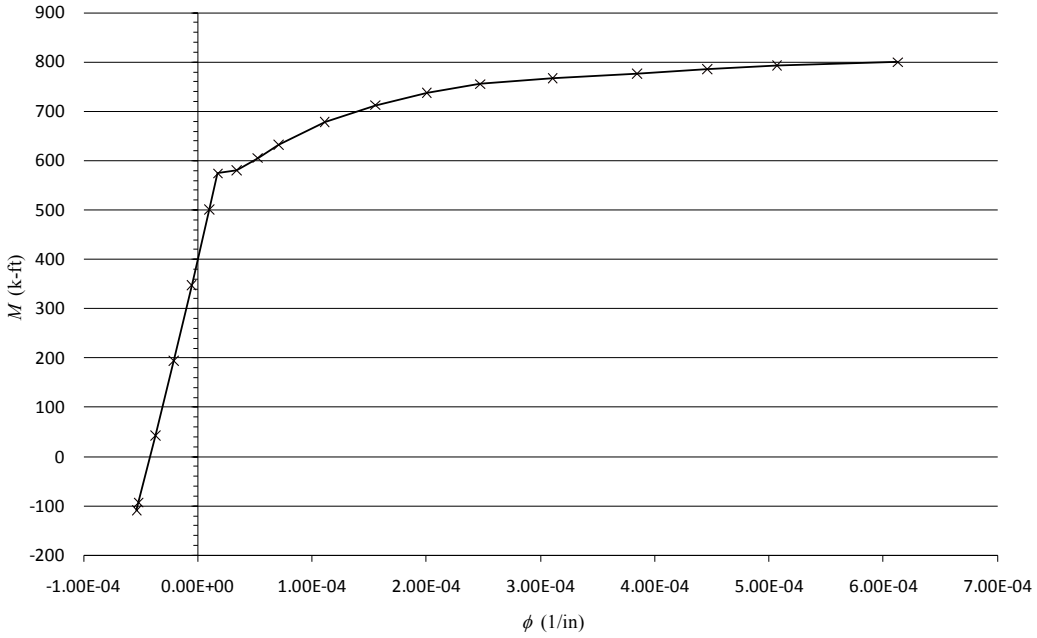

Fig. E.33: LF2 Undamaged Condition at x = 28 ft

LF6 MIXTURE (f_c = 3740 psi) –DAMAGED CONDITIONS

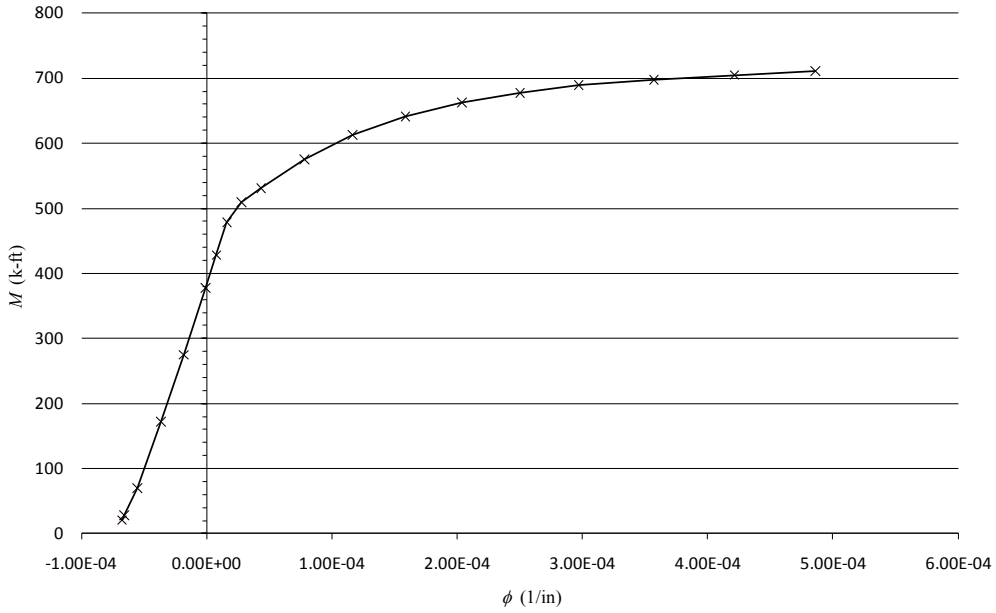

Fig. E.34: LF6 Damaged Condition at x = 22.5 ft

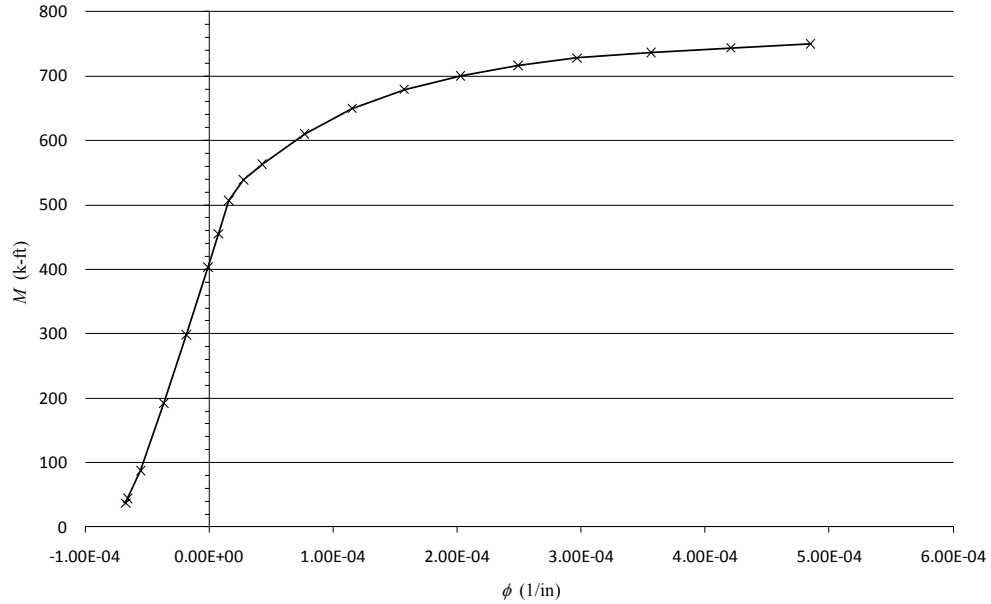

Fig. E.35: LF6 Damaged Condition at x = 25.5 ft

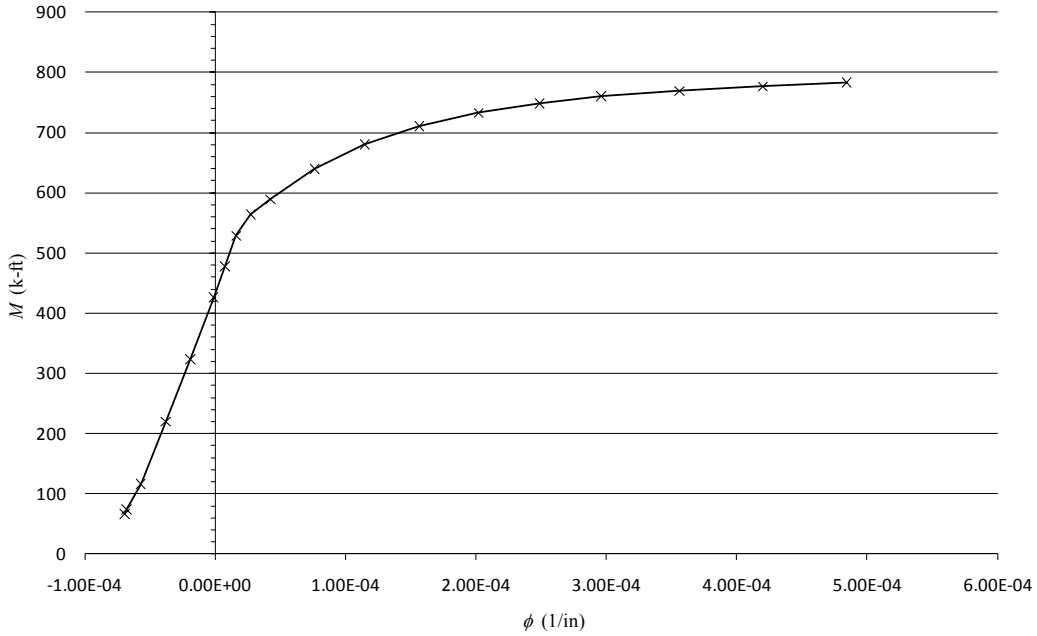

Fig. E.36: LF6 Damaged Condition at x = 28 ft (Spalling)

LF6 MIXTURE (f_c = 3740 psi) –UNDAMAGED CONDITIONS

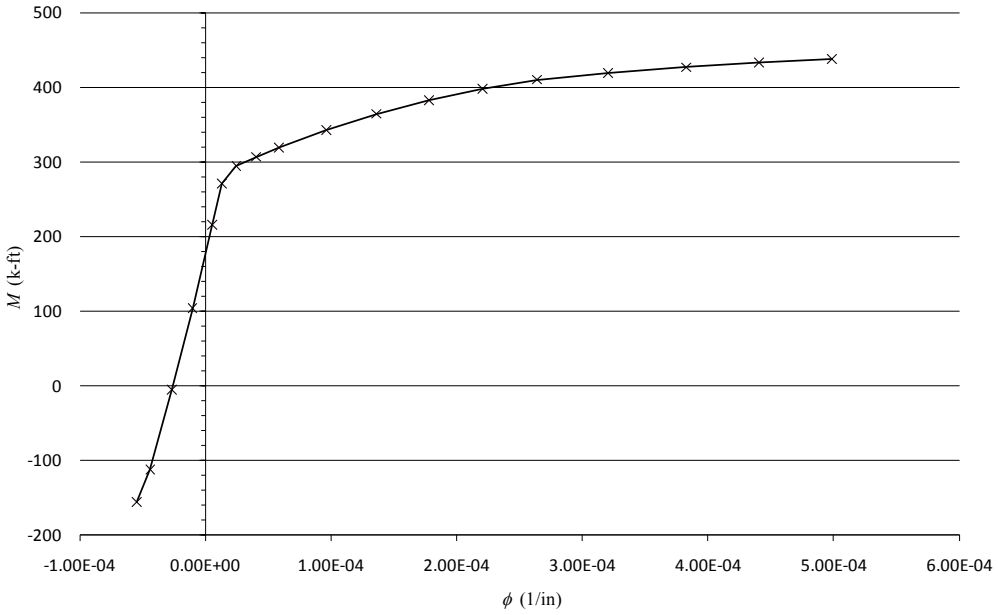

Fig. E.37: LF6 Undamaged Condition at x = 1.5 ft

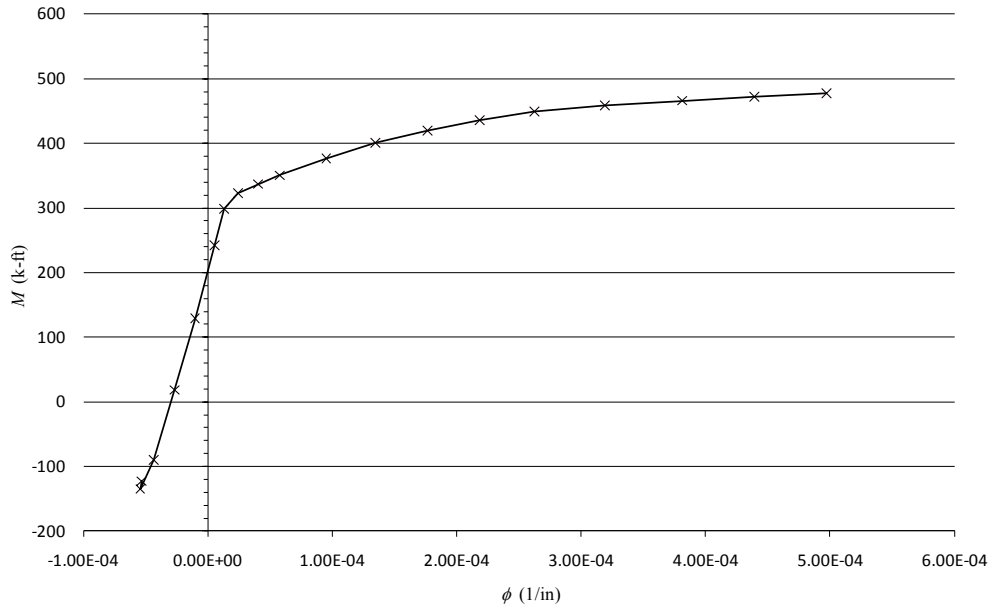

Fig. E.38: LF6 Undamaged Condition at x = 4.5 ft

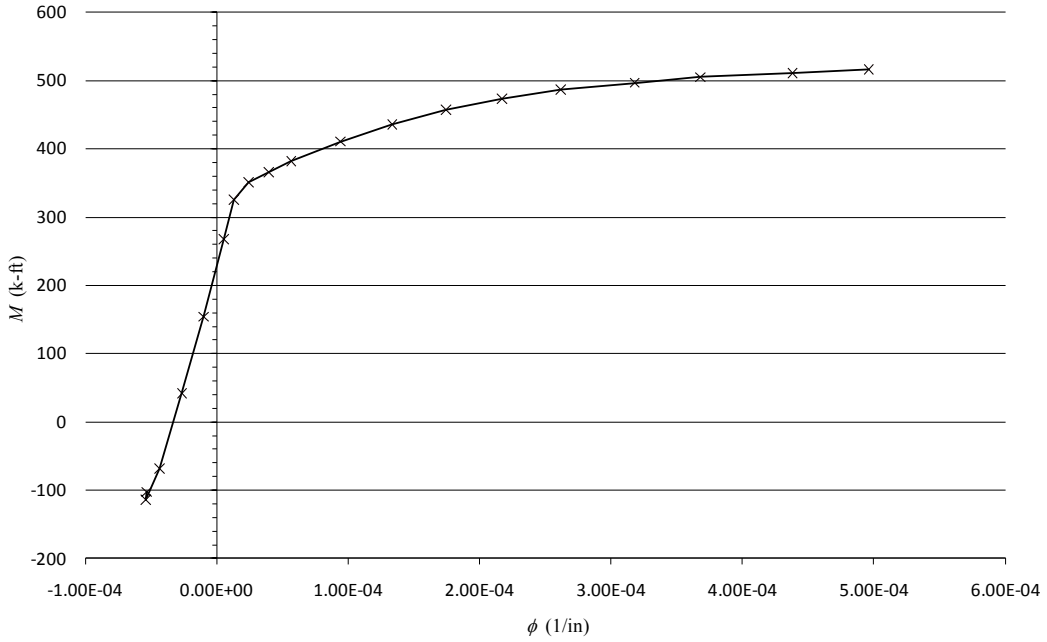

Fig. E.39: LF6 Undamaged Condition at x = 7.5 ft

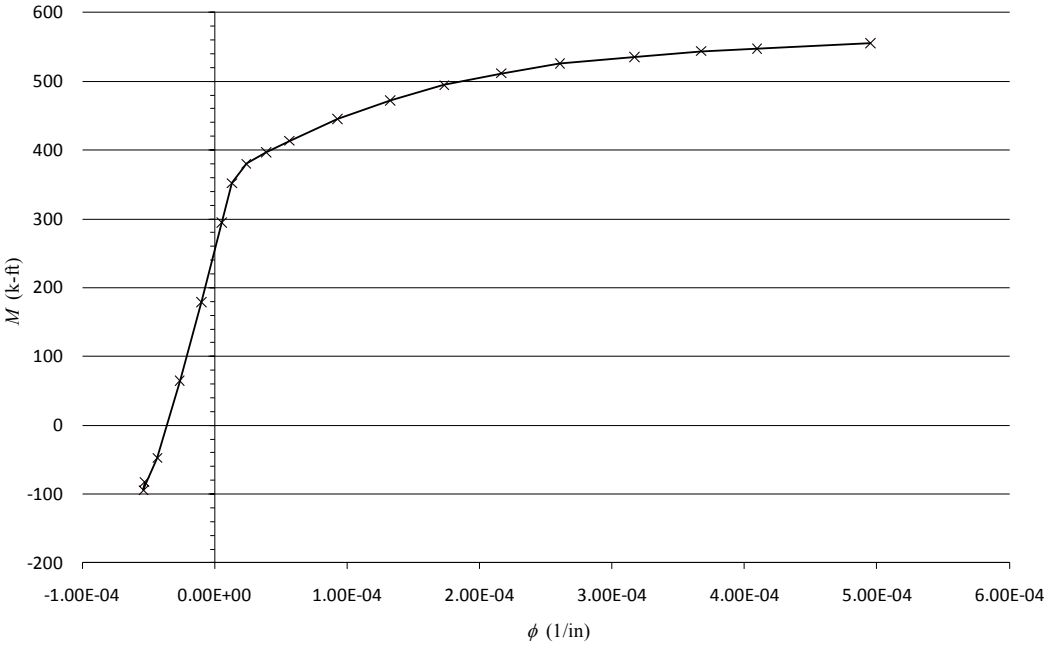

Fig. E.40: LF6 Undamaged Condition at x = 10.5 ft

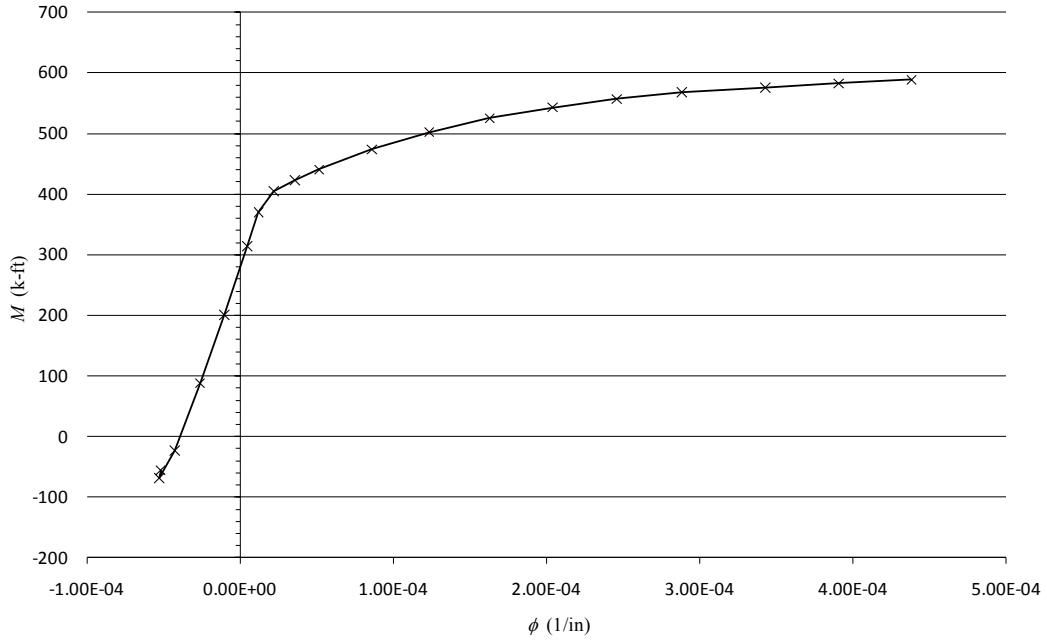

Fig. E.41: LF6 Undamaged Condition at x = 13.5 ft

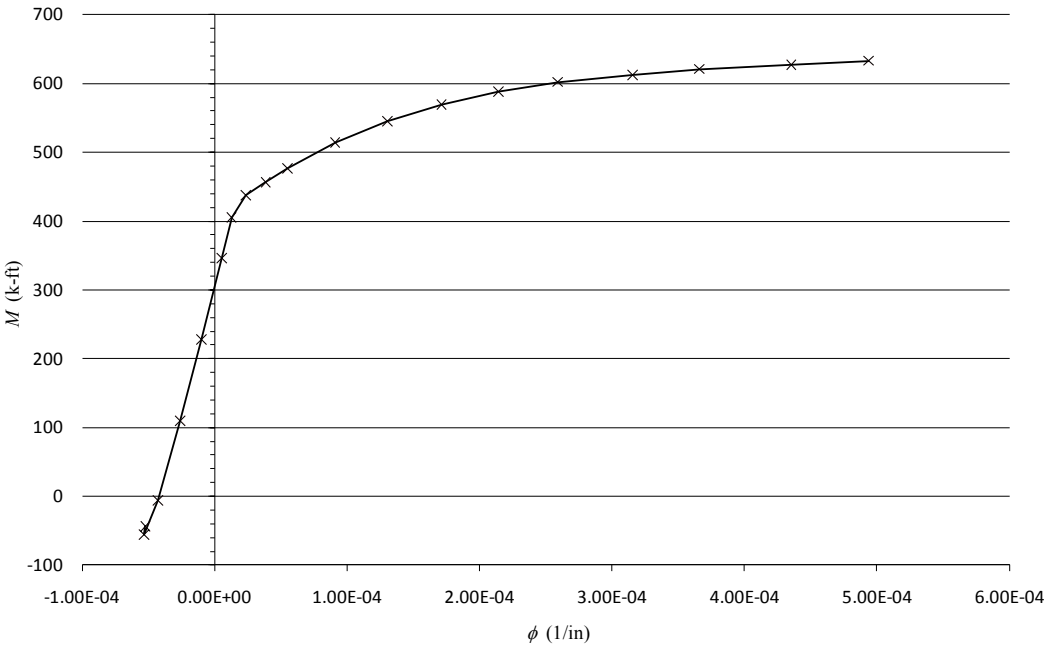

Fig. E.42: LF6 Undamaged Condition at x = 16.5 ft

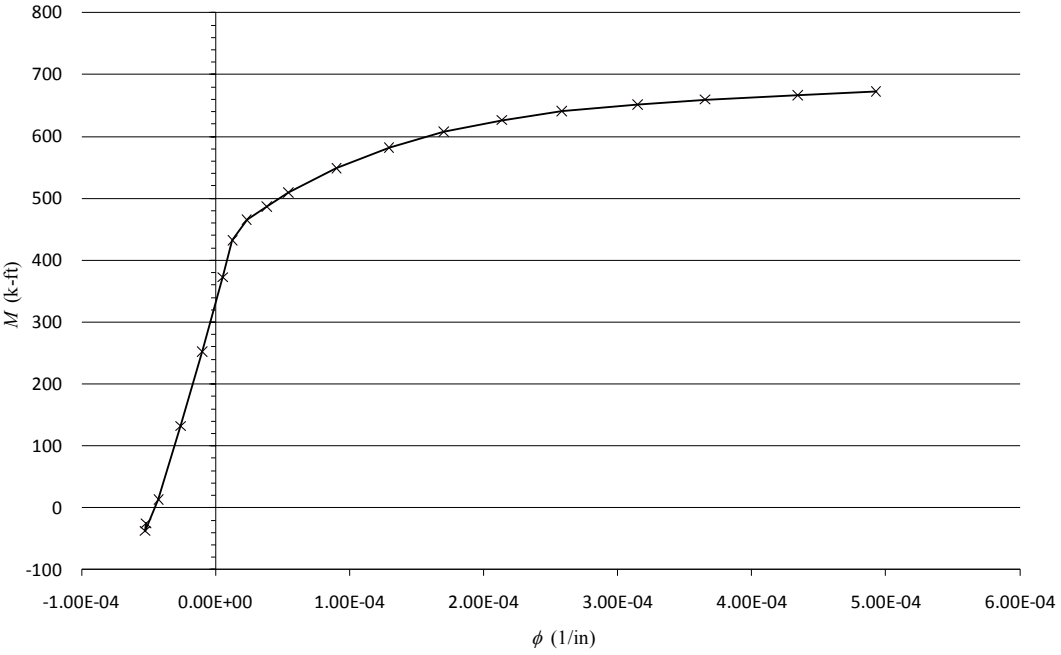

Fig. E.43: LF6 Undamaged Condition at x = 19.5 ft

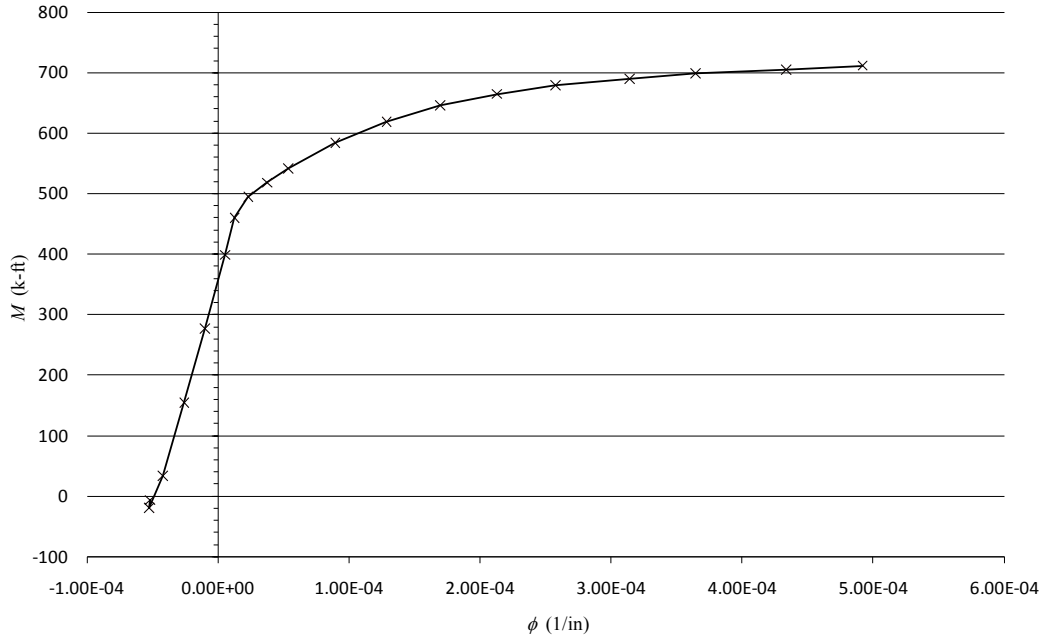

Fig. E.44: LF6 Undamaged Condition at x = 22.5 ft

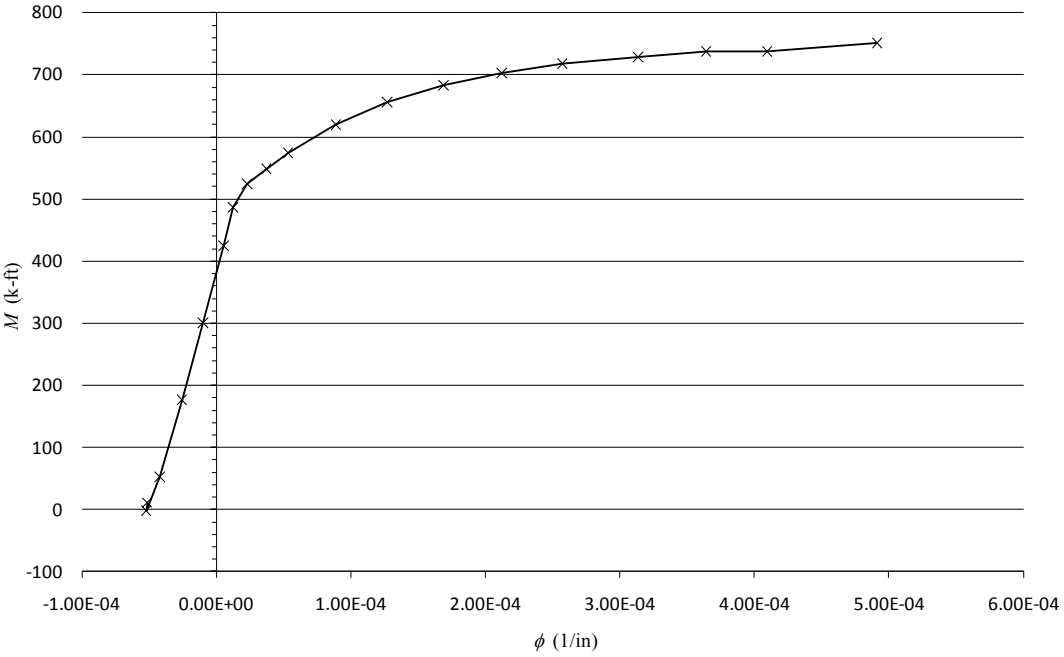

Fig. E.45: LF6 Undamaged Condition at x = 25.5 ft

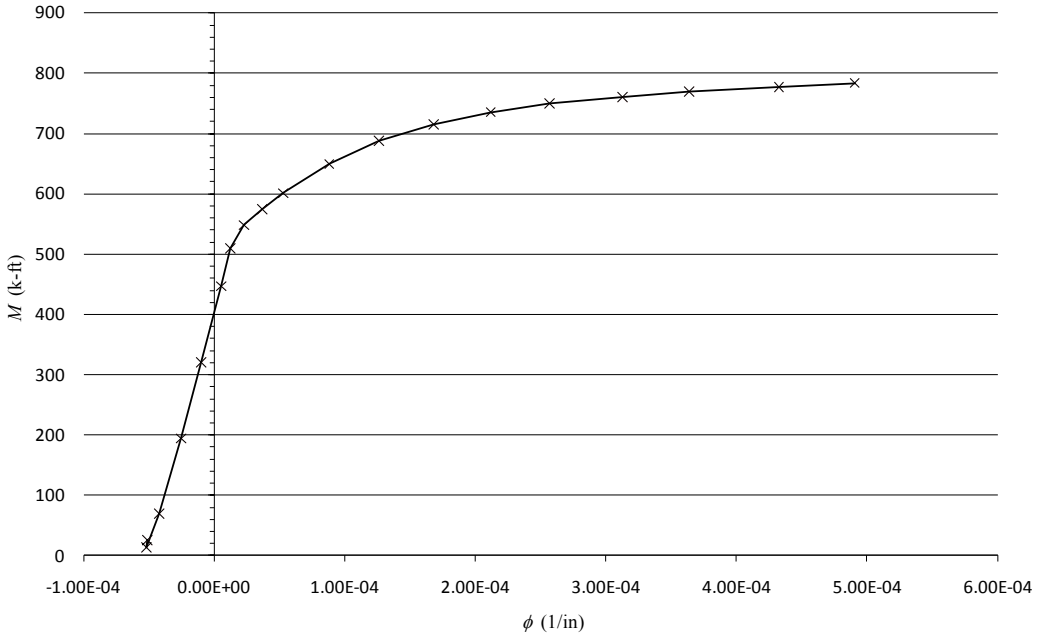

Fig. E.46: LF6 Undamaged Condition at x = 28 ft

APPENDIX F:

Air Permeability Index Test Methodology and Results

F.1 Air Permeability Index Test Methodology

Previous studies have examined the relationship between E_d and fluid penetrability as measured using the air permeability index (API) method developed by Schonlin and Hilsdorf (1988). Dilek and Leming (2007, 2008), Dilek, Leming and Guth (2004), and Recalde and Leming (2009) found the relationship between E_d and log(API) to be roughly linear for a wide variety of concrete mixtures including specimens damaged by load or by fire. The API is determined using the apparatus shown in Figure F.1, and Equation F.1.

$$API = \frac{(p_1 - p_0)V_s}{(s_1 - s_0)(p_a - \frac{p_0 + p_1}{2})}\frac{t}{A} \tag{F.1}$$

where

p_0, p_1 = start and end pressures, in. Hg (atm)

p_a = atmospheric pressure, in. Hg (atm)

s_1-s_0 = duration of measurement, sec.

V_s = volume of chamber, in.^{3} (mm^3)

t = thickness of concrete specimen, in. (mm)

A = cross-sectional area of concrete specimen, in.^{2} (mm^2)

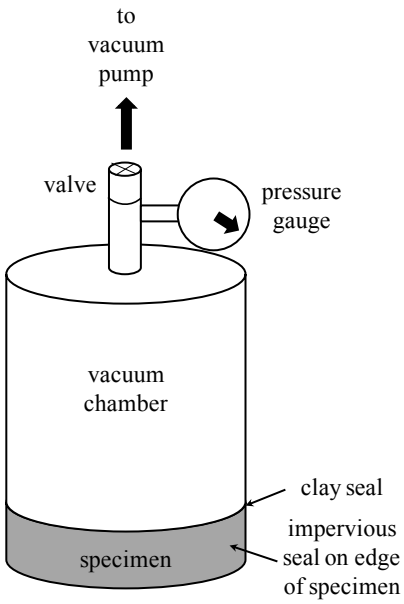

Fig. F.1: Air Permeability Index Test Apparatus

F.2 Air Permeability Index Results

The log(API) values are shown relative to E_d in Figure F.2. The general relationship was consistent with previous studies (Dilek, Leming and Guth 2004; Dilek and Leming 2008; Recalde and Leming 2009). The linearity in Figure F.2 is also consistent with the statistical indication that exposure to 300 C (570 F) only and exposure to 150 C and 300 C (300 F and 570 F) are not significantly different in that the linear change in E_d with log(API) between 150 C (300 F) and 300 C (570 F) exposures and the linear change between no exposure and 300 C (570 F) exposure have approximately the same slope. The combined r^2 of the regression model was 81%, as illustrated in Figure F.2. Figure F.3 shows $\%\Delta$ log(API) relative to $\Delta\in$. Research is ongoing to evaluate this relationship and determine applicability to the findings of this project.

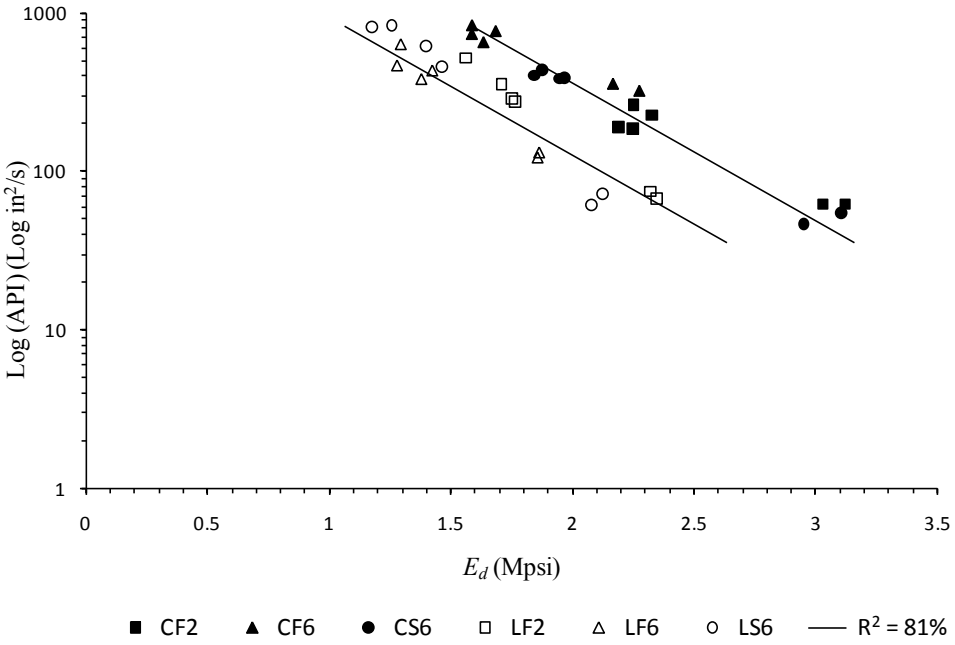

Fig. F.2: Log(API) with E_d
(1.0 Mpsi = 6.89 GPa; 1.0 in^2/s = 645.2 mm^2/s)

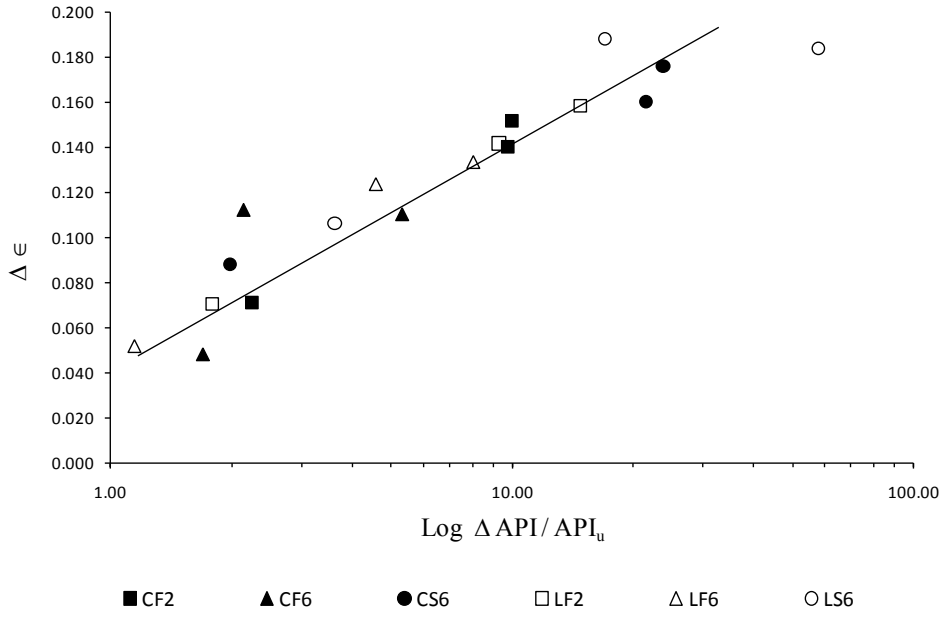

Fig. F.3: Δ∈ with %Δ Log(API)